PittPublicHealth

Department of Human Genetics

PhD Qualifying Exam & MS Comprehensive Exam

Preparation Materials

Updated August 31, 2019

The doctoral Qualifying Exam and Master's Comprehensive Exam begins with an oral presentation by the student of a research article from the primary literature. The paper serves as a starting point for an oral examination of the student's understanding of the paper and knowledge of the field.

Students will be required to demonstrate expertise in their chosen areas of concentration, which may include deeper knowledge than covered in the required coursework. In addition to mastery in their specific area, students will be required to demonstrate broad knowledge of the field of Human Genetics as a whole. Students will be responsible for showcasing their ability to utilize knowledge and skills obtained through coursework and research experiences to inform their interpretation, synthesis, and evaluation of the contemporary peer-reviewed literature.

The following list of knowledge requirements that students are expected to master may be used to assist in preparing for the qualifying exam. Likewise, course objectives for the core Human Genetics curriculum are provided below and may serve as an outline of topics to assist in students' preparations. Material covered in additional courses relevant to an individual student's academic experience and trajectory may also be germane. Lastly, example qualifying exam questions pertaining to specific example papers are provided. Please be aware that some questions raised during the oral examination may not have clear or objective "right" answers, but may instead reflect current uncertainties in the field of human genetics. In these cases, students may be expected to provide thoughtful discussion regarding prevailing hypotheses or themes, demonstrate knowledge of ambiguities in the scientific evidence or limitations of our current knowledge, and propose new experiments that could yield insight into the question at hand.

Knowledge requirements:

- DNA, Genes, Chromosomes, and Genomes
    - definition, structure, function, and organization of genes, chromosomes, and genomes
    - mitosis, meiosis, and recombination
    - central dogma and mechanisms of DNA replication, transcription, and translation
    - gene expression and regulation during development, normal, and abnormal cellular functions
    - genetic variation at the nucleotide, gene, chromosome, and genome levels
- Genetic Control of Phenotypes
    - modes of inheritance (autosomal/sex-linked, dominant/additive/recessive, mitochondrial, etc.) and corresponding patterns of phenotypic variation in human pedigrees

  - basic principles and examples of inborn errors of metabolism and classic genetic syndromes
  - the multifactorial nature of complex traits and the principles of multifactorial inheritance
  - molecular techniques for detecting genetic mutations and polymorphisms
  - use of model organisms to study human genetic diseases
  - principals of cancer genetics, the two-hit hypothesis, and somatic mutations
- Disease Gene Discovery and Gene Mapping
  - genetic epidemiology: modeling genotype-phenotype relationships, and identifying the genetic contributors of a phenotype
  - how multifactorial inheritance impacts disease gene mapping in humans
  - rationale, advantages, and limitations of linkage analysis study designs
  - rationale, advantages, and limitations of genetic association study designs
  - interpretation of classical statistical tests commonly used in genetic studies
  - approaches for studying the role of copy number variation (CNV) in complex disease
  - applications of next-generation sequencing (NGS) in the studying human disease
  - the role of rare variants in common complex disease and how rare variants are tested for association
  - approaches for finding functional variations
  - examples of complex disease genes that have been successfully identified
  - definition of multiple testing and common methods for correction
  - use of animal models to define the pathophysiology of disease
- Population Genetics
  - impact of fundamental principles of population genetics including Hardy-Weinberg Equilibrium, its assumptions, and the effects of violations of these assumptions
  - how evolutionary principles (like bottlenecks, founder effects, and population isolates) can affect or be exploited for human genetic studies
  - how allele frequencies differ in populations and the impact on genetic studies
  - linkage disequilibrium, how it is described and measured, how it relates to haplotypes, and how it impacts association studies
- Genetics in Society
  - how novel scientific discoveries are evaluated in a clinical context and applied appropriately to the care of patients, the function of genetic counseling
  - issues in genetic testing
  - how legal and ethical issues affect research, including informed consent
- Molecular Techniques
  - definition, implementation, advantages, and limitations of PCR, genotyping methods, gene expression methods, sequencing methods

Course objectives:

HUGEN 2022: Human Population Genetics

- apply the Law of Hardy-Weinberg Equilibrium and its assumptions to calculate allele and genotype frequencies
- predict the consequences of genetic inheritance and recombination in populations including the concepts of linkage and linkage disequilibrium
- interpret the qualitative effects of violations of Hardy-Weinberg Equilibrium and solve simple quantitative problems demonstrating these effects

- express the fundamental goals and principles of genetic epidemiology by modeling genotype-phenotype relationships, quantitative traits, and heritability
- interpret results from gene discovery methods such as linkage analysis and large-scale genetic association studies, and critically evaluate the strengths, limitations, and appropriate applications of these methods.

HUGEN 2031: Chromosomes and Human Disease

- compare and contrast the strengths and limitations of the various cytogenetic assays
- describe chromosomal alterations, their causes, and their clinical implications
- describe the role of chromosomal alterations in development of cancer and their use in cancer diagnostics
- apply principles of effective written and oral communication to cytogenetics topics
- critique published cytogenetics literature
- write a research proposal related to cytogenetics or chromosomes
- interpret cytogenetic nomenclature
- describe a variety of cytogenetic concepts and methodologies
    - the cellular basis of chromosome segregation, chromosome structure, meiosis and mitosis, numerical and structural chromosome abnormalities in clinical disorders, including chromosomal syndromes, chromosome breakage syndromes, cancer, sex determination and sex chromosome abnormalities, genomic imprinting, trinucleotide repeat disorders, classical and molecular cytogenetic methods including copy number arrays and nomenclature, the role of cytogenetic techniques in diagnosis of disorders, the history of cytogenetic methods, and ethical issues related to cytogenetic testing and results.

HUGEN 2034: Biochemical and Molecular Genetics of Complex Disease

- Describe the epidemiology and biochemical and molecular bases of selected common diseases
- Describe the underlying genetic architecture and environmental risk factors that influence genetic susceptibility to a variety of common, complex diseases ranging from cardiovascular disease to neurological disorders
- Describe and discuss the public health impact of a variety of common, complex diseases, including potential pharmacogenomics applications.

HUGEN 2040: Molecular Genetics of Human Inherited Disease

- Explain the structural components and functions of genes
- Evaluate the utility of molecular testing methods to diagnose inherited diseases, and calculate key test measures (specificity, sensitivity, etc.)
- Differentiate Mendelian disorders based on clinical manifestations
- Distinguish inherited diseases based on the molecular mechanisms
- Compare different treatment approaches to inherited diseases
- Recognize unique human populations, which harbor alleles for inherited diseases
- Compile clinical, molecular, diagnostic and treatment information on inherited diseases

Example qualifying exam (Ph.D.) and comprehensive exam (M.S.) questions pertaining to Guissart et al. (2018) *American Journal of Human Genetics*.

1. Why do many human genes have two paralogs in zebrafish? Why are both often retained? How does the presence of two paralogs affect the design of zebrafish models of human disease?

2. In Figure 4C the authors present an immunoblot for RORA in skin fibroblasts of patients and a control. In the samples from patients 2 and 6, is the detected protein a product of the WT allele, mutant allele, or both? Explain your reasoning.

3. The authors speculate that the Gly92Ala and Lys94Arg mutations might prevent the access of WT RORA to its target sites. Is this speculation consistent with the findings in figure 4 and the authors' conclusion that these mutations act through a toxic gain of function mechanism?

4. Discuss the mechanisms by with one gene can produce different transcripts. Which of these mechanisms are illustrated by the human RORA gene and which by the zebrafish roraa gene?

5. What method would you use to test if the number or strength of roraa binding sites are altered by certain missense mutations? How would you test if binding at those sites result in an increase or a decrease of transcription?

6. Would you expect individual 11, who has the largest deletion, to show any different symptoms in addition to those shared with the others? Why or why not? Are there any particular traits or biomarkers you might choose to investigate?

7. What is the difference between a gain-of-function mutation and a dominant-negative one? Give an example of a human genetic disorder that is caused by a dominant negative mutation.

8. Explain array CGH, whole exome sequencing, and Sanger sequencing. What information do you get from each technique and to what type of research question would you apply each technique?

9. Cultured fibroblasts from patient #6 (p.Arg340Profs817) show no change in protein level via Western. Authors suggest that the transcript, which is a deletion with frame shift and early stop, is not degraded

by NMD. What is NMD? Do you think their explanation is likely, and why? How could they prove this? Can you suggest other reasons why the protein level might not be lower in this sample?

10. The authors conclude that mutations in the DNA binding domain (DBD) generate gain-of-function and are more deleterious than mutations in the ligand binding domain that generate loss of function (haploinsufficiency). Do you agree? Why or why not? What further experiments could you perform to prove their hypothesis and distinguish whether location of the mutation is important?

11. The specific *RORA* variants reported in this paper had not been discovered in previous GWAS studies of ASD or IQ. What is a likely reason for this?

12. The authors concluded that ectopic expression of each of the four WT *RORA* mRNAs did not lead to cerebellar phenotypes, but Figure S9 shows increased cerebellar area in zebrafish embryos injected with 200 pg of RORA1 mRNA. The p-value is 0.03. Does this result contradict their conclusion? Consider both the statistical significance and the scientific significance of this result.

13. What is the "multiple comparisons problem" and what strategies can be used to accommodate or resolve this problem? Does the multiple comparisons problem impact this paper? Why or why not?

14. Consider the deletion segregating in Family 10 that shows a dominant mode of inheritance with respect to the clinical phenotype. What do you speculate about the variant's impact on fitness? Do you expect that it is adaptive, maladaptive, or neutral? How then do you expect the frequency of the variant will fluctuate across future generations due to selection? What if instead the variant showed a recessive mode of inheritance – how would selection differ?

ARTICLE

Dual Molecular Effects of Dominant *RORA* Mutations Cause Two Variants of Syndromic Intellectual Disability with Either Autism or Cerebellar Ataxia

Claire Guissart,[1,37] Xenia Latypova,[2,3,4,37] Paul Rollier,[5,37] Tahir N. Khan,[3,37] Hannah Stamberger,[6,7,8] Kirsty McWalter,[9] Megan T. Cho,[9] Susanne Kjaergaard,[10] Sarah Weckhuysen,[6,7,8] Gaetan Lesca,[11,12] Thomas Besnard,[2,4] Katrin Õunap,[13] Lynn Schema,[14] Andreas G. Chiocchetti,[15] Marie McDonald,[16] Julitta de Bellescize,[17] Marie Vincent,[2,4] Hilde Van Esch,[18] Shannon Sattler,[19] Irman Forghani,[20] Isabelle Thiffault,[21,22,23] Christine M. Freitag,[15] Deborah Sara Barbouth,[20] Maxime Cadieux-Dion,[21] Rebecca Willaert,[9] Maria J. Guillen Sacoto,[9] Nicole P. Safina,[23,24,25] Christèle Dubourg,[26] Lauren Grote,[23,24,25] Wilfrid Carré,[26] Carol Saunders,[21,22,23] Sander Pajusalu,[13]

(Author list continued on next page)

RORα, the RAR-related orphan nuclear receptor alpha, is essential for cerebellar development. The spontaneous mutant mouse *staggerer*, with an ataxic gait caused by neurodegeneration of cerebellar Purkinje cells, was discovered two decades ago to result from homozygous intragenic *Rora* deletions. However, *RORA* mutations were hitherto undocumented in humans. Through a multi-centric collaboration, we identified three copy-number variant deletions (two *de novo* and one dominantly inherited in three generations), one *de novo* disrupting duplication, and nine *de novo* point mutations (three truncating, one canonical splice site, and five missense mutations) involving *RORA* in 16 individuals from 13 families with variable neurodevelopmental delay and intellectual disability (ID)-associated autistic features, cerebellar ataxia, and epilepsy. Consistent with the human and mouse data, disruption of the *D. rerio* ortholog, *roraa*, causes significant reduction in the size of the developing cerebellum. Systematic *in vivo* complementation studies showed that, whereas wild-type human *RORA* mRNA could complement the cerebellar pathology, missense variants had two distinct pathogenic mechanisms of either haploinsufficiency or a dominant toxic effect according to their localization in the ligand-binding or DNA-binding domains, respectively. This dichotomous direction of effect is likely relevant to the phenotype in humans: individuals with loss-of-function variants leading to haploinsufficiency show ID with autistic features, while individuals with *de novo* dominant toxic variants present with ID, ataxia, and cerebellar atrophy. Our combined genetic and functional data highlight the complex mutational landscape at the human *RORA* locus and suggest that dual mutational effects likely determine phenotypic outcome.

Introduction

Nuclear receptors appeared in the metazoan lineage as an adaptation to multicellular organization requiring distant cellular signaling through non-peptidic growth and differentiation factors.[1] The nuclear receptor superfamily is a group of transcription factors regulated by small hydrophobic hormones, such as retinoic acid, thyroid hormone, and steroids.[2] Mutations in nuclear receptors cause a diverse range of disorders, including central nervous system (CNS) pathologies, cancer, and metabolic disorders. For example, haploinsufficiency of *RORB* (MIM: 601972), encoding the nuclear receptor RORβ, results in behavioral and cognitive impairment and epilepsy,[3] while biallelic mutations in *RORC* (MIM: 602943), encoding RORγ, result in immunodeficiency (MIM: 616622[4]). Nuclear Receptor Subfamily 0, Group B, Member 1 (NR0B1 [MIM: 300473]) is an orphan member of the nuclear receptor superfamily and has been implicated in sex reversal (MIM: 300018[5]) and congenital adrenal hypoplasia (MIM: 300200[6]). RORα (RORA) is most closely related to Retinoic Acid Receptor (RAR) yet functions differently; RAR acts as a ligand responsive heterodimer with retinoid X receptor (RXR). However, RORα isoforms 1 and 2 constitutively activate transcription and bind DNA as monomers at responsive elements which consist of 6-bp

[1]EA7402 Institut Universitaire de Recherche Clinique, and Laboratoire de Génétique Moléculaire, CHU and Université de Montpellier, 34093 Montpellier, France; [2]Service de Génétique Médicale, CHU Nantes, 9 quai Moncousu, 44093 Nantes Cedex 1, France; [3]Center for Human Disease Modeling, Duke University Medical Center, Durham, NC 27701, USA; [4]l'institut du thorax, INSERM, CNRS, UNIV Nantes, 44007 Nantes, France; [5]Service de Génétique Clinique, Centre Référence "Déficiences Intellectuelles de causes rares" (CRDI), Centre de référence anomalies du développement CLAD-Ouest, CHU Rennes, 35203 Rennes, France; [6]Division of Neurology, University Hospital Antwerp (UZA), 2610 Antwerp, Belgium; [7]Neurogenetics Group, Center for Molecular Neurology, VIB, 2650 Antwerp, Belgium; [8]Laboratory of Neurogenetics, Institute Born-Bunge, University of Antwerp, 2650 Antwerp, Belgium; [9]GeneDx, 207 Perry Parkway, Gaithersburg, MD 20877, USA; [10]Chromosome Laboratory, Department of Clinical Genetics, Copenhagen University Hospital, Rigshospitalet, 2100 Copenhagen, Denmark; [11]Service de génétique, Groupement Hospitalier Est, Hospices Civils de Lyon, Lyon, France; [12]INSERM U1028, CNRS UMR5292, Centre de Recherche en Neurosciences de Lyon, Université Claude Bernard Lyon 1, Lyon, France; [13]Department of Clinical Genetics, United Laboratories, Tartu University Hospital and Institute of Clinical Medicine, University of Tartu, 2 L.Puusepa street, Tartu 51014, Estonia; [14]University of Minnesota-Fairview, Minneapolis, MN 55454, USA; [15]Department of Child and Adolescent Psychiatry, Psychosomatics and Psychotherapy, JW Goethe

(Affiliations continued on next page)

© 2018 American Society of Human Genetics.

Emily Farrow,[21,23,24] Anne Boland,[27] Danielle Hays Karlowicz,[16] Jean-François Deleuze,[27] Monica H. Wojcik,[28] Rena Pressman,[20] Bertrand Isidor,[2,4] Annick Vogels,[18] Wim Van Paesschen,[29] Lihadh Al-Gazali,[30] Aisha Mohamed Al Shamsi,[31] Mireille Claustres,[1] Aurora Pujol,[32] Stephan J. Sanders,[33] François Rivier,[34] Nicolas Leboucq,[35] Benjamin Cogné,[2,4] Souphatta Sasorith,[1] Damien Sanlaville,[11,12] Kyle Retterer,[9] Sylvie Odent,[5,36] Nicholas Katsanis,[3] Stéphane Bézieau,[2,4] Michel Koenig,[1,38] Erica E. Davis,[3,38,*] Laurent Pasquier,[5,38] and Sébastien Küry[2,4,38,*]

AT-rich sequences.[7] The amino-terminal domain of the RORα1 isoform determines its affinity and specific DNA-binding properties by acting in concert with the zinc finger domain.[7]

RORα deficiency is known to cause the mouse *staggerer* (*sg*) phenotype, a cerebellar degenerative model.[8] In humans, microdeletions overlapping *RORA* on 15q22.2 have been reported in affected individuals as part of a contiguous gene syndrome,[9] with the smallest deletion involving two genes, NMDA receptor-regulated 2 (*NARG2/ICE2*) and *RORA*. All reported individuals with 15q22.2 microdeletion share epileptic seizures, mild intellectual disability (ID), and dysmorphic features, with variable ataxia.[9] Here, we report 16 affected individuals from 13 syndromic ID-affected families with intergenic or intragenic deletions, truncating mutations, or missense changes in *RORA*. We modeled these genetic findings in zebrafish larvae through endogenous *roraa* ablation or heterologous expression of *RORA*, followed by relevant cerebellar phenotyping. In zebrafish models, we recapitulated the neuroanatomical features of affected humans as well as the *staggerer* mouse, and we show that loss of *roraa* leads to reduction of both the Purkinje and granule compartments of the cerebellum. Further, our *in vivo* data indicate that missense variants in the DNA binding domain confer a dominant toxic effect, while a missense change in the ligand binding domain results in a loss-of-function effect. Together, our data highlight how different mutation effects at the *RORA* locus can produce overlapping but distinct phenotypic outcomes.

Subjects and Methods

Genetic Studies and Ethics Statement

Human genetic studies conducted in research laboratories were approved by local ethics committees from participating centers (Antwerp, Belgium; Lyon, France; Frankfurt, Germany; Copenhagen, Denmark; Montpellier, France; Tartu, Estonia; Minneapolis and Kansas City, USA). Written informed consent was obtained from all study participants. All 16 affected individuals underwent extensive clinical examination by at least one expert clinical geneticist. Routine genetic testing was performed whenever clinically relevant, including copy-number variation (CNV) analysis by high-resolution array-based comparative genomic hybridization (aCGH) using (1) 180k CytoSure ISCA v2 array (Oxford Gene Technology; individuals 10A–D), (2) 180k SurePrint G3 CGH microarray as described[10] (Agilent; individual 11), or (3) 400k SurePrint G3 CGH microarray, as described[11] (Agilent, individuals 12 and 13). Affected individuals with a negative aCGH result underwent whole-exome sequencing (WES) on an Illumina HiSeq platform according to the following paradigms: (1) trio-based clinical diagnostic WES (individuals 1, 2, 6, 7, and 9), (2) trio-based WES in a research laboratory (individuals 3 and 4), or (3) WES of an affected individual followed by single site testing in parental DNA samples (individuals 5 and 8; see Table S1 for further details). Point mutations were confirmed by Sanger sequencing of DNA sample from all available family members, when possible.

Establishment and Culture of Primary Fibroblasts

We conducted biochemical studies in primary cultures of skin fibroblasts from individuals 2, 3, and 6 and from two control individuals (WT1 and WT2). Fibroblasts were grown in RPMI 1640 medium, containing 5% fetal calf serum (FCS, ThermoFisher, Waltham), 2 mM L-glutamine (ThermoFisher), 1% Ultroser G

University Frankfurt, Deutschordenstraße 50, Frankfurt am Main 60528, Germany; [16]Division of Medical Genetics, Department of Pediatrics, Duke University, Durham, NC 27710, USA; [17]Epilepsy, Sleep and Pediatric Neurophysiology Department, Hospices Civils, Lyon, 69677 Bron, France; [18]Center for Human Genetics, University Hospitals Leuven, Herestraat 49, 3000 Leuven, Belgium; [19]Carle Physician Group, Urbana, IL 61801, USA; [20]Dr. John T. Macdonald Foundation Department of Human Genetics, University of Miami, Miller School of Medicine, 1501 NW 10th Avenue, BRB, room 359 (M-860), Miami, FL 33136, USA; [21]Center for Pediatric Genomic Medicine, Children's Mercy Hospital, Kansas City, MO 64108, USA; [22]Department of Pathology and Laboratory Medicine, Children's Mercy Hospital, Kansas City, MO 64108, USA; [23]University of Missouri Kansas City, School of Medicine, Kansas City, MO 64108, USA; [24]Division of Clinical Genetics, Children's Mercy Hospital, Kansas City, MO 64108, USA; [25]Department of Pediatrics, Children's Mercy Hospital, Kansas City, MO 64108, USA; [26]Laboratoire de Génétique Moléculaire & Génomique, CHU de Rennes, 35033 Rennes, France; [27]Centre National de Recherche en Génomique Humaine (CNRGH), Institut de Biologie François Jacob, DRF, CEA, Evry, France; [28]The Broad Institute of MIT and Harvard, Cambridge, MA 02142, USA; [29]Department of Neurology, University Hospitals Leuven, Herestraat 49, 3000 Leuven, Belgium; [30]Department of Paediatrics, College of Medicine and Health Sciences, United Arab Emirates University, PO Box 17666, Al Ain, United Arab Emirates; [31]Department of Paediatrics, Tawam Hospital, PO Box 15258, Al-Ain, United Arab Emirates; [32]Neurometabolic Diseases Laboratory, IDIBELL, Gran Via, 199, L'Hospitalet de Llobregat, 08908 Barcelona, and CIBERER U759, Center for Biomedical Research on Rare Diseases, 08908 Barcelona, Spain, Catalan Institution of Research and Advanced Studies (ICREA), 08010 Barcelona, Spain; [33]Department of Psychiatry, UCSF Weill Institute for Neurosciences, University of California, San Francisco, San Francisco, CA 94158, USA; [34]Department of Neuropaediatrics and CR Maladies Neuromusculaires, CHU Montpellier, PhyMedExp, INSERM, CNRS, University of Montpellier, Montpellier, France; [35]Neuroradiologie, CHU de Montpellier, 34090 Montpellier, France; [36]CNRS UMR 6290, Université de Rennes, 2 Avenue du Professeur Léon Bernard, 35043 Rennes, France

[37]These authors contributed equally to this work

[38]These authors contributed equally to this work

*Correspondence: erica.davis@duke.edu (E.E.D.), sebastien.kury@chu-nantes.fr (S.K.)

https://doi.org/10.1016/j.ajhg.2018.02.021.

(Pall, Cortland), 1 × Antibiotic-Antimycotic (ThermoFisher) and were maintained in a humidified incubator at 37°C/5% CO_2. Both RT-PCR and western blotting studies were performed using individual fibroblasts plated in 6-well plates (200,000 cells/well).

RT-PCR Studies in Primary Fibroblasts

Total RNA was extracted using the RNeasy Plus Mini kit (QIAGEN) and reverse transcribed with the Moloney Murine Leukemia Virus Reverse Transcriptase (ThermoFisher). PCR amplification was performed with primers located in exons 3 and 4 (Table S2) and the Promega MasterMix (Promega). PCR products were separated on a 1.5% agarose gel and fragments were cut from the gel. After extraction from gel slices, the PCR products were purified with ExoSAP-IT (ThermoFisher) and sequenced by standard cycle-sequencing reactions with Big Dye terminators (ThermoFisher) with the PCR forward and reverse primers in an ABI PRISM 3130xl Genetic Analyzer (Applied Biosystems). Mutation detection analysis was performed using 4Peaks.

RORA Immunoblotting

Total protein lysate was extracted from primary fibroblasts using 1 × Laemmli buffer. Proteins were separated on 10% SDS-PAGE gels and transferred to PVDF membrane (Westran Clear Signal Whatman; Dominique Dutscher, Brumath). The membranes were incubated overnight with 1:200 diluted anti-RORα (sc-6062, Santa Cruz biotechnology) primary antibody in 5% skim milk. Protein levels of the housekeeping protein GAPDH were assayed for internal control of protein loading with 1:1,000 diluted GAPDH antibody (sc-25778, Santa Cruz Biotechnology).

Three-Dimensional (3D) Protein Modeling

Missense changes located in the DNA-binding domain of RORA isoform a were studied by 3D modeling. Wild-type (WT) and mutated RORA DNA binding domain homology models were generated according to the crystal structure of the RXR-RAR DNA-binding complex on the retinoic acid response element DR1 using Modeler[12] software with standard parameters.

RORA Expression Analysis in Neuronal Cell Types

There are four RefSeq transcripts of *RORA* (GenBank): NM_134261.2 (*RORA* 1), NM_134260.2 (*RORA* 2), NM_002943.3 (*RORA* 3), and NM_134262.2 (*RORA* 4). Relative mRNA levels of the four *RORA* transcripts were assessed in three different commercially obtained human cDNAs by quantitative (q)RT-PCR: (1) cerebellar cDNA from a 26-year-old male (Amsbio), (2) whole-brain cDNA pooled from two males of Northern European descent aged 43–55 years, Human multiple tissue cDNA (MTC) panel I (Clontech), and (3) Human Universal QUICK-Clone II (Clontech) using transcript-specific primers (Table S2) and SYBR Green PCR Master Mix (Thermo Fisher) on an ABI 7900HT real-time PCR system. We determined relative gene expression levels in quadruplicate samples according to the ΔCt method. After normalization to *β-actin* levels, $-\log^2$ of ΔCt for each of the four transcripts was added together to determine total expression levels from the *RORA* locus for each cDNA. Relative *RORA* transcript expression levels expressed in $-\log^2$ of ΔCt were obtained by calculating the percentage of each transcript compared to total *RORA* expression.

Zebrafish Lines and Husbandry

All zebrafish work was performed in accordance with protocols approved by the Duke University Institutional Animal Care and Use Committee. Zebrafish embryos were obtained by natural matings of WT (ZDR strain, Aquatica BioTech) or transgenic (*neurod:egfp*) adults[13] and maintained on a 14 hr/10 hr light-dark cycle. Embryos were reared in embryo media (0.3 g/L NaCl, 75 mg/L $CaSO_4$, 37.5 mg/L $NaHC0_3$, 0.003% methylene blue) at 28°C until processing for phenotypic analyses at 3 days post-fertilization (dpf).

CRISPR/Cas9 Genome Editing of *roraa* in Zebrafish

We designed two guide (g) RNAs targeting *roraa* (GRCz10: ENSDARG00000031768) using the CHOPCHOP v2 tool[14] and synthesized them *in vitro* with the GeneArt precision gRNA synthesis kit (Table S2; Thermo Fisher) as described.[15–17] We targeted the *roraa* locus by microinjection into the cell of zebrafish embryos with 1 nL of cocktail containing 100 pg gRNA and 200 pg Cas9 protein (PNA Bio) at the 1-cell stage. We harvested individual embryos (n = 8) at 1 dpf for DNA extraction to assess targeting efficiency. We PCR-amplified the region flanking the targeted site (Table S2), denatured the resulting product, and reannealed it slowly to form heteroduplexes (95°C for 5 min, ramped down to 85°C at 1°C/s and then to 25°C at 0.1°C/s). We performed polyacrylamide gel electrophoresis (PAGE) on a 20% precast 1 mm gel (Thermo Fisher) to visualize heteroduplexes. To estimate mosaicism of F0 mutants, PCR products were cloned into a TOPO-TA vector (Thermo Fisher) and individual colonies (n = 24) were sequenced (n = 3 larvae/gRNA).

Transient *roraa* Suppression, *In Vivo* Complementation, and Heterologous Expression Experiments

We designed splice blocking (sb) morpholinos (MO) targeting either the splice donor site of exon 2 (e2i2) or exon 3 (e3i3) of *roraa* (GeneTools, LLC; Table S2) and injected 1 nL of MO into the yolk of zebrafish embryos at 1- to 4-cell stage. To confirm expression of the two annotated *roraa* transcripts (GRCz10: ENSDART00000148537.2 and ENSDART00000121449.2) and to determine MO efficiency, we harvested uninjected control and MO-injected larvae in Trizol (Thermo Fisher) at 3 dpf, extracted total RNA, and conducted first-strand cDNA synthesis with the QuantiTect Reverse Transcription kit (QIAGEN). The targeted region of *roraa* was PCR amplified using primers complementary to sites in flanking exons (Table S2) and migrated by electrophoresis on a 1% agarose gel; bands were excised, gel purified using QIAquick gel extraction kit (QIAGEN) and resulting clones were Sanger sequenced. The optimal MO dose for *in vivo* complementation experiments was determined by injection of three concentrations of MO (2, 3, 4 ng of e2i2; or 6, 7, 8 ng of e3i3). To generate mRNA for injections, we purchased Gateway-compatible open reading frame (ORF) clones from Genecopoeia (*RORA* 1, *RORA* 2, and *RORA* 3) or Thermo Fisher (*RORA* 4) and transferred the ORFs to a pCS2+ vector by LR clonase II-mediated recombination (Thermo Fisher). We performed site-directed mutagenesis of *RORA* 4 according to the QuikChange protocol (Table S2; Agilent), using described methodology;[18] sequences were validated by Sanger sequencing. Linearized pCS2+ vectors containing WT or mutant ORFs were transcribed *in vitro* with the mMessage mMachine SP6 Transcription kit (Ambion).

Whole-Mount Immunostaining

We stained axonal tracts of the cerebellum with monoclonal anti-acetylated tubulin antibody produced in mouse (Sigma-Aldrich, T7451, 1:1,000), as described.[19] We fixed larvae in Dent's solution (80% methanol and 20% DMSO) and carried out primary antibody detection overnight and secondary detection for 1 hr with

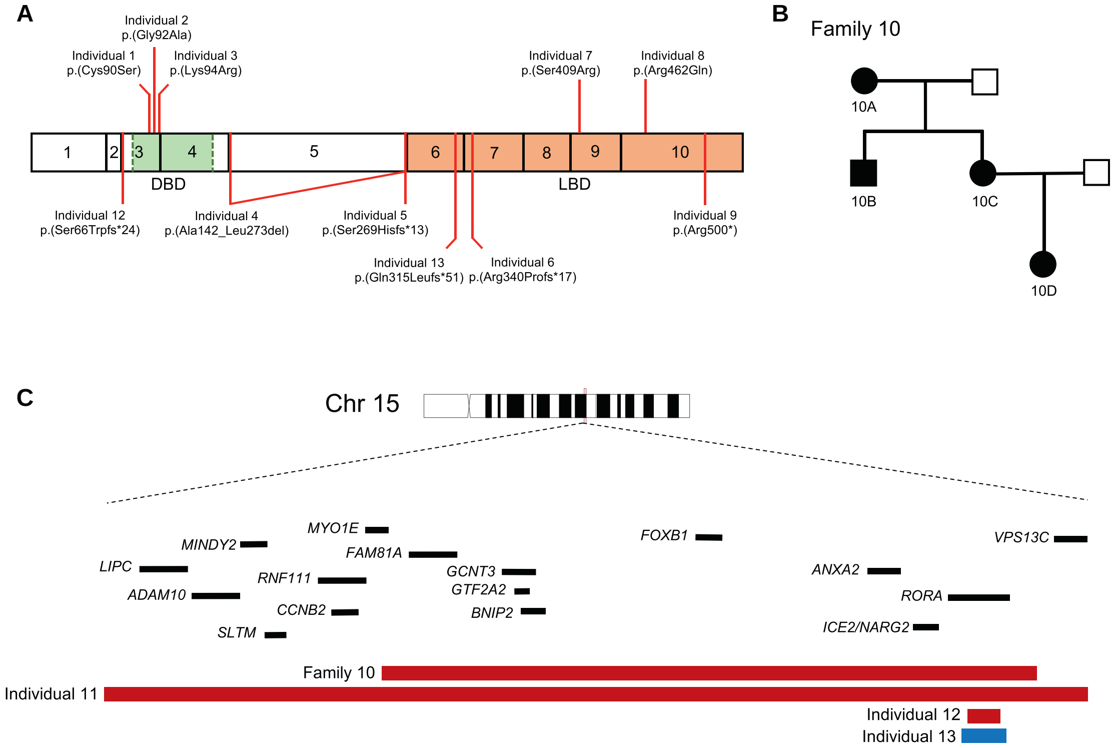

Figure 1. *RORA* Variants Cause Intellectual Disability with Autistic Features or Cerebellar Hypoplasia

(A) Schematic of RORα isoform a (GenBank: NP_599023.1; encoded by *RORA* transcript 1) depicting exons (black outlined boxes with numbers 1–10) and domains; green, DNA binding domain (DBD); orange, ligand binding domain (LBD). Missense variants (top) and truncating variants (bottom) are shown.

(B) Autosomal-dominant pedigree (family 10) in which a ~1.5 Mb intergenic deletion containing *RORA* segregates with disease. Filled shapes, affected individuals; unfilled shapes, healthy individuals. Individuals 10A, 10B, 10C, 10D, and the spouse of 10C were tested.

(C) Schematic depicting the *RORA* locus at 15q22. Zoomed region shows two intergenic deletions (individuals 10A–D and individual 11), one intragenic deletion (individual 12), and an intragenic duplication (individual 13) involving *RORA*. Genes are indicated by black bars; copy number loss, red; copy number gain, blue.

Alexa Fluor 488 goat anti-mouse IgG (A11001, Invitrogen; 1:1,000). We visualized the Purkinje compartment of the zebrafish cerebellum with anti-zebrin II antibody (a gift from Dr. Richard Hawkes) in *neurod:egfp* transgenic larvae. Briefly, zebrafish larvae were fixed in 4% paraformaldehyde and incubated overnight in mouse anti-zebrin II antibody (1:100); secondary antibody was applied for 1 hr (Alexa Fluor 594 goat anti-mouse IgG, A11005, Invitrogen; 1:1,000). Fluorescent signal was imaged manually on dorsally positioned larvae using an AxioZoom.V16 microscope and Axiocam 503 monochromatic camera, using Zen Pro 2012 software (Zeiss). Cerebellar structures of interest or optic tecta were measured using ImageJ.[20] Total cerebellar area was measured on acetylated tubulin-stained larvae by outlining structures with fluorescent signal; regions comprised of Purkinje cells were measured on zebrin II-stained regions; region comprised of granule cells were measured on GFP-positive regions. Statistical analyses were performed using a two-tailed parametric t test (GraphPad software).

Results

Identification of Point Mutations or Copy-Number Variants Disrupting RORA

As part of our ongoing studies to understand the molecular basis of neurodevelopmental disorders, we identified a total of 16 individuals with rare variants suspected to alter *RORA* function (Figure 1; Tables 1, S3, and S4). The first individual under investigation was a female with severe syndromic ID, multifocal seizures, mild cerebellar hypoplasia, and hypotonia (individual 6, Table 1; Figure 2A). Upon performing WES, we identified a *de novo* frameshifting mutation in *RORA* (GenBank: NM_134261.2; c.1019delG [p.Arg340Profs*17]) that was not present in the genome aggregation database (gnomAD; >246,000 chromosomes) or the NHLBI Exome Variant Server (EVS; >13,000 alleles). Information exchange on community data-sharing platforms including GeneMatcher,[21] the DatabasE of genomiC varIation and Phenotype in Humans using Ensembl Resources (DECIPHER), and the Broad Institute matchbox repository facilitated the identification of an additional 15 affected individuals with *RORA* variants who displayed overlapping phenotypes. These variants were present *de novo* in 11 simplex families with affected individuals and segregated in one three-generation pedigree under a dominant paradigm, bolstering the candidacy of this locus. Of note, segregation analysis was impossible in individual 1's family, since the child had been adopted.

Of the 16 affected individuals, 4 harbored likely pathogenic SNVs predicted to alter RORA protein sequence or

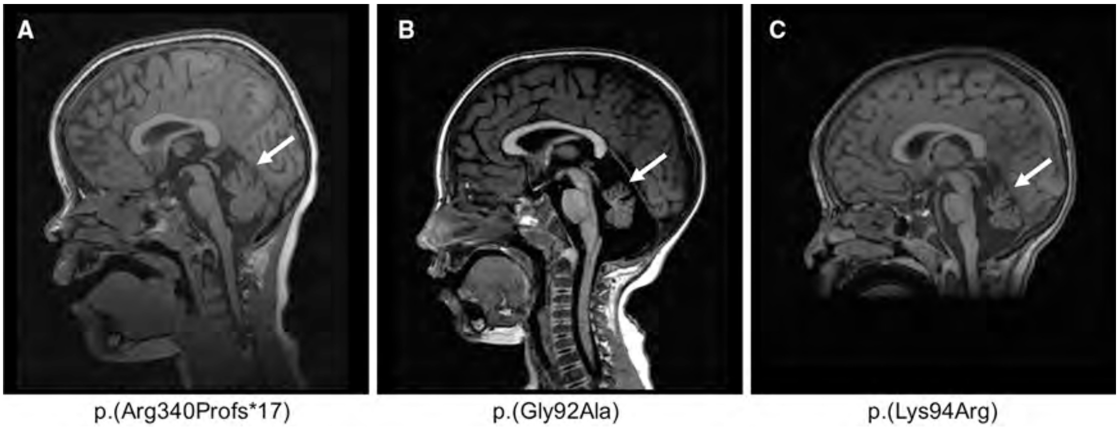

Figure 2. Brain MRI of Individuals with Cerebellar Hypoplasia
MRI of individual 6 done at 6.5 years old (A), individual 2 done at 2 years and 1 month old (B), and individual 3 done at 2 years old (C) showing cerebellar hypoplasia, predominant on the vermis (white arrow). T1-weighted sequence, sagittal section through cerebellum.

dose. In addition to individual 6, three affected individuals had *de novo* SNVs or small indels in *RORA*; these included one frameshifting mutation, one nonsense mutation, and one mosaic canonical splice acceptor site change (Figure 1A; Tables 1 and S3). These three *RORA* variants are predicted to result in protein sequence with either complete (c.804_805delGT [p.Ser269Hisfs*13]) or partial (c.1019delG [p.Arg340Profs*17] and c.1498C>T [p.Arg500*]) truncation of the ligand binding domain at the C terminus and/or nonsense-mediated mRNA decay (NMD). Notably, analyses of fibroblast protein lysates from individual 6 (p.Arg340Profs*17) showed that RORA protein levels were not decreased compared to control subjects, suggesting that related mRNA harboring the premature stop codon would not be eliminated by NMD. According to Alamut software (compiling five different prediction tools: Splicesite Finder-like, MaxEntScan, NNSPLICE, GeneSplicer, and Human Splicing Finder), the splice acceptor site mutation, c.425−1G>A, is predicted to cause in-frame exon skipping and deletion of 77 amino acids (p.Ala142_Leu273del); however, cell lines were unavailable from the affected individual to confirm this prediction; mosaicism was estimated at about 20% from exome and Sanger sequencing data.

An additional seven affected individuals had non-recurrent CNVs impacting the *RORA* locus detected by high-resolution aCGH (Tables 1 and S4; Figures 1A–1C and S1). We identified one ~63 kb duplication interrupting *RORA* exons 3–6, which is predicted to result in a premature termination of the protein (p.Gln315Leufs*51), one intragenic CNV that resulted in a ~27 kb deletion of *RORA* exon 3 and its flanking intronic regions to produce a putative frameshifting truncation, and one ~3.7 Mb intergenic deletion impacting 17 genes on 15q22.3q22.2 including *RORA*. Segregation in each of the three families showed that all three CNVs occurred *de novo*. Furthermore, we detected a ~1.5 Mb intergenic deletion in four individuals segregating neurological phenotypes in an autosomal-dominant pedigree (Figure 1B); this CNV encompasses nine genes, including *RORA*.

Finally, an additional five affected individuals had missense mutations predicted to be deleterious (Tables 1 and S3; Figure S2). All five alleles were absent from all available public databases queried (gnomAD, ExAC, EVS). Two of the five variants, c.1225A>C (p.Ser409Arg) and c.1385G>A (p.Arg462Gln), map to the ligand binding domain; both residues are conserved in vertebrate orthologs of RORα but not in the human paralogous nuclear receptor proteins, indicating that these positions are specific to the ROR sub-family. The other three variants—c.269C>G (p.Cys90Ser), c.275G>C (p.Gly92Ala), and c.281A>G (p.Lys94Arg)—are located in the conserved zinc-finger DNA-binding domain of RORα. The three residues Cys90, Gly92, and Lys94, together with Cys93, belong to the P box motif that is part of the alpha-helix of the first zinc-finger domain of the nuclear receptors and interacts directly with DNA (Figure S3A).[22] Because the c.281A>G variant lies in the donor splice site of exon 3, we examined whether it impacts mRNA splicing in primary skin fibroblasts from individual 3; RT-PCR showed neither abnormal sized product nor semiquantitative differences in cDNA amounts (Figures S4A and S4B). Additionally, western blotting of lysates from primary fibroblasts harboring the c.275G>C change (individual 2) showed a modest increase of RORα levels when compared to a matched control (Figure S4C).

Clinical Features of Individuals with RORA Variants

The 16 affected individuals in our cohort display complex phenotypes with regards to their cognition, motor function, and electrophysiology (Table 1). The predominant phenotype was ID. However, cognitive function was variable among the 16 individuals and ranged from mild to moderate (13/16) to severe (2/16), while one individual had a low intelligence quotient (IQ) without ID. We noted IQ regression in one affected individual (individual 4) who had cognitive decline at ~10 years

Table 1. Molecular and Clinical Data from the 15 Individuals with *RORA* Variants

Individual ID	**1**	**2**	**3**	**4**	**5**	**6**	**7**
DECIPHER ID	–	–	–	–	–	–	–
Sex	female	male	female	female	female	female	male
Geographic origin	USA	Estonia	France	USA	USA	France	USA
Age at last investigation (years)	4	3.5	6	28	3	10	9
Mutation type	missense	missense	missense	splice site	frameshift	frameshift	missense
Mutation (GRCh37)[a]	c.269G>C	c.275G>C	c.281A>G	c.425-1G>A	c.804_805delGT	c.1019delG	c.1225A>C
Protein variant[b]	p.Cys90Ser	p.Gly92Ala	p.Lys94Arg	p.Ala142_ Leu273del	p.Ser269Hisfs*13	p.Arg340Profs*17	p.Ser409Arg
Mode of inheritance	unknown (adopted)	*de novo*	*de novo*	*de novo* (mosaic, 20% in blood) [c]	*de novo*	*de novo*	*de novo*
Functional effect[d]	NA	dominant toxic	dominant toxic	NA	NA	NA	NA
Growth Parameters							
Birth weight (grams/SD)	NA	3,500/0	3,310/0	4,238/+2	4,054/+1.4	2,655/−1.5	3,487/0
Birth length (cm/SD)	NA	52/+1	49/0	NA	54.6/+1.9	46/−2	52/+1
Birth head circumference (cm/SD)	NA	38/+2.5	34.5/0	NA	NA	33/−1	34/−0.5
Height at age last investigation (cm/SD)	102/0	102/+0.5	104/−2	167.8/+0.5	89/−1.5	132/−1	120.8/−2 (8 y 5 mo)
Weight at age last investigation (kg/SD)	17.2/+0.5	17.8/+1	16/−1.5	69.4/+1	14.5/+0.3	26.2/−1.3	31/+1.3 (9 y 3 mo)
Head circumference at age last investigation (cm/SD)	49/0	50.6/0	50/0	58.4/+1.9	NA	53/0	51.7/−0.3 (8 y 4 mo)
Degree of developmental delay or ID	mild	mild-moderate	severe	mild (regression at 10 years)	mild	severe	mild
Age of walking	2 years	3 years	6 years	14 months	20 months	3 years	15 months
Age of first words	2 years	delayed	before 1 year	14–15 months	12–13 months	5 years	>2 years
Current language ability	speaking with sentences	speaking with sentences	no phrase	normal	around 20 words	no phrase	delayed
Behavioral anomalies	no	no	no	no	ASD	ASD	ASD

(*Continued on next page*)

8	**9**	**10D**	**10C**	**10B**	**10A**	**11**	**12**	**13**
–	**–**	**–**	**–**	**–**	**289628**	**–**	**255754**	**293939**
male	male	female	female	male	female	male	male	male
Germany	USA	Belgium	Belgium	Belgium	Belgium	France	Denmark	Denmark
4	14	25	50	44	80	15	8	6,5
missense	nonsense	15q22 deletion including *RORA*	15q22 deletion including *RORA*	15q22 deletion including *RORA*	15q22 deletion including *RORA*	15q22.3q22.2 deletion including *RORA*	15q22 intragenic deletion of *RORA*	15q22 disruptive duplication of *RORA*
c.1385G>A	c.1498C>T	15q22.2 (59,641,986-61,104,231) x1	15q22.2 (59,641,986-61,104,231) x1	15q22.2 (59,641,986-61,104,231) x1	15q22.2 (59,641,986-61,104,231) x1	15q21.3q22.2 (58,622,268 −62,320,616) x1	15q22.2 (60,809,984-60,837,029) x1	15q22.2 (60,797,691-60,860,668) x3
p.Arg462Gln	p.Arg500*	–	–	–	–	–	p.Ser66Trpfs*24	p.Gln315Leufs*51
de novo	*de novo*	dominant; inherited from mother (ID 10C)	dominant; inherited from mother (ID 10A)	dominant; inherited from mother (ID 10A)	dominant	*de novo*	*de novo*	*de novo*
loss-of-function	NA	NA	NA	NA	NA	NA	NA	NA
NA	3,340/−0.4	NC/+0.7	NA	NA	NA	3,200/−0.5	4050/+1	NC; unremarkable
NA	48.3/−0.7	NC/+0.7	NA	NA	NA	49.5/0	56/+2.5	NC; unremarkable
NA	46.5/+2 (6 mo)	NC/+0.7	NA	NA	NA	34/−0.5	NA	NC; unremarkable
NA	150.4/−0.7 (13 y)	166/+0.7	NA	NA	NA	170/0	NC/+2.5	NC/−1
NA	44.4/−0.2 (13 y)	74.3/+1.3	NA	NA	NA	58/+0.7	NC/+1	NC/−1
NA	58/+2.6 (13 y)	54/−0.7	NA	NA	NA	56/+0.7	NA	NA
no ID (IQ 85)	moderate	mild	mild	mild	mild	moderate	mild	mild
NA	24 months	16 months	NA	NA	NA	21 months	normal	mild delay
NA	delayed	14 months	NA	NA	NA	2 years	delayed	delayed
normal	rudimentary sentences	delayed	NA	NA	NA	normal	delayed	delayed
ASD	no	behavioral problems	no	borderline personality disorder	no	hyperactivity	no	ASD

(*Continued on next page*)

Table 1. *Continued*

Individual ID	1	2	3	4	5	6	7
DECIPHER ID	–	–	–	–	–	–	–
Neurological Examination							
Seizures (age at onset/type)	no	no	yes (4 years/ absences)	yes (8 years/ tonic-clonic seizures)	yes (ND/ 1 episode of absence)	yes (5 years/ multifocal)	yes (neonatal/ myoclonic seizures)
Neurological examination	tremor, hypotonia, coordination disorder	tremor, hypotonia, ataxia	tremor, hypotonia, ataxia, pyramidal syndrome	tremor, hypotonia, ataxia	hypotonia, poor coordination	tremor, hypotonia, ataxia	occasional fine tremor
Brain imaging	normal	cerebellar hypoplasia (mainly vermis)	pontocerebellar atrophy (mainly vermis)	NA	normal	mild global cerebellar hypoplasia	corpus callosal hypoplasia
Global Examination							
Eye anomalies	strabismus, esotropia, nystagmus, amblyopia	no	mild oculomotor apraxia, strabismus	visual processing deficits	no	no	esotropia, hyperopia
Other	–	spina bifida occulta	recurrent vomiting, constipation	hypoglycemia in childhood	bilateral hydronephrosis	hypercholesterolemia	popliteal contractures
Other genetic findings	VUS in *NR4A2*	–	maternally inherited heterozygous p.(Arg662*) in *DNM1L*	–	maternally inherited deletions of 3p26.3 and 10q21.3 (both classified as VUS), mother reports no history of developmental delays	–	*HSPG2* c.7006+1G>A (maternally inherited), *HSPG2* c.4391G>A (paternally inherited), *GSK3B* c.625dupC (*de novo*), *CACNA1A* c.5883G>A (maternally inherited)
Initial diagnostic hypotheses	none	ID and disorders with cerebellar involvement	congenital ataxia with pontocerebellar atrophy	disorder of mitochondrial metabolism	none	none	speech delay, toe walking

Abbreviations: LoF, loss of function; GoF, gain of function; ND, not determined; ASD, autism spectrum disorder; ID, intellectual disability; IQ, intelligence quotient; GGE, genetic generalized epilepsy; NA, not analyzed; NC, not communicated; ND, not determined; y, years.

[a] Nomenclature HGVS V2.0 according to mRNA reference sequence GenBank: NM_134261.2. Nucleotide numbering uses +1 as the A of the ATG translation initiation codon in the reference sequence, with the initiation codon as codon 1.

[b] Inferred from bioinformatic predictions but not verified from the individual's mRNA.

[c] Mosaicism was inferred and estimated initially from raw exome sequencing data and confirmed by Sanger sequencing.

[d] Effect inferred from *in vivo* tests in zebrafish or analyses from patient fibroblasts; *in vitro* experiments.

of age. Developmental milestones were also delayed. The mean age of walking was delayed in 8/12 individuals; 11/12 walked by 3 years of age. Further, 11/13 individuals had speech delay and/or poor verbal communication abilities, and 2 were not speaking in sentences by the age of 6. We diagnosed epilepsy in 11/16 individuals (Table 1); the predominant seizure semiology was that of a generalized epilepsy with absences, drop attacks, and tonic-clonic seizure sub-types. None of the patients with *RORA* intragenic mutation had overt dysmorphic facial features. Of the nine individuals who underwent brain MRI, six had normal results and three were diagnosed with cerebellar hypoplasia, which predominantly affected the vermis (individuals 2 and 3; Figures 2B and 2C). These individuals developed early-onset ataxia and hypotonia by age 1.

Modeling RORA Disruption in Zebrafish

To corroborate the *Rora*^{sg} mouse mutant phenotype data[8,23] and to determine the effect of missense variants identified in affected individuals, we developed zebrafish models of *RORA* ablation and expression. We and others have shown previously that zebrafish is a robust model of neuroanatomical phenotypes observed in humans.[19,24–26] In particular,

8	9	10D	10C	10B	10A	11	12	13
–	**–**	**–**	**–**	**–**	**289628**	**–**	**255754**	**293939**
no	yes (ND/ generalized seizures)	yes (4 years/ absences, drop attacks)	yes	yes (ND/ generalized, *status epilepticus*)	no	yes (ND/ generalized, febrile seizures)	no	yes
NA	mild hand tremor, hypotonia	NA	NA	tremor	no	palpebral myoclonia	no	no
NA	CSF spaces mildly prominent	normal	NA	normal	NA	NA	NA	NA
NA	strabismus, hyperopia	strabismus	strabismus	NA	NA	strabismus	no	no
–	cryptorchidism, renal cysts	–	–	–	–	–	atopic dermatitis	–
–	*NGLY1* c.1516C>T, p.Arg506* (maternally inherited), *PKD2* c.2143delC, (p.Leu715*) (paternally inherited), 3p26.2 deletion (maternally inherited; VUS)	intragenic *DISC1* deletion (1q42.2(231, 834,554–231, 885,282)x1	intragenic *DISC1* deletion (1q42.2(231, 834,554–231, 885,282)x1	intragenic *DISC1* deletion (1q42.2(231, 834,554–231, 885,282)x1	intragenic *DISC1* deletion (1q42.2(231, 834,554–231, 885,282)x1	–	–	–
idiopathic ASD F84.0	*CUL4B*-related disorder	GGE and ID	ID and possible epilepsy	ID?	epilepsy (GGE?) and ID	deletion of *RORB*	none	none

assay of cerebellar defects in zebrafish has provided crucial insights toward understanding underlying pathomechanism,[27–29] especially given the high conservation of granule and Purkinje cell types between mammals and teleost species.[30] First, we aimed to model *RORA* disruption *in vivo* by targeting and knocking down the relevant zebrafish ortholog. Through reciprocal BLAST of the zebrafish genome and four annotated human *RORA* transcripts (GenBank: NM_134261, NM_134260, NM_002943, and NM_134262; Figure S5A), we identified two zebrafish orthologs: *roraa* (Ensembl ID: ENSDARG00000031768; GRCz10; 88%, 91%, 91%, and 91% identity to proteins encoded by *RORA* 1, *RORA* 2, *RORA* 3, *RORA* 4, respectively) and *rorab* (Ensembl ID: ENSDARG00000001910; 69%, 72%, 72%, and 73% identity to *RORA* 1, *RORA* 2, *RORA* 3, *RORA* 4, respectively). Next, we considered endogenous expression data to determine the most appropriate *D. rerio* transcript(s) to modulate *in vivo*. RNA *in situ* hybridization studies in zebrafish larvae have documented *roraa* expression patterns in the developing cerebellum as well as other anterior structures (optic tecta, hindbrain, and retina). However, *rorab* expression is restricted to the hindbrain.[31,32] Considering both the amino acid conservation and also the spatiotemporal expression of *roraa* in the

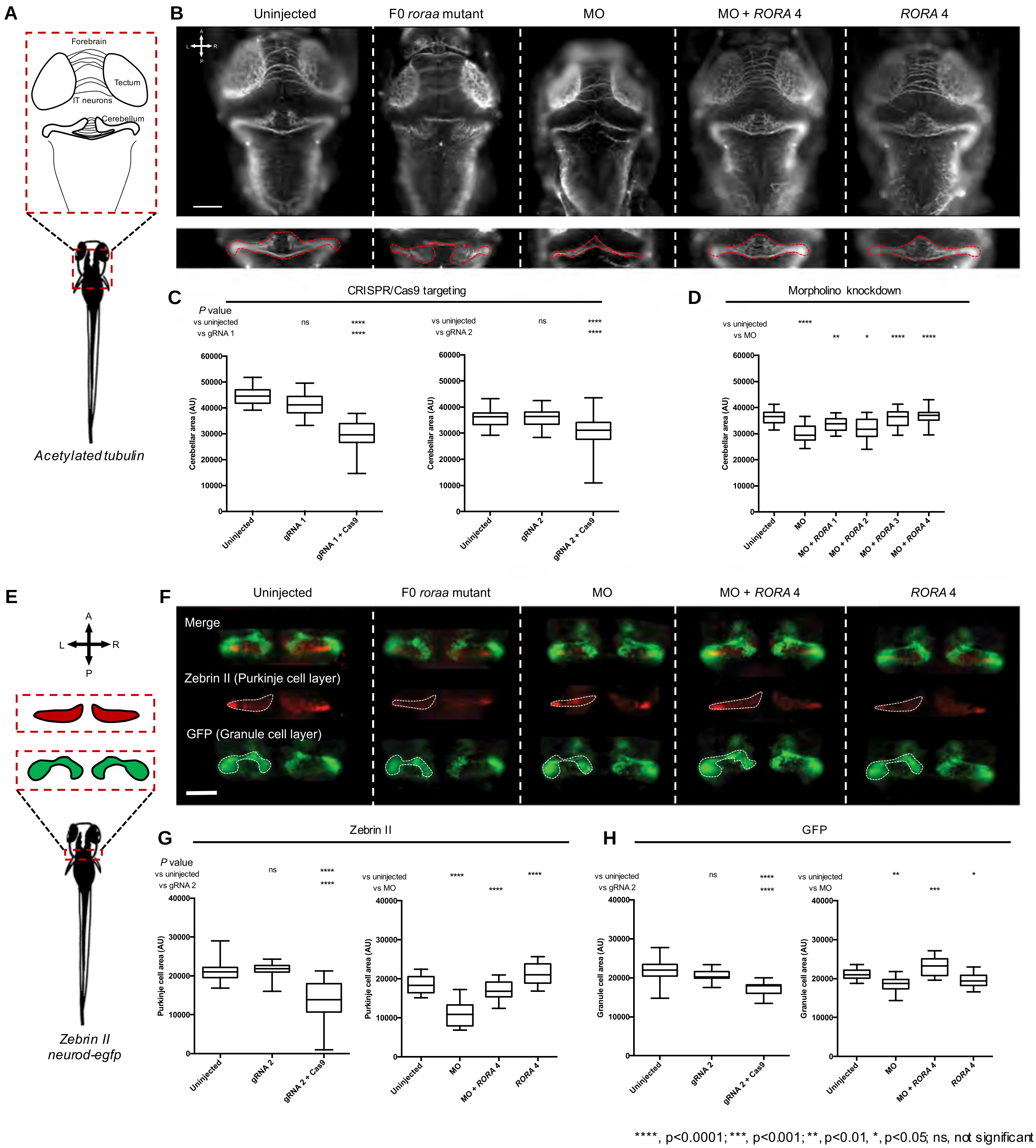

Figure 3. Disruption of *roraa* in Zebrafish Larvae Results in Cerebellar Hypoplasia Driven by Purkinje and Granule Cell Loss

(A) Schematic of neuroanatomical structures painted with anti-acetylated tubulin antibody at 3 days post fertilization (dpf); IT, intertectal.

(B) Representative dorsal images of acetylated tubulin immunostained larvae show that *roraa* ablation causes cerebellar defects in CRISPR/Cas9 F0 mutants and morphants. Cerebellar size was measured as indicated by the dashed red outline on inset panels.

(C) Quantification of cerebellar area in larval batches is shown for two guide (g)RNAs targeting either *roraa* exon 5 (gRNA 1) or exon 8 (gRNA 2).

(D) *roraa* morphants (injected with 3 ng morpholino; MO) display a cerebellar phenotype that can be rescued by four different wild-type *RORA* mRNA transcripts: co-injection of *roraa* e2i2 splice-blocking MO with *RORA* splice variants (*RORA* 1, GenBank: NM_134261, *RORA* 2: NM_134260, *RORA* 3: NM_002943 and *RORA* 4: NM_134262).

(E) Schematic of cerebellar cell types assessed in 3 dpf larvae using either a *neurod:egfp* transgene (green) or anti-zebrin II immunostaining (red). Orientation is indicated with A, anterior; P, posterior; L, left; R, right.

(legend continued on next page)

developing cerebellum, we deemed *roraa* as the most relevant *D. rerio* locus to test the activity of *RORA* mutations in humans.

Haploinsufficiency or knockout of *Rora* in mice lead to abnormal cerebellar layer morphology.[8,23] Therefore, to assess the effect of loss of RORA function consistent with deletion or truncating mutations identified in affected individuals, we compared the size of the developing cerebellum between *roraa* knock-down and uninjected controls. The zebrafish *roraa* locus has two annotated transcripts (GRCz10: [*roraa*-201] ENSDART00000121449.2 and [*roraa*-202] ENSDART00000148537.2), the latter of which has an incomplete 5′ coding sequence; RT-PCR using cDNA originating from 3 dpf embryos confirmed that both transcripts are detectable in this time window (Figures S6A and S6B). Next, we generated CRISPR/Cas9-based zebrafish F0 mutant models by targeting exon 5 or exon 8 of *roraa*-201 (corresponding to exon 4 or exon 7 of *roraa*-202) to produce mosaic mutants with >90% mosaicism (Figure S7). Immunostaining of the central nervous system (CNS) with anti-acetylated tubulin antibody and measurements of neuroanatomical structures showed that *roraa* F0 mutants display a reduced cerebellar area and smaller optic tecta area compared to either control larvae or larvae injected with gRNA alone ($p < 0.0001$, for gRNA 1 and gRNA 2, $n = 33–43$ and 41–45 larvae/batch, respectively, repeated, masked scoring; Figures 3A–3C and S8A–S8C).

To assess phenotype specificity and to determine the effect of *RORA* missense variants, we performed MO-mediated transient suppression of *roraa*. We designed two sb MOs targeting the splice donor site of exons 2 and 3 of *roraa*-201, which we injected into embryo batches, generated cDNA at 3 dpf, and performed RT-PCR to determine efficiency; subsequent Sanger sequencing confirmed a frameshifting deletion of *roraa* exon 2 or exon 3 (Figures S6C and S6D). Next, we injected increasing concentrations of either MO (2, 3, 4 ng e2i2; or 6, 7, 8 ng e3i3). Consistent with our CRISPR F0 mutant data, we observed a dose-dependent reduction in cerebellar size for both reagents ($p < 0.0001$, 30 to 94 larvae/condition, Figure S6E). Co-injection of e2i2 sb MO with each of the four RefSeq annotated WT human *RORA* mRNAs rescued cerebellar and optic tecta defects, indicating MO specificity ($p = 0.0060$, 0.0387, < 0.0001, < 0.0001 for *RORA* 1, 2, 3, and 4, respectively, versus MO, $n = 31–60$ larvae/batch, repeated, Figures 3B, 3D, S8A, and S8D). In parallel, heterologous expression of each of the four WT *RORA* mRNAs did not lead to cerebellar phenotypes that differed from uninjected controls ($n = 40–52$ larvae/batch, Figure S9). To investigate further the relative expression of the four annotated *RORA* transcripts and to identify the most relevant isoform for *in vivo* modeling in zebrafish, we performed qRT-PCR on commercial human adult cDNA; we identified *RORA* 4 as the most abundantly expressed transcript in the human CNS (Figures S5A and S5B), potentially explaining the observation that WT *RORA* 4 mRNA produced the most significant restoration of cerebellar size when co-injected with MO.

Altered Purkinje and Granule Layers in *roraa* Zebrafish Models

Similar to mammals, Purkinje and granule cell crosstalk is vital for the function of the zebrafish cerebellum.[30] Cerebellar cell subpopulations have been characterized previously in zebrafish with lineage-specific markers and transgenic lines. In *neurod:egfp* transgenic zebrafish, granule cells are marked with GFP.[29] Furthermore, zebrin II is a specific marker of the Purkinje compartment,[27] which develops between 2.3 and 4 dpf.[33] To assess whether *roraa* suppression affects granule or Purkinje cell layers of zebrafish cerebellum, we conducted whole-mount zebrin II immunostaining on *neurod:egfp* transgenic zebrafish larvae at 3 dpf. F0 *roraa* mutants presented with a significantly decreased size of Purkinje and granule cell layers compared to controls ($p < 0.0001$ for both cell types; Purkinje cells, $n = 26–55$; granule cells, $n = 11–55$, repeated; Figures 3E–3H and S10A–S10C). Importantly, gRNA injected alone was indistinguishable from controls (Figures 3G and 3H). Injection of e2i2 MO recapitulated these observations ($p < 0.0001$ or $p < 0.001$ for Purkinje [$n = 29–55$] and granule [$n = 30–55$] cells, respectively, in morphants versus controls; repeated; Figures 3E–3H and S10). Further, co-injection of e2i2 MO with WT human *RORA* 4 mRNA rescued the measured area of each of the granule and Purkinje compartments ($p < 0.0001$ or $p < 0.001$ versus MO alone for Purkinje or granule cells, respectively; Figures 3E–3H and S10). Together, our data confirm that in F0 mutant or transient knockdown zebrafish models, *roraa* disruption leads to defects of Purkinje and granule cell layers, consistent with the *Rora*^{sg} mouse model.[34–36]

In Vivo Complementation Studies Indicate Dual Direction of RORA Allele Effect

To determine the pathogenicity of *RORA* missense variants (c.275G>C [p.Gly92Ala], c.281A>G [p.Lys94Arg], and c.1385G>A [p.Arg462Gln]), we assessed the effect of mutant *RORA* 4 mRNA in the presence or absence of MO.

(F) Representative dorsal images show that reduction of Purkinje and granule cells contributes to cerebellar defects induced by *roraa* targeting. Transgenic *neurod:egfp* larvae were fixed and immunostained with anti-zebrin II antibody (red), and the area comprised of each cell type was measured (as indicated in the schematic). Dashed white lines indicate measured area.
(G) Quantification of granule layer cells (GFP-positive).
(H) Quantification of Purkinje cells (zebrin II-positive). Both cell populations are reduced significantly in *roraa* F0 mutants as well as morphant zebrafish.
Scale bar in (B) and (F): 100 μm. AU, arbitrary units. Stars indicate p value compared to uninjected controls (CRISPR/Cas9 and MO) or to morphants (MO + RORA). ****$p < 0.0001$, ***$p < 0.001$, **$p < 0.01$, *$p < 0.05$; ns, not significant. Error bars in (C), (D), (G), and (H) represent the 5th and 95th percentiles.

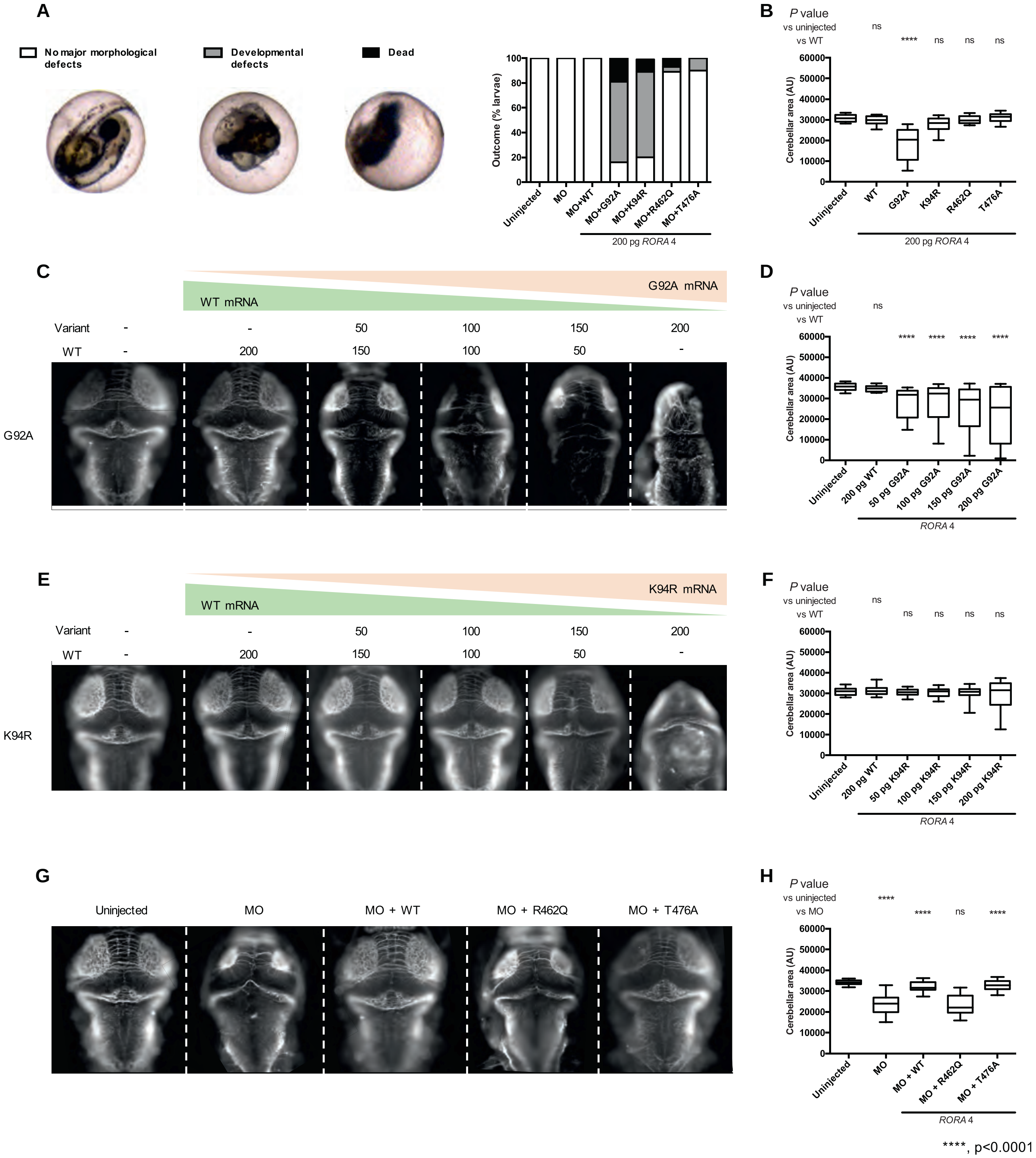

Figure 4. *RORA* Missense Variant Located in the DNA Binding Domain and Ligand Binding Domain Confer a Dominant Toxic and Loss-of-Function Effect, Respectively

(A) Complementation of *roraa* morpholino (MO) with variant mRNA results in severe gross morphological defects or larval death before 3 days post-fertilization (dpf). Left, representative embryo classes are shown; right, quantification of outcomes. p.Gly92Ala (G92A), p.Lys94Arg (K94R) are located in the DNA binding domain; p.Arg462Gln (R462Q) localizes to the ligand-binding domain; T476A (rs190933482) is a negative control for the assay with an allele frequency of 0.001091 in gnomAD).

(B) Quantification of cerebellar area of larval batches with ectopic expression of *RORA* mRNA. G92A mRNA confers a significant reduction in cerebellar size.

(C) Representative dorsal images of 3 dpf larvae injected with gradually modified doses of WT and G92A RNA (top, amount in pg) and stained with anti-acetylated tubulin antibody.

(D) Quantification of cerebellar measurements from the batches shown in (C).

(legend continued on next page)

First, we tested a loss-of-function hypothesis by co-injecting *roraa* e2i2 MO with WT or variant *RORA* 4 mRNA. *In vivo* complementation of *roraa* MO with p.Gly92Ala or p.Lys94Arg encoding mRNA resulted in early developmental defects including a reduction in the size of anterior structures and tail extension failure (65% and 69%, respectively) and a high mortality rate (19% and 10%, respectively), while co-injection of MO with p.Arg462Gln, WT, or a potentially benign variant p.Thr476Ala (rs190933482, minor allele frequency 0.001 in gnomAD) induced no appreciable morphological defects (Figure 4A). The gross morphological phenotype observed by co-injection of MO with mutant mRNAs located in the DNA binding domain was more severe than the morphant phenotype and suggested either a dominant-negative or a gain-of-function effect. To investigate these possibilities, we injected 200 pg of each mutant mRNA alone and again observed notable mortality at 3 dpf (2% for controls [1 dead larva/54] versus 31% for p.Gly92Ala [14/45]; 9% for p.Lys94Arg [4/46]; and 7% for p.Arg462Gln [3/41]). Of the larvae that survived to 3 dpf, we performed anti-acetylated immunostaining and measurement of the cerebellar area; p.Gly92Ala encoding mRNA induced a reduction in the mean cerebellar area compared to WT ($p < 0.0001$, 31–53 larvae/batch, Figure 4B). To determine whether WT mRNA could rescue the phenotypes induced by p.Gly92Ala, we titrated increasing amounts of p.Gly92Ala mRNA together with *RORA* 4 WT mRNA and observed a dose-dependent effect that correlated with the injected dose of p.Gly92Ala (Figures 4C and 4D). These data suggested a dominant toxic effect as the likely mechanism for the p.Gly92Ala variant. Although expression of p.Lys94Arg induced morphological defects similar to p.Gly92Ala and we observed a broadened distribution of cerebellar measurements at the highest dose of mutant mRNA that was consistent with p.Gly92Ala, these results did not reach statistical significance (Figures 4E and 4F). Finally, *in vivo* complementation of *roraa* MO with p.Arg462Gln encoding mRNA did not rescue the size of the cerebellum (Figures 4G and 4H, $p < 0.001$, $n = 40–41$), suggesting a loss-of-function effect as the possible disease mechanism for this change impacting the ligand binding domain (Figures 4G and 4H).

Discussion

Here, we describe a cohort of 16 affected individuals who harbor 13 different rare variants disrupting *RORA*. We observe a clinical spectrum of neurodevelopmental delay with at least two different presentations: (1) a cognitive and motor phenotype and (2) a cognitive and behavioral phenotype. The first sub-phenotype is characterized by a moderate to severe ID with a marked ataxic component, severe cerebellar vermis hypoplasia, and epilepsy with predominant generalized seizures as already reported in *RORB*,[3] whereas the hallmark of the second sub-phenotype is ASD with mild ID or normal cognition frequently associated with epilepsy. In addition to these two groups, three individuals exhibit only mild ID without behavioral problems.

Although the size of our cohort limits the delineation of an unambiguous genotype-phenotype correlation, we can infer pathomechanisms related to specific phenotypes from our *in vivo* complementation data. Individuals 2 and 3, who harbor the two dominant toxic mutations of the RORα DNA binding domain, display severe ID and motor phenotypes likely due to cerebellar hypoplasia. A similar severe phenotype is coincident with the truncating deletion (individual 6; p.Arg340Profs*17), raising the possibility that this mutation could also result in a dominant toxic effect by encoding a truncated protein; immunoblotting studies from fibroblast protein lysates showed RORA protein levels to be similar to that of controls, arguing against haploinsufficiency (Figure S4C). Individual 6 also displayed autistic traits, but these phenotypes occurred secondary to established ID, potentially excluding her from the Autism Diagnosis Interview (ADI) criteria for idiopathic ASD.[37,38]

By contrast, we note variability in cognitive function and behavioral phenotypes in individuals with likely haploinsufficiency. One individual displays an ASD phenotype in the absence of ID (individual 8), and *in vivo* complementation testing in zebrafish indicate that the p.Arg462Gln mutation confers a loss-of-function effect. Further, 6/12 individuals from simplex families who likely have a reduction in protein dosage display mild to moderate ID but with normal behavior, while the remaining 5/12 affected individuals from simplex families present with both ID and autistic features. Notably, there is phenotypic variability among the individuals within multiplex family 10: all four individuals display mild ID, but only two display behavioral anomalies. However, we cannot exclude the possibility of *trans* effects from elsewhere in the genome, especially from *DISC1* affected by the CNVs harbored by individuals 10A–C or individual 11 (Figure S1; Table S4). Phenotypic variability is not uncommon for neurodevelopmental disorders,[39] and here

(E) Representative dorsal images of 3 dpf larvae injected with gradually modified doses of WT and K94R RNA (top, amount in pg) and stained with anti-acetylated tubulin antibody.
(F) Quantification of cerebellar measurements from the batches shown in (E).
(G) Representative dorsal images of 3 dpf larvae injected either with e2i2 splice-blocking MO or MO co-injected with WT *RORA* mRNA, R462Q or population control T476A variant *RORA* mRNA.
(H) Quantification of cerebellar measurements from the batches shown in (E).
AU, arbitrary units. Stars indicate p value compared to WT. ****$p < 0.0001$; ns, not significant. Error bars in (B), (D), (F), and (H) represent the 5th and 95th percentiles.

we account, in part, for variability due to allelism at the *RORA* locus by elucidating the direction of allele effect for missense changes.

The sub-group of our cohort who show a constellation of cognitive and motor defects are reminiscent of the homozygous *staggerer* (*sg/sg*) mouse, an early reported animal model of *Rora* ablation. The *staggerer* mutation consists of an intragenic CNV that results in a 122-bp frameshifting deletion that truncates the ligand binding domain, leading to the loss of RORα activity.[8] This phenotype is similar to *Rora*$^{-/-}$ mice[40] in which the most obvious symptom is an ataxic gait associated with defective Purkinje cell development leading to an abnormal cerebellar size.[41] Heterozygous *Rora*$^{+/-}$ mice present with a comparable phenotype, although they display a late onset of neuronal loss and reduced phenotypic severity.[42] Further studies will be required to understand the precise molecular mechanisms of p.Gly92Ala and p.Lys94Arg to account for their apparent toxic effects. We speculate that these changes in the DNA binding domain might hamper access of WT RORα to its natural target sites (Figure S3B), thereby leading to a phenotype resembling to the *staggerer* and *Rora*$^{-/-}$ homozygous mutants.

The autistic signs observed in two individuals with truncating mutations (individuals 6 and 13) and two individuals with missense mutations altering the ligand binding domain of *RORA* (individuals 7 and 8) are in agreement with recent reports suggesting that *RORA* is a candidate gene for ASD.[43] ChIP-on-chip analysis has revealed that RORα can be recruited to the promoter regions of 2,544 genes across the human genome, with a significant enrichment in biological functions including neuronal differentiation, adhesion, and survival, synaptogenesis, synaptic transmission and plasticity, and axonogenesis, as well as higher-level functions such as development of the cortex and cerebellum, cognition, memory, and spatial learning.[44] Independent ChIP-quantitative PCR analyses confirmed binding of RORA to promoter regions of selected ASD-associated genes, including *A2BP1*, *CYP19A1*, *ITPR1*, *NLGN1*, and *NTRK2*, whose expression levels are also decreased in *RORA*-repressed human neuronal cells and in prefrontal cortex tissues from individuals with ASD.[44] Additionally, two *RORA* polymorphisms (rs11639084 and rs4774388) have been associated with ASD risk in Iranian individuals.[45] Consistent with these data, treatment with a synthetic RORα/γ agonist, SR1078, reduced repetitive behavior in the BTBR mouse model of autism, suggesting that *RORA* upregulation could be a viable therapeutic option for ASD.[46]

In summary, our data implicate a diverse series of disruptive mutations in *RORA* with neurological phenotypes hallmarked by ID and either severe motor phenotypes or behavioral anomalies. Through combined clinical, genetic, and functional studies, we expand the genetic basis of rare neurodevelopmental syndromes and show how *in vivo* modeling can reveal dual molecular mutational effects.

Supplemental Data

Supplemental Data include ten figures and four tables and can be found with this article online at https://doi.org/10.1016/j.ajhg.2018.02.021.

Acknowledgments

We are grateful to Dr. R. Hawkes and Dr. C. Armstrong (University of Calgary) for providing the zebrin II antibody. We also thank Mr. Z. Kupchinsky for zebrafish husbandry, Mr. D. Morrow for assisting with reagents for the *in vivo* modeling study, and members of the Center for Human Disease Modeling for helpful comments. We are also grateful to Ms. J.A. Rosenfeld (Mokry) for her precious help in our search for similar affected individuals and for her review of the manuscript. This work was supported by funds from the Agence Nationale pour la Recherche/E-rare Joint-Transnational-Call 2011 (2011-RARE-004-01 "Euro-SCAR") to M.K.; from the National Human Genome Research Institute with supplemental funding provided by the National Heart, Lung, and Blood Institute under the Trans-Omics for Precision Medicine (TOPMed) program and the National Eye Institute (to the Broad Center for Mendelian Genomics [UM1 HG008900]); from the NIH grant T32 HD07466 (to M.H.W.); US NIH grant R01 MH106826 to E.E.D.; and from the Estonian Research Council, grant PUT355 (to S.P. and K.Õ.). We also acknowledge the Deciphering Developmental Disorders (DDD) Study.

K.M., M.T.C., R.W., M.J.G.S., and K.R. are employees of GeneDx, Inc., a wholly owned subsidiary of OPKO Health, Inc. N.K. is a paid consultant for and holds significant stock of Rescindo Therapeutics, Inc.

Received: December 18, 2017
Accepted: February 26, 2018
Published: April 12, 2018

Web Resources

1000 Genomes, http://www.internationalgenome.org/
CHOPCHOP, http://chopchop.cbu.uib.no/
Clustal: Multiple Sequence Alignment, http://www.clustal.org/
Database of Genomic Variants (DGV), http://dgv.tcag.ca/dgv/app/home
DECIPHER, https://decipher.sanger.ac.uk/
dbSNP, https://www.ncbi.nlm.nih.gov/projects/SNP/
Ensembl Genome Browser, http://www.ensembl.org/index.html
ExAC Browser, http://exac.broadinstitute.org/
GenBank, https://www.ncbi.nlm.nih.gov/genbank/
GeneMatcher, https://genematcher.org/
gnomAD Browser, http://gnomad.broadinstitute.org/
ImageJ Fiji, http://fiji.sc/Fiji
NHLBI Exome Sequencing Project (ESP) Exome Variant Server, http://evs.gs.washington.edu/EVS/
OMIM, http://www.omim.org/
PLINK, https://www.partners.org/~purcell/plink/
QuickChange Primer Design, https://www.genomics.agilent.com/primerDesignProgram.jsp
seqr, https://seqr.broadinstitute.org/
The Human Protein Atlas, http://www.proteinatlas.org/
UCSC Genome Browser, http://genome.ucsc.edu
UniProt, http://www.uniprot.org/
ZFIN, http://zfin.org

References

1. Escriva, H., Langlois, M.C., Mendonça, R.L., Pierce, R., and Laudet, V. (1998). Evolution and diversification of the nuclear receptor superfamily. Ann. N Y Acad. Sci. *839*, 143–146.
2. Sladek, F.M. (2011). What are nuclear receptor ligands? Mol. Cell. Endocrinol. *334*, 3–13.
3. Rudolf, G., Lesca, G., Mehrjouy, M.M., Labalme, A., Salmi, M., Bache, I., Bruneau, N., Pendziwiat, M., Fluss, J., de Bellescize, J., et al. (2016). Loss of function of the retinoid-related nuclear receptor (RORB) gene and epilepsy. Eur. J. Hum. Genet. *24*, 1761–1770.
4. Okada, S., Markle, J.G., Deenick, E.K., Mele, F., Averbuch, D., Lagos, M., Alzahrani, M., Al-Muhsen, S., Halwani, R., Ma, C.S., et al. (2015). IMMUNODEFICIENCIES. Impairment of immunity to *Candida* and *Mycobacterium* in humans with bi-allelic RORC mutations. Science *349*, 606–613.
5. Bardoni, B., Zanaria, E., Guioli, S., Floridia, G., Worley, K.C., Tonini, G., Ferrante, E., Chiumello, G., McCabe, E.R., Fraccaro, M., et al. (1994). A dosage sensitive locus at chromosome Xp21 is involved in male to female sex reversal. Nat. Genet. *7*, 497–501.
6. Muscatelli, F., Strom, T.M., Walker, A.P., Zanaria, E., Récan, D., Meindl, A., Bardoni, B., Guioli, S., Zehetner, G., Rabl, W., et al. (1994). Mutations in the DAX-1 gene give rise to both X-linked adrenal hypoplasia congenita and hypogonadotropic hypogonadism. Nature *372*, 672–676.
7. Giguère, V., Tini, M., Flock, G., Ong, E., Evans, R.M., and Otulakowski, G. (1994). Isoform-specific amino-terminal domains dictate DNA-binding properties of ROR alpha, a novel family of orphan hormone nuclear receptors. Genes Dev. *8*, 538–553.
8. Hamilton, B.A., Frankel, W.N., Kerrebrock, A.W., Hawkins, T.L., FitzHugh, W., Kusumi, K., Russell, L.B., Mueller, K.L., van Berkel, V., Birren, B.W., et al. (1996). Disruption of the nuclear hormone receptor RORalpha in staggerer mice. Nature *379*, 736–739.
9. Yamamoto, T., Mencarelli, M.A., Di Marco, C., Mucciolo, M., Vascotto, M., Balestri, P., Gérard, M., Mathieu-Dramard, M., Andrieux, J., Breuning, M., et al. (2014). Overlapping microdeletions involving 15q22.2 narrow the critical region for intellectual disability to NARG2 and RORA. Eur. J. Med. Genet. *57*, 163–168.
10. Boutry-Kryza, N., Labalme, A., Till, M., Schluth-Bolard, C., Langue, J., Turleau, C., Edery, P., and Sanlaville, D. (2012). An 800 kb deletion at 17q23.2 including the MED13 (THRAP1) gene, revealed by aCGH in a patient with a SMC 17p. Am. J. Med. Genet. A. *158A*, 400–405.
11. Grønborg, S., Kjaergaard, S., Hove, H., Larsen, V.A., and Kirchhoff, M. (2015). Monozygotic twins with a de novo 0.32cMb 16q24.3 deletion, including TUBB3 presenting with developmental delay and mild facial dysmorphism but without overt brain malformation. Am. J. Med. Genet. A. *167A*, 2731–2736.
12. Sali, A., and Blundell, T.L. (1993). Comparative protein modelling by satisfaction of spatial restraints. J. Mol. Biol. *234*, 779–815.
13. Obholzer, N., Wolfson, S., Trapani, J.G., Mo, W., Nechiporuk, A., Busch-Nentwich, E., Seiler, C., Sidi, S., Söllner, C., Duncan, R.N., et al. (2008). Vesicular glutamate transporter 3 is required for synaptic transmission in zebrafish hair cells. J. Neurosci. *28*, 2110–2118.
14. Montague, T.G., Cruz, J.M., Gagnon, J.A., Church, G.M., and Valen, E. (2014). CHOPCHOP: a CRISPR/Cas9 and TALEN web tool for genome editing. Nucleic Acids Res. *42*, W401-7.
15. Küry, S., Besnard, T., Ebstein, F., Khan, T.N., Gambin, T., Douglas, J., Bacino, C.A., Craigen, W.J., Sanders, S.J., Lehmann, A., et al. (2017). De novo disruption of the proteasome regulatory subunit PSMD12 causes a syndromic neurodevelopmental disorder. Am. J. Hum. Genet. *100*, 352–363.
16. Stankiewicz, P., Khan, T.N., Szafranski, P., Slattery, L., Streff, H., Vetrini, F., Bernstein, J.A., Brown, C.W., Rosenfeld, J.A., Rednam, S., et al.; Deciphering Developmental Disorders Study (2017). Haploinsufficiency of the chromatin remodeler BPTF causes syndromic developmental and speech delay, postnatal microcephaly, and dysmorphic features. Am. J. Hum. Genet. *101*, 503–515.
17. Ta-Shma, A., Khan, T.N., Vivante, A., Willer, J.R., Matak, P., Jalas, C., Pode-Shakked, B., Salem, Y., Anikster, Y., Hildebrandt, F., et al. (2017). Mutations in TMEM260 cause a pediatric neurodevelopmental, cardiac, and renal syndrome. Am. J. Hum. Genet. *100*, 666–675.
18. Niederriter, A.R., Davis, E.E., Golzio, C., Oh, E.C., Tsai, I.-C., and Katsanis, N. (2013). In vivo modeling of the morbid human genome using Danio rerio. J. Vis. Exp., e50338.
19. Margolin, D.H., Kousi, M., Chan, Y.-M., Lim, E.T., Schmahmann, J.D., Hadjivassiliou, M., Hall, J.E., Adam, I., Dwyer, A., Plummer, L., et al. (2013). Ataxia, dementia, and hypogonadotropism caused by disordered ubiquitination. N. Engl. J. Med. *368*, 1992–2003.
20. Schneider, C.A., Rasband, W.S., and Eliceiri, K.W. (2012). NIH Image to ImageJ: 25 years of image analysis. Nat. Methods *9*, 671–675.
21. Sobreira, N., Schiettecatte, F., Valle, D., and Hamosh, A. (2015). GeneMatcher: a matching tool for connecting investigators with an interest in the same gene. Hum. Mutat. *36*, 928–930.
22. Ruff, M., Gangloff, M., Wurtz, J.M., and Moras, D. (2000). Estrogen receptor transcription and transactivation: Structure-function relationship in DNA- and ligand-binding domains of estrogen receptors. Breast Cancer Res. *2*, 353–359.
23. Sidman, R.L., Lane, P.W., and Dickie, M.M. (1962). Staggerer, a new mutation in the mouse affecting the cerebellum. Science *137*, 610–612.
24. Marin-Valencia, I., Novarino, G., Johansen, A., Rosti, B., Issa, M.Y., Musaev, D., Bhat, G., Scott, E., Silhavy, J.L., Stanley, V., et al. (2018). A homozygous founder mutation in*TRAPPC6B* associates with a neurodevelopmental disorder characterised by microcephaly, epilepsy and autistic features. J. Med. Genet. *55*, 48–54.
25. Schaffer, A.E., Eggens, V.R.C., Caglayan, A.O., Reuter, M.S., Scott, E., Coufal, N.G., Silhavy, J.L., Xue, Y., Kayserili, H., Yasuno, K., et al. (2014). CLP1 founder mutation links tRNA splicing and maturation to cerebellar development and neurodegeneration. Cell *157*, 651–663.
26. Borck, G., Hög, F., Dentici, M.L., Tan, P.L., Sowada, N., Medeira, A., Gueneau, L., Thiele, H., Kousi, M., Lepri, F., et al. (2015). BRF1 mutations alter RNA polymerase III-dependent transcription and cause neurodevelopmental anomalies. Genome Res. *25*, 155–166.
27. Akizu, N., Cantagrel, V., Zaki, M.S., Al-Gazali, L., Wang, X., Rosti, R.O., Dikoglu, E., Gelot, A.B., Rosti, B., Vaux, K.K., et al. (2015). Biallelic mutations in SNX14 cause a syndromic form of cerebellar atrophy and lysosome-autophagosome dysfunction. Nat. Genet. *47*, 528–534.

28. Frosk, P., Arts, H.H., Philippe, J., Gunn, C.S., Brown, E.L., Chodirker, B., Simard, L., Majewski, J., Fahiminiya, S., Russell, C., et al.; FORGE Canada Consortium; and Canadian Rare Diseases: Models & Mechanisms Network (2017). A truncating mutation in CEP55 is the likely cause of MARCH, a novel syndrome affecting neuronal mitosis. J. Med. Genet. *54*, 490–501.

29. Anttonen, A.-K., Laari, A., Kousi, M., Yang, Y.J., Jääskeläinen, T., Somer, M., Siintola, E., Jakkula, E., Muona, M., Tegelberg, S., et al. (2017). ZNHIT3 is defective in PEHO syndrome, a severe encephalopathy with cerebellar granule neuron loss. Brain *140*, 1267–1279.

30. Hibi, M., and Shimizu, T. (2012). Development of the cerebellum and cerebellar neural circuits. Dev. Neurobiol. *72*, 282–301.

31. Bertrand, S., Thisse, B., Tavares, R., Sachs, L., Chaumot, A., Bardet, P.-L., Escrivà, H., Duffraisse, M., Marchand, O., Safi, R., et al. (2007). Unexpected novel relational links uncovered by extensive developmental profiling of nuclear receptor expression. PLoS Genet. *3*, e188.

32. Katsuyama, Y., Oomiya, Y., Dekimoto, H., Motooka, E., Takano, A., Kikkawa, S., Hibi, M., and Terashima, T. (2007). Expression of zebrafish ROR alpha gene in cerebellar-like structures. Dev. Dyn *236*, 2694–2701.

33. Hamling, K.R., Tobias, Z.J.C., and Weissman, T.A. (2015). Mapping the development of cerebellar Purkinje cells in zebrafish. Dev. Neurobiol. *75*, 1174–1188.

34. Gold, D.A., Gent, P.M., and Hamilton, B.A. (2007). ROR alpha in genetic control of cerebellum development: 50 staggering years. Brain Res. *1140*, 19–25.

35. Vogel, M.W., Sinclair, M., Qiu, D., and Fan, H. (2000). Purkinje cell fate in staggerer mutants: agenesis versus cell death. J. Neurobiol. *42*, 323–337.

36. Yoon, C.H. (1972). Developmental mechanism for changes in cerebellum of “staggerer” mouse, a neurological mutant of genetic origin. Neurology *22*, 743–754.

37. Tammimies, K., Marshall, C.R., Walker, S., Kaur, G., Thiruvahindrapuram, B., Lionel, A.C., Yuen, R.K.C., Uddin, M., Roberts, W., Weksberg, R., et al. (2015). Molecular diagnostic yield of chromosomal microarray analysis and whole-exome sequencing in children with autism spectrum disorder. JAMA *314*, 895–903.

38. Chérot, E., Keren, B., Dubourg, C., Carré, W., Fradin, M., Lavillaureix, A., Afenjar, A., Burglen, L., Whalen, S., Charles, P., et al. (2018). Using medical exome sequencing to identify the causes of neurodevelopmental disorders: Experience of 2 clinical units and 216 patients. Clin. Genet. *93*, 567–576.

39. Hu, W.F., Chahrour, M.H., and Walsh, C.A. (2014). The diverse genetic landscape of neurodevelopmental disorders. Annu. Rev. Genomics Hum. Genet. *15*, 195–213.

40. Doulazmi, M., Frédéric, F., Capone, F., Becker-André, M., Delhaye-Bouchaud, N., and Mariani, J. (2001). A comparative study of Purkinje cells in two RORalpha gene mutant mice: staggerer and RORalpha(-/-). Brain Res. Dev. Brain Res. *127*, 165–174.

41. Herrup, K., Shojaeian-Zanjani, H., Panzini, L., Sunter, K., and Mariani, J. (1996). The numerical matching of source and target populations in the CNS: the inferior olive to Purkinje cell projection. Brain Res. Dev. Brain Res. *96*, 28–35.

42. Doulazmi, M., Capone, F., Frederic, F., Bakouche, J., Lemaigre-Dubreuil, Y., and Mariani, J. (2006). Cerebellar purkinje cell loss in heterozygous rora+/- mice: a longitudinal study. J. Neurogenet. *20*, 1–17.

43. Nguyen, A., Rauch, T.A., Pfeifer, G.P., and Hu, V.W. (2010). Global methylation profiling of lymphoblastoid cell lines reveals epigenetic contributions to autism spectrum disorders and a novel autism candidate gene, RORA, whose protein product is reduced in autistic brain. FASEB J. *24*, 3036–3051.

44. Sarachana, T., and Hu, V.W. (2013). Genome-wide identification of transcriptional targets of RORA reveals direct regulation of multiple genes associated with autism spectrum disorder. Mol. Autism *4*, 14.

45. Sayad, A., Noroozi, R., Omrani, M.D., Taheri, M., and Ghafouri-Fard, S. (2017). Retinoic acid-related orphan receptor alpha (RORA) variants are associated with autism spectrum disorder. Metab. Brain Dis. *32*, 1595–1601.

46. Wang, Y., Billon, C., Walker, J.K., and Burris, T.P. (2016). Therapeutic effect of a synthetic RORα/γ agonist in an animal model of autism. ACS Chem. Neurosci. *7*, 143–148.

Example qualifying exam (Ph.D.) and comprehensive exam (M.S.) questions pertaining to Minster et al. (2016) *Nature Genetics* **48**:1049-1054.

---

1. The Samoan population has a high prevalence of obesity and includes many individuals with extremely high BMI. Explain the rationale for why geneticists often study (1) high-risk populations and (2) individuals with extreme phenotypes.

2. In Samoans, the heritability of BMI is 45%. How does this compare to other populations? How is this heritability estimate related, if at all, to the high BMI observed in the Samoan population?

3. The authors were careful to adjust their statistical model for population substructure and inferred relatedness. What is the reason behind this?

4. The investigators used sequence data from 96 individuals in order to impute unmeasured variants in the entire cohort. Explain the purpose of imputation and describe the logic behind it.

5. The authors state that because of high linkage disequilibrium in the region, conditional analyses were not able to distinguish between the top variants on statistical grounds. Explain the reason for this.

6. Authors used the p-value threshold of 5×10^{-8} for statistical significance. This is considerably smaller than the typical p-value threshold of 0.05. Explain why investigators used the stricter p-value threshold?

7. In the LocusZoom plot, some of the points form horizontal bands? Explain why this phenomenon may occur and what, if anything, can be inferred about the linkage disequilibrium and allele frequencies of these SNPs.

8. The investigators report that they have identified evidence of positive selection at the missense variant in Samoans. What is positive selection?

nature genetics

A thrifty variant in *CREBRF* strongly influences body mass index in Samoans

Ryan L Minster[1,13], Nicola L Hawley[2,13], Chi-Ting Su[1,12,13], Guangyun Sun[3,13], Erin E Kershaw[4], Hong Cheng[3], Olive D Buhule[5,12], Jerome Lin[1], Muagututi‘a Sefuiva Reupena[6], Satupa‘itea Viali[7], John Tuitele[8], Take Naseri[9], Zsolt Urban[1,14], Ranjan Deka[3,14], Daniel E Weeks[1,5,14] & Stephen T McGarvey[10,11,14]

© 2016 Nature America, Inc. All rights reserved.

Samoans are a unique founder population with a high prevalence of obesity[1–3], making them well suited for identifying new genetic contributors to obesity[4]. We conducted a genome-wide association study (GWAS) in 3,072 Samoans, discovered a variant, rs12513649, strongly associated with body mass index (BMI) ($P = 5.3 \times 10^{-14}$), and replicated the association in 2,102 additional Samoans ($P = 1.2 \times 10^{-9}$). Targeted sequencing identified a strongly associated missense variant, rs373863828 (p.Arg457Gln), in *CREBRF* (meta $P = 1.4 \times 10^{-20}$). Although this variant is extremely rare in other populations, it is common in Samoans (frequency of 0.259), with an effect size much larger than that of any other known common BMI risk variant (1.36–1.45 kg/m^2 per copy of the risk-associated allele). In comparison to wild-type CREBRF, the Arg457Gln variant when overexpressed selectively decreased energy use and increased fat storage in an adipocyte cell model. These data, in combination with evidence of positive selection of the allele encoding p.Arg457Gln, support a ‘thrifty’ variant hypothesis as a factor in human obesity.

Obesity is essentially a disorder of energy homeostasis and has strong genetic and environmental components. As diets have modernized and physical activity has decreased, the prevalence of overweight and obesity in Samoa has escalated to be among the highest in the world. In 2003, 68% of men and 84% of women in Samoa were overweight or obese by Polynesian cutoffs (BMI >26 kg/m^2)[1]; by 2010, prevalence had increased to 80% and 91%, respectively[3]. Although the contribution of environmental factors to this trend is clear, the estimated 45% heritability of BMI in Samoans remains largely unexplained[1]. Genetic susceptibility to obesity in the contemporary obesogenic environment may have resulted from putative selective advantages from efficient energy metabolism acquired during 3,000 years of Polynesian island discoveries, settlement, and population dynamics[5–8] and/or from genetic drift due to founder effects, small population sizes, and population bottlenecks[9–11].

To discover genes influencing BMI, we genotyped 659,492 markers across the genome in our discovery sample of 3,072 Samoans recruited from 33 villages across Samoa using the Affymetrix 6.0 chip (**Supplementary Fig. 1** and **Supplementary Table 1**). We adjusted for population substructure and inferred relatedness using an empirical kinship matrix and then tested for association with BMI using linear mixed models. Quantile–quantile plots indicated that *P*-value inflation was well controlled ($\lambda_{GC} = 1.07$) (**Supplementary Fig. 2**).

By far, the strongest association with BMI occurred at rs12513649 ($P = 5.3 \times 10^{-14}$) on chromosome 5q35.1 (**Fig. 1a**), and this association was strongly replicated ($P = 1.2 \times 10^{-9}$) in 2,102 adult Samoans from a 1990–1995 longitudinal study and a 2002–2003 family study, with participants of each study drawn from both American Samoa and Samoa (**Table 1** and **Supplementary Table 1**). To fine-map the region encompassing this signal, we used the Affymetrix-based genotypes to select 96 individuals optimal for targeted sequencing of a 1.5-Mb region centered on rs12513649. The haplotypes generated from the sequencing data were used to impute genotypes for the rest of the discovery sample. Analyses of the imputed data highlighted two significantly associated variants in *CREBRF* (encoding CREB3 regulatory factor), rs150207780 and rs373863828 (**Fig. 1b**). Because of high linkage disequilibrium (LD) in the region, conditional analyses were not able to distinguish between the top variants on statistical grounds (**Supplementary Fig. 3**). Annotation indicated that neither rs12513649, located between *ATP6V0E1* and *CREBRF*, nor rs150207780, located in intron 1 of *CREBRF*, had any predicted regulatory function, drawing our attention to rs373863828, which was

[1]Department of Human Genetics, Graduate School of Public Health, University of Pittsburgh, Pittsburgh, Pennsylvania, USA. [2]Department of Epidemiology (Chronic Disease), Yale University School of Public Health, New Haven, Connecticut, USA. [3]Department of Environmental Health, University of Cincinnati College of Medicine, Cincinnati, Ohio, USA. [4]Division of Endocrinology, Department of Medicine, University of Pittsburgh, Pittsburgh, Pennsylvania, USA. [5]Department of Biostatistics, Graduate School of Public Health, University of Pittsburgh, Pittsburgh, Pennsylvania, USA. [6]Bureau of Statistics, Government of Samoa, Apia, Samoa. [7]Samoa National Health Service, Apia, Samoa. [8]Department of Health, American Samoa Government, Pago Pago, American Samoa, USA. [9]Ministry of Health, Government of Samoa, Apia, Samoa. [10]International Health Institute, Department of Epidemiology, Brown University School of Public Health, Providence, Rhode Island, USA. [11]Department of Anthropology, Brown University, Providence, Rhode Island, USA. [12]Present addresses: Department of Internal Medicine, National Taiwan University Hospital, Yun-Lin Branch, Yun-Lin, Taiwan (C.-T.S.) and Biostatistics and Bioinformatics Branch, Division of Intramural Population Health Research, Eunice Kennedy Shriver National Institute of Child Health and Human Development, US National Institutes of Health, Bethesda, Maryland, USA (O.D.B.). [13]These authors contributed equally to this work. [14]These authors jointly supervised this work. Correspondence should be addressed to S.T.M. (stephen_mcgarvey@brown.edu).

Received 7 December 2015; accepted 15 June 2016; published online 25 July 2016; doi:10.1038/ng.3620

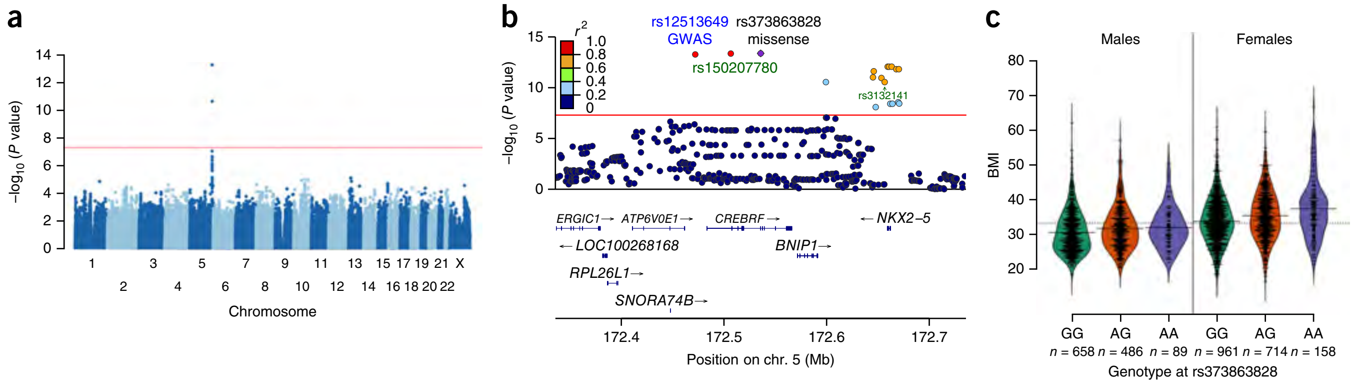

Figure 1 Association results from genome-wide and targeted sequencing and beanplots of BMI versus genotype in men and women from the discovery sample. (**a**) Manhattan plot of the genome-wide association scan for association with BMI. The red line corresponds to a P value of 5×10^{-8}. (**b**) Association results using imputed data for the region encompassing *CREBRF*. The strength of LD, as measured by the squared correlation of genotype dosages, between each variant and the missense variant rs373863828 is represented by the color of each point. The red line corresponds to a P value of 5×10^{-8}. The plot was generated using LocusZoom[32]. (**c**) Beanplots of BMI versus genotype in men (n = 1,233) and women (n = 1,833) from the discovery sample. Each bean consists of a mirrored density curve containing a one-dimensional scatterplot of the individual data. A solid line shows the average for each group, and the dashed line represents the overall average. The plot was generated using the R beanplot package[33].

© 2016 Nature America, Inc. All rights reserved.

the only strongly associated missense variant among the 775 variants with $P \leq 1 \times 10^{-5}$ in the targeted sequencing region. The rs373863828 missense variant (c.1370G>A, p.Arg457Gln) is located at a highly conserved position (GERP score 5.49) with a high probability of being damaging (SIFT, 0.03; PolyPhen-2, 0.996). The BMI-increasing A allele of rs373863828 has an overall frequency of 0.259 in Samoans but is unobserved or extremely rare in other populations, with an allele count in the Exome Aggregation Consortium of only 5 among 121,362 measured alleles (**Table 1**)[12]. Bayesian fine-mapping with PAINTOR[13] strongly supported following up the missense variant. The two variants in the region with the highest posterior probability (PP) of being causal were rs373863828 (PP = 0.80) and rs150207780 (PP = 0.22); when Encyclopedia of DNA Elements (ENCODE) functional annotation was included, these probabilities increased to 0.92 and 0.34, respectively.

We then genotyped the missense variant rs373863828 in the discovery and replication samples, obtaining very significant evidence of association with BMI in adults ($P = 7.0 \times 10^{-13}$ and $P = 3.5 \times 10^{-9}$, respectively), with a combined meta-analysis P value of 1.4×10^{-20} (**Table 1**). The meta-analysis showed no evidence of heterogeneity (I^2 = 0%; Q = 1.12; P = 0.571). In our discovery sample, each copy of the A allele increased BMI by 1.36 kg/m^2 (**Fig. 1c**). In our adult replication sample, each copy of the A allele increased BMI by 1.45 kg/m^2. There was a strong effect on BMI at this locus even after stratifying by sex and cohort (**Supplementary Fig. 4**; however, sex–genotype interactions were not significant (discovery P = 0.060; replication P = 0.555)). There was also suggestive evidence ($P = 1.1 \times 10^{-3}$) that this variant increased BMI in our sample of 409 Samoan children (**Table 1**). The rs373863828 variant (encoding p.Arg457Gln) accounted for 1.93% of the variance in BMI in our discovery sample and 1.08% of the variance in BMI in our replication sample. In comparison, rs1558902, the main risk-associated variant in *FTO*, increases BMI by 0.39 kg/m^2 per copy of the risk-associated allele and accounts for only 0.34% of the variance in BMI in Europeans[14,15]. In searches of the literature and databases (including GRASP[16,17]), we were unable to identify any significant associations with BMI in the *CREBRF* region in other human studies.

In addition to BMI, the A allele of rs373863828 was also positively associated with obesity risk (odds ratio (OR) = 1.305 and 1.441 in the discovery and replication cohorts, respectively) as well as measures of total and regional adiposity, including percent body fat, abdominal circumference, and hip circumference, in both cohorts (**Table 2** and **Supplementary Table 2**). The A allele was also positively associated with serum leptin levels in women (both cohorts) and men (replication cohort) before but not after adjusting for BMI. These data indicate that the association between the missense variant and BMI is indeed due to an association with adiposity.

Higher BMI and adiposity are usually associated with greater insulin resistance (higher fasting insulin levels and homeostatic model assessment–insulin resistance (HOMA-IR)), an atherogenic lipid profile (especially higher serum triglyceride and lower HDL cholesterol levels), and lower adiponectin levels. We therefore expected the BMI-increasing A allele of rs373863828 to also be associated with these metabolic variables. However, even though the A allele was consistently associated with higher BMI and adiposity in both the discovery and replication cohorts, the expected associations with the above obesity-related comorbidities were not observed and, in some cases, were even in the opposite direction to that expected (**Table 2** and **Supplementary Table 2**). Notably, when considering all subjects, the risk of diabetes was actually lower (OR = 0.586 for the discovery cohort, $P = 6.68 \times 10^{-9}$) or trended lower (0.742 for the replication cohorts, P = 0.029) in carriers of the A allele. Likewise, even in non-diabetic subjects, the variant was associated with moderately but significantly lower fasting glucose levels in both the discovery and replication cohorts (1.65 mg/dl ($P = 9.5 \times 10^{-5}$) and 1.54 mg/dl ($P = 8.8 \times 10^{-4}$) lower for each copy of the A allele, respectively). These effects became even more significant after adjusting for BMI (2.25 mg/dl, $P = 6.9 \times 10^{-8}$ and 2.09 mg/dl, $P = 7.6 \times 10^{-6}$), suggesting an independent effect of the variant on glucose homeostasis and diabetes risk. Such effects are unlikely to be due to survival bias, as no correlation between age and genotype was observed (linear regression P = 0.849). These effects seem to be independent of obesity-associated insulin resistance, as associations with fasting insulin levels and HOMA-IR were not consistently observed across the cohorts (associations were stronger only in the replication cohort before adjusting for BMI). Furthermore, although the variant was associated with lower total cholesterol levels in the discovery cohort, consistent effects on serum lipid or adiponectin levels were likewise not observed. Together, these data suggest that the missense variant does not promote, and may even protect against, obesity-associated comorbidities; however, additional studies will be required to confirm these findings and directly test this hypothesis.

Table 1 Association details for rs12513649 and rs373863828

	Discovery variant	Missense variant
SNP rs ID	rs12513649	rs373863828
Chromosome	5	5
Physical position (GRCh37.p13) (bp)	172,472,052	172,535,774
Effect allele	G	A
Other allele	C	G
Nearest gene upstream of the SNP	*ATP6V0E1*	*CREBRF*
Distance to nearest upstream gene (bp)	10,152	0
Nearest gene downstream of the SNP	*CREBRF*	*CREBRF*
Distance to nearest downstream gene (bp)	11,302	0
Sample sizes (phenotyped and genotyped)		
GWAS Samoans from the 2010s (discovery)	3,072	3,066
Samoans from the 1990s (replication)	1,020	1,020
Samoans from the 2000s (replication)	1,082	1,083
Meta-analysis of the 1990s and 2000s samples	2,102	2,103
Meta-analysis of the 1990s, 2000s, and 2010s samples	5,174	5,169
Samoan children from the 2000s	409	409
P values for log-transformed BMI		
GWAS Samoans from the 2010s (discovery)	5.3×10^{-14}	7.0×10^{-13}
Samoans from the 1990s (replication)	5.8×10^{-4}	8.0×10^{-4}
Samoans from the 2000s (replication)	3.0×10^{-7}	6.5×10^{-7}
Meta-analysis of the 1990s and 2000s samples	1.2×10^{-9}	3.5×10^{-9}
Meta-analysis of the 1990s, 2000s, and 2010s samples	4.0×10^{-22}	1.4×10^{-20}
Samoan children from the 2000s	4.1×10^{-3}	1.1×10^{-3}
Effect sizes (β (s.e.)) for log-transformed BMI		
GWAS Samoans from the 2010s (discovery)	0.041 (0.005)	0.039 (0.005)
Samoans from the 1990s (replication)	0.029 (0.008)	0.028 (0.008)
Samoans from the 2000s (replication)	0.056 (0.011)	0.054 (0.011)
Samoan children from the 2000s	0.031 (0.011)	0.035 (0.011)
Effect allele frequencies		
GWAS Samoans from the 2010s	0.276	0.276
Samoans from the 1990s	0.251	0.251
Samoan adults from the 2000s	0.224	0.225
Samoan children from the 2000s	0.236	0.235
All of the 1990s, 2000s and 2010s samples	0.258	0.259
Individuals of East Asian descent from 1000G	0.063	0.000
Individuals of South Asian descent from 1000G	0.003	0.000
Individuals of European descent from 1000G	0.000	0.000
Individuals of admixed American descent from 1000G	0.059	0.000
Individuals of African descent from 1000G	0.001	0.000
Individuals of East Asian descent from ExAC	NA	<0.001[a]
Individuals of South Asian descent from ExAC	NA	0.000
Individuals of European descent from ExAC	NA	<0.001[b]
Individuals of Latino descent from ExAC	NA	0.000
Individuals of African descent from ExAC	NA	0.000
Individuals of other descent from ExAC	NA	0.001[c]

This table provides detailed results for rs12513649 and rs373863828. 1000G, 1000 Genomes Project; ExAC, Exome Aggregation Consortium[12]; s.e., standard error; NA, not available.
[a]Two A alleles in 8,636 measured alleles. [b]Two A alleles in 73,328 measured alleles. [c]One A allele in 908 measured alleles.

Although the majority of genes contributing to obesity do so by influencing the central regulation of energy balance[18], emerging evidence highlights the contribution of altered cellular metabolism to obesity[19]. Therefore, we examined the impact of rs373863828 on cellular bioenergetics. To do so, we selected the established 3T3-L1 mouse adipocyte model for two reasons: (i) *CREBRF* is widely expressed in virtually all tissues, including adipose tissue (**Supplementary Fig. 5**), suggesting a fundamental cellular function, and (ii) several CREB family proteins have been linked to mitochondrial function and metabolic phenotypes in adipocytes[20–23]. Thus, this model is well suited to assess multiple potentially relevant metabolic phenotypes.

We first characterized the effects of adipogenic differentiation and ectopic overexpression of human wild-type or Arg457Gln CREBRF on endogenous *Crebrf* expression in 3T3-L1 cells. *Crebrf* expression was induced during adipogenesis in conjunction with that of adipogenic markers (*Cebpa*, *Pparg*, and *Adipoq*), suggesting a role for CREBRF in this process (**Supplementary Fig. 6**). Indeed, comparable stable overexpression of the transcripts for human wild-type and Arg457Gln CREBRF (**Fig. 2a**), without changing endogenous *Crebrf* levels (**Fig. 2b**), was sufficient to induce the expression of adipogenic markers (**Fig. 2c**–**e**) and promote lipid and triglyceride accumulation (**Fig. 2f**–**h**) in the absence of standard hormonal induction of adipogenesis. Although Arg457Gln CREBRF resulted in slightly weaker induction of adipogenic markers than wild-type protein (**Fig. 2c**,**e**), it promoted significantly ($P < 0.02$) greater lipid and triglyceride accumulation (**Fig. 2f**–**h**). To determine whether this increased energy storage was associated with decreased energy use, we next assessed glycolysis, mitochondrial respiration, and ATP production. Consistent with published data[24,25], glycolysis was suppressed and mitochondrial respiration and ATP production were enhanced by hormonally induced adipogenic differentiation (**Supplementary Fig. 7**). Stable overexpression of wild-type CREBRF increased whereas Arg457Gln CREBRF decreased multiple measures of cellular energy use, including basal and maximal mitochondrial respiration, mitochondrial ATP production, and basal glycolysis (**Fig. 2i**). These data indicate that the Arg457Gln CREBRF variant promotes more lipid storage while using less energy than wild-type CREBRF.

In addition to having a role in cellular energy storage and use, the *Drosophila melanogaster CREBRF* ortholog *REPTOR* has recently been implicated in both cellular and organismal adaptation to nutritional stress by mediating the downstream transcriptional response to the cellular energy sensor TORC1 (refs. 26,27). In support of this hypothesis, expression of *CREBRF* orthologs is highly induced by starvation in all tissues of *Drosophila*[26,27] as well as in human lymphoblasts[28,29]. Moreover, *REPTOR*-knockout flies[26] and *Crebrf*-knockout mice[30] have lower total energy storage and body weight, respectively. Similarly, we found that nutrient starvation of 3T3-L1 preadipocytes rapidly increased *Crebrf* mRNA levels, which peaked by 4 h at levels 13-fold higher than those seen at 0 h ($P = 1.1 \times 10^{-16}$) and remained elevated by 5-fold at 24 h after the start of starvation ($P = 4.1 \times 10^{-14}$) (**Fig. 3a**). Treatment with rapamycin, a TORC1 inhibitor, also rapidly increased *Crebrf* mRNA levels, but did so to a lesser extent than starvation (**Fig. 3b**), indicating that additional TORC1-independent signals converge on *Crebrf*. Furthermore, overexpression of wild-type and

© 2016 Nature America, Inc. All rights reserved.

Table 2 Association of rs373863828 with untransformed adiposity, metabolic, and lipid traits in the discovery sample

Quantitative trait	*n*	*β* (s.e.)	*P*	Covariates[a]
Adiposity traits				
BMI (kg/m^2)	3,066	1.356 (0.183)	**1.12 × 10^{-13}**	A, A^2, S, A × S
Body fat (%)	2,893	2.199 (0.345)	**1.78 × 10^{-10}**	A, A^2, S, A × S
Abdominal circumference (cm)	3,057	2.842 (0.404)	**2.05 × 10^{-12}**	A, A^2, S, A × S, A^2 × S
Hip circumference (cm)	3,058	2.361 (0.332)	**1.19 × 10^{-12}**	A, A^2, S, A^2 × S
Abdominal–hip ratio	3,056	0.005 (0.002)	2.23 × 10^{-3}	A, A^2, S, A × S, A^2 × S
Metabolic traits				
Fasting glucose (mg/dl)[b]	2,393	−1.652 (0.423)	**9.52 × 10^{-5}**	A, A^2, S
Fasting insulin (μU/ml)[b]	2,392	1.342 (0.449)	2.83 × 10^{-3}	A, S, A × S
HOMA-IR[b]	2,392	0.241 (0.114)	0.035	A, S, A × S
Adiponectin (μg/ml)	2,858	−0.228 (0.083)	0.006	A, A^2, S, A × S
Leptin in men (ng/ml)[c]	1,151	0.719 (0.326)	0.027	A
Leptin in women (ng/ml)[c]	1,707	1.888 (0.525)	**3.25 × 10^{-4}**	
Metabolic traits adjusted for BMI				
Fasting glucose (mg/dl)[b]	2,383	−2.248 (0.417)	**6.89 × 10^{-8}**	A, A^2, S, B
Fasting insulin (μU/ml)[b]	2,382	0.225 (0.420)	0.592	A, A^2, S, B, A × S, A^2 × S
HOMA-IR[b]	2,382	−0.034 (0.107)	0.754	A, B
Adiponectin (μg/ml)	2,844	−0.066 (0.080)	0.412	A, A^2, S, B, A × S
Leptin in men (ng/ml)[c]	1,143	−0.262 (0.210)	0.213	A, A^2, B
Leptin in women (ng/ml)[c]	1,701	−0.516 (0.366)	0.159	A, A^2, B
Serum lipid levels				
Total cholesterol (mg/dl)	2,858	−3.203 (1.029)	**1.84 × 10^{-3}**	A, A^2, S, A × S, A^2 × S
Triglycerides (mg/dl)	2,858	0.349 (2.769)	0.900	A, S, A × S
HDL cholesterol (mg/dl)	2,858	−0.322 (0.321)	0.317	A, A^2, S
LDL cholesterol (mg/dl)	2,851	−2.347 (0.945)	0.013	A, A^2, S, A^2 × S
Dichotomous traits	***n***	**OR (95% CI)**	***P***	**Covariates[a]**
Obesity (>32 kg/m^2)	3,066	1.305 (1.159–1.470)	**1.12 × 10^{-5}**	A, A^2, S, A × S
Diabetes	2,876	0.637 (0.536–0.758)	**3.86 × 10^{-7}**	A
Diabetes adjusted for BMI	2,861	0.586 (0.489–0.702)	**6.68 × 10^{-9}**	A, B
Hypertension	3,041	1.014 (0.898–1.145)	0.818	A, S

Boldface represents a *P* value <2.17 × 10^{-3}. s.e., standard error; OR, odds ratio; 95% CI, 95% confidence interval. [a]A, age; A^2, age^2; S, sex; A × S, age × sex interaction; A^2 × S = age^2 × sex interaction, B, log(BMI). [b]Analysis was conducted only in non-diabetics. [c]Leptin was not analyzed in men and women together because the distributions were very different for the sexes.

Arg457Gln human CREBRF equivalently reduced the cell death rate to approximately one-third of that in controls within the first 6 h of nutrient starvation in 3T3-L1 preadipocytes ($P = 5 \times 10^{-6}$ and $P = 4 \times 10^{-5}$, respectively; **Fig. 3c,d**). These data indicate that CREBRF is a starvation-responsive factor and that wild-type and Arg457Gln CREBRF when overexpressed confer similar protection against cellular nutritional stress.

Complementing the functional evidence of 'thriftiness', we identified evidence of positive selection at the missense variant in Samoan genomes. The core haplotype carrying the derived BMI-increasing allele exhibited long-range LD (corresponding to the single thick branch in **Fig. 4b** versus **Fig. 4a**) and had elevated extended haplotype homozygosity (EHH) relative to haplotypes carrying the ancestral allele (**Fig. 4c**). Haplotypes carrying the derived allele were longer than haplotypes carrying the ancestral allele (**Fig. 4d**). Evidence of positive selection was provided by an integrated haplotype score (iHS) of 2.94 ($P \approx 0.003$) and a number of segregation sites by length (nS$_L$) score of 2.63 ($P \approx 0.008$) (**Supplementary Fig. 8**).

In 1962, James Neel posited the existence of a thrifty gene that provides a metabolic advantage in times of famine but promotes metabolic disease in times of nutritional excess[31]. By carrying out a genome-wide association analysis of BMI in Samoans, we discovered and replicated a strong association with a missense variant in *CREBRF* that has a much larger effect size than any other known common risk-associated variant for BMI[18]. Functional evidence from an adipocyte model further demonstrated that CREBRF with this missense variant promotes cellular energy conservation by increasing fat storage and decreasing energy use in comparison to the wild-type protein.

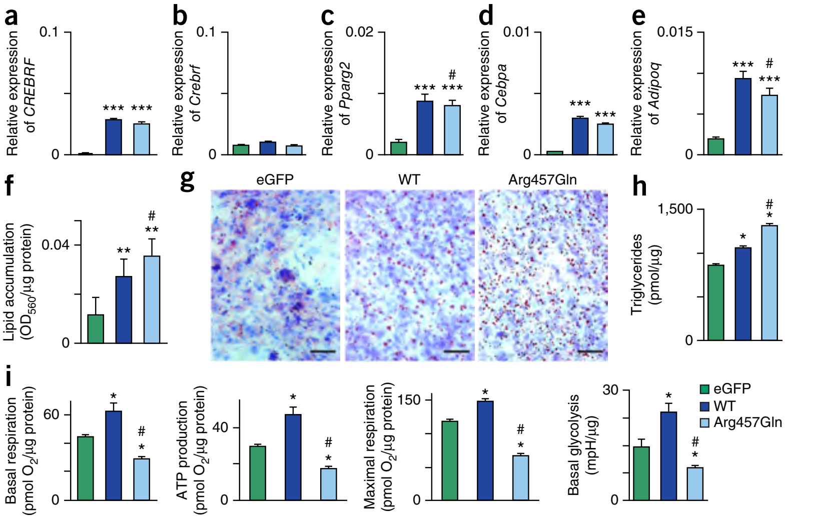

Figure 2 CREBRF variants, adipogenic differentiation, lipid accumulation, and energy homeostasis. 3T3-L1 mouse preadipocytes overexpressing enhanced GFP–only negative control (eGFP), wild-type human CREBRF (WT), or Arg457Gln human CREBRF were collected at 8 d after confluence in the absence of hormonal stimulation of adipogenic differentiation. (**a**–**e**) mRNA levels of human *CREBRF* (**a**) and endogenous mouse *Crebrf* (**b**), *Pparg2* (**c**), *Cebpa* (**d**), and *Adipoq* (**e**) relative to those of the β-actin (*Actb*) reference gene determined using quantitative RT–PCR. Values are given as means ± s.e.m. from three biological replicates with four technical replicates each ($n = 3 \times 4 = 12$). Representative results from one of four experiments are shown. (**f**) Quantification of lipid accumulation with Oil Red O staining normalized to protein content (OD$_{560}$/μg protein). Data are shown as means ± s.e.m. from three transfection replicates with eight wells for each transfection ($n = 3 \times 8 = 24$). (**g**) Representative photomicrographs of Oil Red O staining to visualize lipid droplets (red) with counterstaining of nuclei with hematoxylin (blue). Scale bars, 50 μm. (**h**) Biochemical assay for triglycerides. Data are shown as means ± s.e.m., $n = 2$ biological replicates. (**i**) Key bioenergenic variables as determined on the basis of oxygen consumption rate (OCR) and extracellular acidification rate (ECAR) normalized to protein content. Values are given as means ± s.e.m. ($n = 6$ biological replicates). mpH, 0.01 pH unit. Statistical analysis: one-way analysis of variance (ANOVA), two-sided Games–Howell *post-hoc* test. $^{*}P < 0.03$, $^{**}P < 1 \times 10^{-3}$, $^{***}P < 1 \times 10^{-4}$ compared to 3T3-L1 cells transfected with eGFP control construct; $^{\#}P < 0.05$ compared to 3T3-L1 cells transfected with construct for wild-type CREBRF.

© 2016 Nature America, Inc. All rights reserved.

© 2016 Nature America, Inc. All rights reserved.

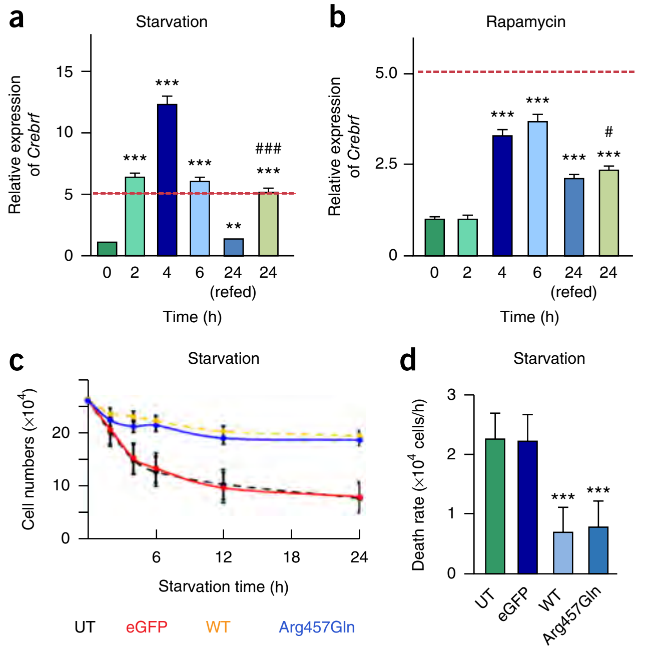

Figure 3 Induction of *Crebrf* expression by nutritional stress and protection against starvation. (**a**,**b**) 3T3-L1 preadipocytes were starved (**a**) or treated with 20 ng/ml rapamycin (**b**) for 0, 2, 4, 12, or 24 h. A set of cells was starved or treated with rapamycin for 12 h and then refed with fresh growth medium for an additional 12 h (24 h (refed)). *Crebrf* mRNA levels were determined relative to *Actb* levels and normalized to baseline levels (0 h). Values are given as means ± s.e.m. from three biological replicates with four technical replicates each ($n = 3 \times 4 = 12$). Statistical analysis: one-way ANOVA and two-sided Bonferroni *post-hoc* tests. $^{**}P = 0.002$, $^{***}P < 1 \times 10^{-11}$ compared to cells at 0 h; $^{\#}P = 0.02$, $^{\#\#\#}P = 8.8 \times 10^{-13}$ compared to cells at 24 h (refed). (**c**,**d**) 3T3-L1 preadipocytes were either untransfected (UT) or transfected with plasmid encoding eGFP-only negative control, wild-type human CREBRF, or Arg457Gln CREBRF and starved. (**c**) Time course of 3T3-L1 cell survival upon starvation up to 24 h. (**d**) Cell death rates after 0–6 h of starvation. Values are given as means ± s.e.m. from two transfection replicates with six wells for each transfection and three technical (cell counting) replicates ($n = 2 \times 6 \times 3 = 36$). This experiment was performed once following a pilot experiment with fewer time points showing similar results. Statistical analysis: one-way ANOVA and two-sided Games–Howell *post-hoc* tests. $^{***}P < 5 \times 10^{-5}$ compared to cells transfected with control eGFP construct.

The potential importance of this variant in organismal energy homeostasis is further supported by the 'lean' phenotype of mice[30] and flies[26] lacking the ortholog for this gene. These data, in combination with evidence of positive selection, support a thrifty variant hypothesis for human obesity and underscore the value of examining unique populations to identify new genetic contributions to complex traits.

However, many questions remain unanswered. More detailed studies in animal models and humans are required to define the systemic and tissue-specific (particularly central) contributions of the missense variant to overall energy balance. Such studies would also help confirm and clarify the mechanism by which this missense variant might protect against obesity-associated metabolic disease, which perhaps involves preferential promotion of more metabolically 'safe' or efficient energy storage and use. Studies that consider potential modifying and mediating environmental influences of this variant as well as gene–gene interactions might illuminate additional new factors contributing to these complex traits. Finally, additional anthropological genetic studies might determine the evolutionary origin of this variant or the potential role of drift in determining its frequency. Such research is urgently needed to inform decisions about how to use knowledge of this obesity risk variant to benefit Samoans at both individual and population health levels and to determine how this discovery might contribute to the understanding and treatment of more common obesity in general.

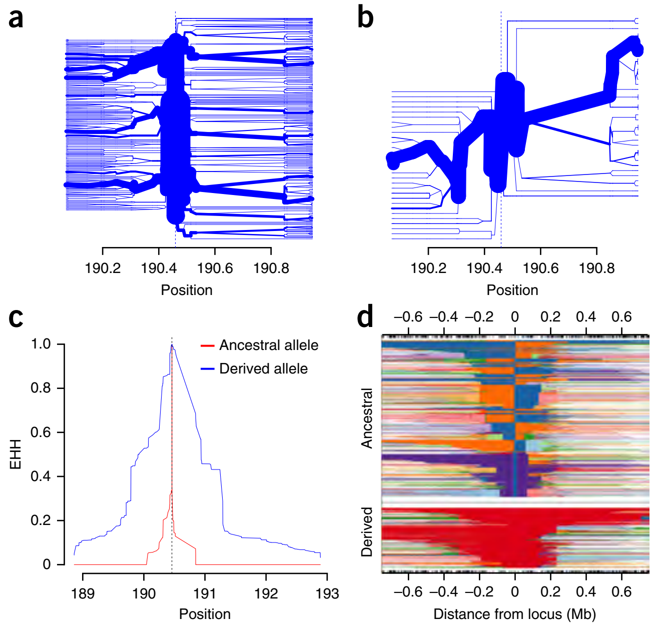

Figure 4 Evidence of positive selection centered on the missense variant rs373863828. Findings are shown for 626 Samoans who are not closely related. (**a**,**b**) Haplotype bifurcation plots for haplotypes carrying the ancestral allele (**a**) and the derived allele (**b**) at rs373863828 show that haplotypes carrying the derived allele have unusual long-range homozygosity. (**c**,**d**) Haplotypes carrying the derived allele have elevated EHH values as one moves away from rs373863828 (vertical dashed line) (**c**) and are longer than those carrying the ancestral allele (**d**).

URLs. BGTEx portal, http://www.gtexportal.org/; BioGPS portal, http://biogps.org/.

METHODS

Methods and any associated references are available in the online version of the paper.

Accession codes. The discovery data set is available from the database of Genotypes and Phenotypes (dbGaP) under accession phs000914.v1.p1.

Note: Any Supplementary Information and Source Data files are available in the online version of the paper.

ACKNOWLEDGMENTS

The authors would like to thank the Samoan participants of the study, and local village authorities and the many Samoan and other field workers over the years. We acknowledge the Samoan Ministry of Health and the Samoan Bureau of Statistics, and the American Samoan Department of Health for their support of this research. We also acknowledge S.S. Shiva and C.G. Corey at the University of Pittsburgh Center for Metabolism and Mitochondrial Biology for assistance with cellular bioenergetic profiling. This work was funded by NIH grants R01-HL093093 (S.T.M.), R01-AG09375 (S.T.M.), R01-HL52611 (I. Kamboh), R01-DK59642 (S.T.M.), P30 ES006096 (S.M. Ho), R01-DK55406. (R.D.), R01-HL090648 (Z.U.), and R01-DK090166 (E.E.K.) and by Brown University student research funds. Genotyping was performed in the Core Genotyping Laboratory at the University of Cincinnati, funded by NIH grant

P30 ES006096 (S.M. Ho). Illumina sequencing was conducted at the Genetic Resources Core Facility, Johns Hopkins Institute of Genetic Medicine (Baltimore).

AUTHOR CONTRIBUTIONS

R.L.M. performed the genotype quality control and association analyses, with guidance from D.E.W. and assistance from O.D.B. and J.L.; D.E.W. and R.L.M. wrote the relevant sections of the manuscript. N.L.H. led the field work data collection and phenotype analyses with guidance from S.T.M. G.S. led and directed genotyping experiments (using the Affymetrix 6.0 chip) and assay development for validation and replication (using the TaqMan platform) with guidance from R.D. H.C. participated extensively in DNA extraction, genotyping, and quality control of the data under the supervision of G.S. and R.D. Z.U. and C.-T.S. designed and performed the *CREBRF* overexpression, lipid accumulation, and adipocyte differentiation and starvation experiments, analyzed the data, and wrote the relevant sections of the manuscript. E.E.K. contributed mouse and human gene expression profiling data as well as contributed to the design and analysis of the functional studies. M.S.R., S.V., and J.T. facilitated fieldwork in Samoa and American Samoa. T.N. contributed to the discussion of the public health implications of the findings. All authors contributed to this work, discussed the results, and critically reviewed and revised the manuscript.

COMPETING FINANCIAL INTERESTS

The authors declare competing financial interests: details are available in the online version of the paper.

Reprints and permissions information is available online at http://www.nature.com/reprints/index.html.

© 2016 Nature America, Inc. All rights reserved.

1. Åberg, K. *et al.* Susceptibility loci for adiposity phenotypes on 8p, 9p, and 16q in American Samoa and Samoa. *Obesity (Silver Spring)* **17**, 518–524 (2009).
2. McGarvey, S.T. Obesity in Samoans and a perspective on its etiology in Polynesians. *Am. J. Clin. Nutr.* **53** (Suppl. 6), 1586S–1594S (1991).
3. Hawley, N.L. *et al.* Prevalence of adiposity and associated cardiometabolic risk factors in the Samoan genome-wide association study. *Am. J. Hum. Biol.* **26**, 491–501 (2014).
4. Tishkoff, S. Strength in small numbers. *Science* **349**, 1282–1283 (2015).
5. McGarvey, S.T., Bindon, J.R., Crews, D.E. & Schendel, D.E. in *Human Population Biology: A Transdisciplinary Science* (eds. Little, M.A. & Haas, J.D.) 263–279 (Academic Press, 1989).
6. McGarvey, S.T. The thrifty gene concept and adiposity studies in biological anthropology. *J. Polyn. Soc.* **103**, 29–42 (1994).
7. Zimmet, P., Dowse, G., Finch, C., Serjeantson, S. & King, H. The epidemiology and natural history of NIDDM—lessons from the South Pacific. *Diabetes Metab. Rev.* **6**, 91–124 (1990).
8. Kirch, P.V. & Rallu, J.-L. in *The Growth and Collapse of Pacific Island Societies* (eds. Kirch, P.V. & Rallu, J.-L.) 1–14 (University of Hawaii Press, 2007).
9. Friedlaender, J.S. *et al.* The genetic structure of Pacific Islanders. *PLoS Genet.* **4**, e19 (2008).
10. Tsai, H.-J. *et al.* Distribution of genome-wide linkage disequilibrium based on microsatellite loci in the Samoan population. *Hum. Genomics* **1**, 327–334 (2004).
11. Green, R.C. in *The Growth and Collapse of Pacific Island Societies* (eds. Kirch, P.V. & Rallu, J.-L.) 203–231 (University of Hawaii Press, 2007).
12. Exome Aggregation Consortium. Analysis of protein-coding genetic variation in 60,706 humans. Preprint at *bioRxiv* http://dx.doi.org/10.1101/030338 (2016).
13. Kichaev, G. *et al.* Integrating functional data to prioritize causal variants in statistical fine-mapping studies. *PLoS Genet.* **10**, e1004722 (2014).
14. Loos, R.J. & Yeo, G.S. The bigger picture of *FTO*: the first GWAS-identified obesity gene. *Nat. Rev. Endocrinol.* **10**, 51–61 (2014).
15. Speliotes, E.K. *et al.* Association analyses of 249,796 individuals reveal 18 new loci associated with body mass index. *Nat. Genet.* **42**, 937–948 (2010).
16. Eicher, J.D. *et al.* GRASP v2.0: an update on the Genome-Wide Repository of Associations between SNPs and phenotypes. *Nucleic Acids Res.* **43**, D799–D804 (2015).
17. Leslie, R., O'Donnell, C.J. & Johnson, A.D. GRASP: analysis of genotype–phenotype results from 1390 genome-wide association studies and corresponding open access database. *Bioinformatics* **30**, i185–i194 (2014).
18. Locke, A.E. *et al.* Genetic studies of body mass index yield new insights for obesity biology. *Nature* **518**, 197–206 (2015).
19. Pearce, L.R. *et al.* *KSR2* mutations are associated with obesity, insulin resistance, and impaired cellular fuel oxidation. *Cell* **155**, 765–777 (2013).
20. Vankoningsloo, S. *et al.* CREB activation induced by mitochondrial dysfunction triggers triglyceride accumulation in 3T3-L1 preadipocytes. *J. Cell Sci.* **119**, 1266–1282 (2006).
21. Reusch, J.E., Colton, L.A. & Klemm, D.J. CREB activation induces adipogenesis in 3T3-L1 cells. *Mol. Cell. Biol.* **20**, 1008–1020 (2000).
22. Ma, X. *et al.* CREBL2, interacting with CREB, induces adipogenesis in 3T3-L1 adipocytes. *Biochem. J.* **439**, 27–38 (2011).
23. Kim, T.H. *et al.* Identification of Creb3l4 as an essential negative regulator of adipogenesis. *Cell Death Dis.* **5**, e1527 (2014).
24. Wilson-Fritch, L. *et al.* Mitochondrial biogenesis and remodeling during adipogenesis and in response to the insulin sensitizer rosiglitazone. *Mol. Cell. Biol.* **23**, 1085–1094 (2003).
25. Keuper, M. *et al.* Spare mitochondrial respiratory capacity permits human adipocytes to maintain ATP homeostasis under hypoglycemic conditions. *FASEB J.* **28**, 761–770 (2014).
26. Tiebe, M. *et al.* REPTOR and REPTOR-BP regulate organismal metabolism and transcription downstream of TORC1. *Dev. Cell* **33**, 272–284 (2015).
27. Stocker, H. Stress relief downstream of TOR. *Dev. Cell* **33**, 245–246 (2015).
28. Chen, R., Mallelwar, R., Thosar, A., Venkatasubrahmanyam, S. & Butte, A.J. GeneChaser: identifying all biological and clinical conditions in which genes of interest are differentially expressed. *BMC Bioinformatics* **9**, 548 (2008).
29. Dengjel, J. *et al.* Autophagy promotes MHC class II presentation of peptides from intracellular source proteins. *Proc. Natl. Acad. Sci. USA* **102**, 7922–7927 (2005).
30. Martyn, A.C. *et al.* Luman/CREB3 recruitment factor regulates glucocorticoid receptor activity and is essential for prolactin-mediated maternal instinct. *Mol. Cell. Biol.* **32**, 5140–5150 (2012).
31. Neel, J.V. Diabetes mellitus: a "thrifty" genotype rendered detrimental by "progress"? *Am. J. Hum. Genet.* **14**, 353–362 (1962).
32. Pruim, R.J. *et al.* LocusZoom: regional visualization of genome-wide association scan results. *Bioinformatics* **26**, 2336–2337 (2010).
33. Kampstra, P. Beanplot: a boxplot alternative for visual comparison of distributions. *J. Stat. Softw.* **28**, 1–9 (2008).

© 2016 Nature America, Inc. All rights reserved.

ONLINE METHODS

Participants. The participants in this study are derived from the populations of the Independent State of Samoa and the US territory of American Samoa. We used two samples in this study: a discovery sample of 3,072 phenotyped and genotyped Samoans and a replication sample of 2,103 phenotyped and genotyped Samoans and American Samoans (**Supplementary Table 1**). An additional sample of 409 phenotyped and genotyped Samoan children was not included in the main analyses, but analyses with our associated variants were also conducted in this sample. Details about participant recruitment can be found in the **Supplementary Note**. The parent GWAS, sample selection and data collection methods, and phenotype levels, including those of lipids and lipoproteins, have been reported[3]. This study has been approved by the Health Research Committee of the Samoa Ministry of Health and the institutional review boards of Brown University, the University of Cincinnati, and the University of Pittsburgh. All participants gave informed consent.

In the original GWAS study design, our goal of a discovery sample size of 2,500 (which we exceeded) was chosen so as to have high power to detect risk-associated SNPs with realistic effect sizes. Power was estimated as follows: we used Quanto[34,35] to estimate the power to detect the rs9930506 SNP in *FTO*, which in the Sardinia study[36] explained 1.34% of variance in BMI. If we assume that this SNP has the same allele frequencies and that BMI has the same overall mean values and standard deviation as in Scuteri *et al.*[36], then at a significance level of 1×10^{-5} power is ≥80% when the risk-associated SNP explains at least 1.1% of the variance (and power is 90% when the SNP explains 1.3% of the variance). If we instead test at a threshold of 1×10^{-7}, power is ≥80% if the SNP explains at least 1.5% of the variance.

Anthropometric and biochemical measurements. Height, weight, and BMI were measured as previously described[3,37,38]. Polynesian cutoffs were used to classify adults as normal weight, overweight, or obese on the basis of BMI of <26 kg/m^2, 26–32 kg/m^2, and >32 kg/m^2, respectively[39]. Obesity in children was categorized from BMI using the international age- and sex-specific classifications developed by Cole *et al.*[40].

In the discovery sample, abdominal (at the level of the umbilicus) and hip circumferences were measured in duplicate, and the measures were averaged (**Supplementary Table 1**). Bioelectrical impedance measures of resistance and reactance (RJL BIA-101Q device, RJL Systems) were used to estimate percent body fat on the basis of Polynesian-specific equations[38,39]. Serum separated from whole-blood samples, collected after a 10-h overnight fast, was assayed for cholesterol (total, HDL, and LDL), triglycerides, glucose, and insulin. The assay techniques for these metabolic markers have been described previously[1]. Individuals were classified as having type 2 diabetes on the basis of fasting serum glucose levels ≥126 mg/dl or the current use of diabetes medication[41]. Hypertensives either had systolic blood pressure ≥140 mm Hg or diastolic blood pressure ≥90 mm Hg, or were currently taking hypertension medication. Additionally, serum levels of leptin and adiponectin were obtained by using commercially available radioimmunoassay kits (EMD Millipore). HOMA-IR was calculated as glucose (mg/dl) × insulin (μU/ml)/405, as recommended[42].

Genotyping. Genotyping of the discovery sample was performed using Genome-Wide Human SNP 6.0 arrays (Affymetrix). Extensive quality control was conducted on the basis of a pipeline developed by Laurie *et al.*[43]. Additional details for sample genotyping and genotype quality control can be found in the **Supplementary Note**.

Statistical analysis. During quality control, significant relatedness was observed among the discovery sample participants, so empirical kinship coefficients were estimated using genotyped markers, in two iterations. In the first iteration, we selected 10,000 independent autosomal markers using PLINK[44] and used them to generate empirical kinship coefficients with GenABEL[45]. Individuals with kinship coefficients less than 0.0625 (corresponding to first cousins) were considered unrelated. A maximal set of 1,891 unrelated individuals was then determined using previously published methods[46]. In the second iteration, the kinship matrix for all participants was estimated using a new set of 10,000 independent autosomal markers that had been selected using the set of unrelated individuals.

We tested for association between autosomal marker genotypes and BMI residuals while using the empirical kinship matrix to adjust for population substructure and subject relatedness. The tests were conducted using a score test as implemented in the mmscore function in GenABEL[47]. The statistics for association of X-chromosome genotypes with BMI residuals were calculated in GenABEL without adjusting for the empirical kinship estimates.

Meta-analysis of the adult samples was performed using METAL[48] to generate two replication *P* values: one for the adult replication samples and one for the adult replication samples and the discovery sample together (**Table 1**). Additional details of the statistical analyses, including ancestry principal components (**Supplementary Fig. 1** and **Supplementary Video 1**), can be found in the **Supplementary Note**.

Targeted sequencing. Before undertaking targeted sequencing, we first used SHAPEIT[49–53] and IMPUTE2 (refs. 54–56) for imputation in our region of interest centered on rs12513649 with the December 2013 1000 Genomes Project Phase I integrated variant set release haplotype reference panel. The approach implicated only one strongly associated variant (with a predicted allele frequency of 0.075), but when we genotyped this variant in a pilot sample it turned out to be monomorphic (as it was in the subsequent targeted sequencing experiment). On the basis of this experience, as well as what we would expect given the unique population history of Samoans, we believe that the best way to perform accurate imputation in Samoans is by using a Samoan-specific reference panel. This idea is in agreement with recent recommendations for optimal fine-mapping in populations with unique ancestry not found in a cosmopolitan reference panel[57]. A panel of 1,295 Samoans from the discovery sample is currently undergoing whole-genome sequencing by the National Heart, Lung, and Blood Institute (NHLBI) TOPMed Consortium. Additional details for targeted sequencing can be found in the **Supplementary Note**.

Imputation. We prephased the targeted sequencing sample using SHAPEIT[49–53] and then imputed into our discovery sample using IMPUTE2 (refs. 54–56). Association testing was carried out using ProbABEL[58], adjusting for relatedness with the empirical kinship matrix generated by GenABEL. Three variants had nearly equivalent *P* values (rs12513649, rs150207780, and rs373863828) because of nearly perfect LD between them (r^2 ≥0.988); imputation was very good for rs150207780 and rs373863828 (IMPUTE2 info metric = 0.954 for both variants). To determine which of these variants might be the most likely causal candidate, we tested for association in the targeted sequencing region with conditioning on each of these variants as well as the next most significant variant (rs3095870; info metric = 0.957), using ProbABEL and adjusting for relatedness. As expected for variants in such high LD, the signals in the region were eliminated after conditioning (**Supplementary Fig. 3**).

Bayesian fine mapping. Details can be found in the **Supplementary Note**.

Confirmatory genotyping. Genotyping was attempted for both rs150207780 and rs373863828 using TaqMan technology in all discovery and replication sample participants. The assay for rs150207780 failed; genotyping was not reattempted because this SNP showed no residual association signal in the analyses of the imputed data with conditioning on the missense variant rs373863828 (**Supplementary Fig. 3**). The replication plates included the 96 samples that had been sequenced in the targeted sequencing experiment. Laboratory personnel were blinded to the sequence-derived genotypes of these 96 samples, as well as to the phenotypes for all the samples. Association analysis was performed using the same regression models and meta-analysis as for the GWAS and replication analyses above. Effect size estimates were calculated using untransformed BMI separately for men and women from the discovery sample with age and age^2 as covariates.

Association analyses of additional phenotypes. rs373863828 genotype was examined for association with the additional adiposity-related phenotypes listed in **Table 2**. Association was assessed in both the discovery sample (**Table 2** and **Supplementary Table 2a**) and a mega-analysis of the adults from the replication sample (**Supplementary Table 2b**). Although meta-analysis of properly transformed phenotypes generates more accurate *P* values (as in **Table 1**), we chose instead to carry out mega-analyses here because we were primarily interested in estimating effect sizes on the natural scale for each trait. Sex-stratified analyses were also conducted in both samples (**Supplementary Table 2**). Diabetics were excluded from analyses of glucose, insulin, and HOMA-IR. Because the distributions of leptin levels varied greatly for women and men, a combined-sex analysis was not conducted for this trait. Residuals for quantitative traits were generated using linear regression. Age, age^2, sex, and the interactions between age and sex and between age^2 and sex were initially included in sex-combined models. For glucose, insulin, HOMA-IR, adiponectin, leptin, and diabetes status, a second set of models was used that included log-transformed BMI as a covariate. Sex and age × sex interactions were not included in the sex-stratified models. In the replication mega-analysis models, polity (Samoa or American Samoa) and cohort (1990s or 2000s) were initially included in the models as well. Stepwise regression was used to reduce the number of covariates for each trait separately. For quantitative traits, residuals were tested for association using the mmscore function of GenABEL[45], adjusted for the empirical kinship matrix as above. Dichotomous traits were analyzed using the palogist function of ProbABEL[58] while adjusting for covariates and empirical kinship. A Bonferroni-corrected P-value threshold of 2.17×10^{-3} was used to assess significance; this threshold is conservative, as it adjusts for 23 tests even though some traits are correlated with each other. To assess a possible survivor effect as the cause of the association between the BMI-increasing allele and decreased fasting glucose levels and risk of diabetes, we conducted linear regression of age by genotype. In the discovery sample, in regard to the association of rs373863828 with BMI, fasting glucose, fasting insulin, obesity risk, and diabetes risk, addition of the first ten 'local' principal components from **Supplementary Figure 1b** into the statistical models had a negligible effect on the effect estimates and statistical significance (data not shown).

© 2016 Nature America, Inc. All rights reserved.

Expression of *CREBRF* in human and mouse tissues. For human gene expression analysis, a Human Normal cDNA Array was obtained from Origene Technologies (HMRT103 and HBRT101). The human standard curve was prepared from Control Human Total RNA (Thermo Fisher Scientific, 4307281). For mouse gene expression analysis, mouse tissues were collected from 8–10 a.m. from littermate-matched, *ad libitum*–fed male C56BL/6J mice at 10 weeks of age (n = 6 mice/group). The mouse standard curve was prepared from pooled kidney RNA from the above mice. mRNA was prepared using the RNeasy Lipid Tissue Mini kit with on-column DNase treatment (Qiagen) followed by reverse transcription to cDNA using qScript cDNA Supermix (Quanta Biosciences). Gene expression was determined by qPCR (Quanta PerfeCTa SYBR Green FastMix or PerfeCTa qPCR FastMix) using an Eppendorf Realplex System. Human *CREBRF* was amplified using species-specific primers (**Supplementary Table 3**). Mouse *Crebrf* was amplified using a species-specific primer–probe set (Thermo Fisher Scientific, Mm00661538_m1). *CREBRF* expression was normalized to species-specific peptidylprolyl isomerase A or cyclophilin A as the endogenous control gene (Thermo Fisher Scientific, 4333763T and Mm02342430_g1 for human and mouse, respectively). Mouse data are expressed as means plus s.e.m. Data are relative expression values, and so randomization, blinding, and statistical comparisons were not indicated. Gene expression analysis was performed in accordance with Minimum Information for Publication of Quantitative Real–Time PCR Experiments (MIQE) guidelines. Mouse experiments were approved by the University of Pittsburgh Institutional Animal Care and Use Committee and conducted in conformity with the Public Health Service Policy for Care and Use of Laboratory Animals. Human samples from Origene Technologies conform to federal policies for the protection of human subjects (45 CDR 46) and are HIPAA compliant. Additional information and documentation can be obtained by contacting the company.

Plasmid construction and mutagenesis. Expression plasmids with ORFs for eGFP and human *CREBRF* (NM_153607.2) were obtained from GeneCopoeia (EX-EGFP-M10, EX-E3374-M10). The backbone vector was pReceiver-M10, which has a cytomegalovirus promoter and encodes a C-terminal Myc-(His)$_6$ tag. A rare missense variant, c.1447A>G, p.Thr483Ala (rs17854147), affecting a conserved residue was present in the *CREBRF* ORF. To avoid using this potentially function-altering variant, we converted *CREBRF* to the wild-type sequence and introduced the BMI risk-associated mutation c.1370G>A, p.Arg457Gln (rs373863828), using PCR mutagenesis. The segments obtained by PCR in each plasmid were verified by sequencing before large-scale plasmid purification for transfection.

Cell culture and transfection, adipocyte differentiation, Oil Red O plate assays, microscopy, triglyceride assays, and quantitative RT–PCR. These methods are described in detail in the **Supplementary Note**.

Bioenergetic profiling. OCR, a measure of mitochondrial respiration, and ECAR, a measure of glycolysis, were determined using an XF96 extracellular flux analyzer (Seahorse Bioscience). Transfected 3T3-L1 cells were seeded in a 96-well XF96 cell culture microplate (Seahorse Bioscience) at a density of 7,000 cells per well in 200 µl of DMEM (4.5 g/l glucose) supplemented with 10% FBS (Sigma) 36 h before measurement. Six replicates per cell type were included in the experiments, and four wells were chosen evenly in the plate to correct for temperature variation. On the day of the assay, the growth medium was exchanged for assay medium (unbuffered DMEM with 4.5 g/l glucose). Oligomycin at a final concentration of 2.0 µM, FCCP (carbonyl cyanide-*p*-trifluoromethoxyphenylhydrazone) at 1.0 µM, 2-deoxyglucose at 100 mM, and rotenone at 15.0 µM were sequentially injected into each well in accordance with the manufacturer's protocol. Basal mitochondrial respiration, maximal respiration, ATP production, and basal glycolysis were determined according to the manufacturer's instructions. At the conclusion of the assay, cells in the analysis plate were lysed using CelLytic M (Sigma). Protein concentration was measured using the Bradford assay[59] and used to normalize the bioenergetic profile data.

Starvation and rapamycin treatment. 3T3-L1 preadipocytes were subjected to starvation for 0, 2, 4, 12, and 24 h by culturing cells in Hank's balanced salt solution (HBSS). To investigate the response to refeeding starving cells, a set of cells undergoing 12 h of starvation was fed with fresh growth medium for an additional 12 h (**Fig. 3a**). For rapamycin stimulation, preadipocytes were treated with 20 ng/ml rapamycin (Sigma), for 2, 4, 12, and 24 h. A set of cells kept in rapamycin for 12 h was cultured in fresh growth medium for the following 12 h (**Fig. 3b**). To quantify cell survival, 3T3-L1 cells and transfected cells were seeded in six-well plates at 86,000 cells per well. Two days later, the cells were starved in HBSS. At 0, 2, 4, 6, 12, and 24 h, the cells were collected and 100 µl of the cell suspension samples was added to an equal volume of trypan blue (Life Technologies). The mixture was loaded into an automated cell counter (Cellometer Mini, Nexcelom Bioscience), and viable cell numbers were measured. Cell death rates were calculated by subtracting the number of viable cells at 6 h from cell numbers at 0 h and dividing the result by the cell numbers at 6 h.

Cell studies statistical analysis. For the cell studies, adequate sample sizes were determined on the basis of publications using similar methods and pilot experiments. No blinding was used. Each experiment was performed twice with similar results unless otherwise stated in the corresponding figure legend. The data were initially evaluated by one-way ANOVA implemented in SPSS (IBM). The homogeneity of variances was examined using Levene's test. Two-sided Bonferroni and Games–Howell *post-hoc* tests were used to compare data with equal and unequal variance, respectively. Alternatively, pairwise two-sided t tests for unequal variance were used. $P < 0.05$ was considered to be statistically significant. SPSS analyses were verified using the same tests as implemented in R (ref. 60).

Selection analyses. On the basis of the genome-wide Affymetrix 6.0 SNP genotype data, we used Primus[61,62] to select 626 individuals from the discovery sample using a kinship threshold (0.039) halfway between the values expected for first and second cousins, so that first cousins and more closely related relatives were excluded. These 'unrelated' individuals were then haplotyped using SHAPEIT[49–53] and were annotated with ancestral allele information using the selectionTools pipeline[63]. Haplotype bifurcation diagrams and EHH plots were drawn using the rehh R package[64]. The haplotype bifurcation diagram[65] visualizes the breakdown of LD as one moves away from the core allele at the focal SNP; each branch reflects the creation of new haplotypes, and the thickness of the line reflects the number of samples with the haplotype. EHH represents the probability that two randomly chosen chromosomes are identical by descent from the focal SNP to the current position of interest[65]. Selection at the core allele is expected to result in EHH values close to 1 in an extended region centered on the focal SNP. To measure the deviation, we used selscan[66] to compute the iHS[67], which is defined as the log of the ratio of the integrated EHH for the derived allele over the integrated EHH for the ancestral allele. These values are then normalized in frequency bins across the whole genome (we used 25 bins). Note that selscan's definition of iHS differs from earlier definitions where the ancestral allele was in the numerator of the ratio[66,67]. In our case, a large positive iHS indicates that a derived allele has had its frequency increase owing to selection. We computed an approximate two-sided *P* value under the assumption that after normalization the iHS is approximately distributed as a standard normal. We also used selscan to compute nS_L scores (the number of segregation sites by length)[68]. The nS_L is similar to the iHS, but instead of integrating over genetic distance the nS_L uses the number of segregating sites as a measure of 'distance'. Thus, the nS_L is more robust to demographic assumptions than the iHS, as it does not depend on a genetic map. As with the iHS, we normalized the nS_L scores in 25 frequency bins across the whole genome and computed approximate two-sided *P* values assuming a standard normal distribution. The selscan program was run using its assumed default values. As we were focused on testing whether there is positive selection at the missense variant, we did not adjust the *P* values for multiple testing.

© 2016 Nature America, Inc. All rights reserved.

34. Gauderman, W.J. Sample size requirements for association studies of gene–gene interaction. *Am. J. Epidemiol.* **155**, 478–484 (2002).
35. Gauderman, W.J. Sample size requirements for matched case–control studies of gene–environment interaction. *Stat. Med.* **21**, 35–50 (2002).
36. Scuteri, A. *et al.* Genome-wide association scan shows genetic variants in the *FTO* gene are associated with obesity-related traits. *PLoS Genet.* **3**, e115 (2007).
37. McGarvey, S.T., Levinson, P.D., Bausserman, L., Galanis, D.J. & Hornick, C.A. Population-change in adult obesity and blood-lipids in American-Samoa from 1976–1978 to 1990. *Am. J. Hum. Biol.* **5**, 17–30 (1993).
38. Keighley, E.D., McGarvey, S.T., Turituri, P. & Viali, S. Farming and adiposity in Samoan adults. *Am. J. Hum. Biol.* **18**, 112–122 (2006).
39. Swinburn, B.A., Ley, S.J., Carmichael, H.E. & Plank, L.D. Body size and composition in Polynesians. *Int. J. Obes. Relat. Metab. Disord.* **23**, 1178–1183 (1999).
40. Cole, T.J., Bellizzi, M.C., Flegal, K.M. & Dietz, W.H. Establishing a standard definition for child overweight and obesity worldwide: international survey. *Br. Med. J.* **320**, 1240–1243 (2000).
41. American Diabetes Association. Diagnosis and classification of diabetes mellitus. *Diabetes Care* **35** (Suppl. 1), S64–S71 (2012).
42. Matthews, D.R. *et al.* Homeostasis model assessment: insulin resistance and beta-cell function from fasting plasma glucose and insulin concentrations in man. *Diabetologia* **28**, 412–419 (1985).
43. Laurie, C.C. *et al.* Quality control and quality assurance in genotypic data for genome-wide association studies. *Genet. Epidemiol.* **34**, 591–602 (2010).
44. Purcell, S. *et al.* PLINK: a tool set for whole-genome association and population-based linkage analyses. *Am. J. Hum. Genet.* **81**, 559–575 (2007).
45. Aulchenko, Y.S., Ripke, S., Isaacs, A. & van Duijn, C.M. GenABEL: an R library for genome-wide association analysis. *Bioinformatics* **23**, 1294–1296 (2007).
46. Heath, S.C. *et al.* Investigation of the fine structure of European populations with applications to disease association studies. *Eur. J. Hum. Genet.* **16**, 1413–1429 (2008).
47. Chen, W.M. & Abecasis, G.R. Family-based association tests for genomewide association scans. *Am. J. Hum. Genet.* **81**, 913–926 (2007).
48. Willer, C.J., Li, Y. & Abecasis, G.R. METAL: fast and efficient meta-analysis of genomewide association scans. *Bioinformatics* **26**, 2190–2191 (2010).
49. Delaneau, O., Marchini, J. & Zagury, J.F. A linear complexity phasing method for thousands of genomes. *Nat. Methods* **9**, 179–181 (2012).
50. Delaneau, O., Howie, B., Cox, A.J., Zagury, J.F. & Marchini, J. Haplotype estimation using sequencing reads. *Am. J. Hum. Genet.* **93**, 687–696 (2013).
51. Delaneau, O., Zagury, J.F. & Marchini, J. Improved whole-chromosome phasing for disease and population genetic studies. *Nat. Methods* **10**, 5–6 (2013).
52. O'Connell, J. *et al.* A general approach for haplotype phasing across the full spectrum of relatedness. *PLoS Genet.* **10**, e1004234 (2014).
53. Delaneau, O. & Marchini, J.; 1000 Genomes Project Consortium; 1000 Genomes Project Consortium. Integrating sequence and array data to create an improved 1000 Genomes Project haplotype reference panel. *Nat. Commun.* **5**, 3934 (2014).
54. Marchini, J., Howie, B., Myers, S., McVean, G. & Donnelly, P. A new multipoint method for genome-wide association studies by imputation of genotypes. *Nat. Genet.* **39**, 906–913 (2007).
55. Howie, B.N., Donnelly, P. & Marchini, J. A flexible and accurate genotype imputation method for the next generation of genome-wide association studies. *PLoS Genet.* **5**, e1000529 (2009).
56. Marchini, J. & Howie, B. Genotype imputation for genome-wide association studies. *Nat. Rev. Genet.* **11**, 499–511 (2010).
57. Wang, X. *et al.* Evaluation of transethnic fine mapping with population-specific and cosmopolitan imputation reference panels in diverse Asian populations. *Eur. J. Hum. Genet.* **24**, 592–599 (2016).
58. Aulchenko, Y.S., Struchalin, M.V. & van Duijn, C.M. ProbABEL package for genome-wide association analysis of imputed data. *BMC Bioinformatics* **11**, 134 (2010).
59. Bradford, M.M. A rapid and sensitive method for the quantitation of microgram quantities of protein utilizing the principle of protein-dye binding. *Anal. Biochem.* **72**, 248–254 (1976).
60. R Development Core Team. *R: A Language and Environment for Statistical Computing* (R Foundation for Statistical Computing, 2004).
61. Staples, J., Nickerson, D.A. & Below, J.E. Utilizing graph theory to select the largest set of unrelated individuals for genetic analysis. *Genet. Epidemiol.* **37**, 136–141 (2013).
62. Staples, J. *et al.* PRIMUS: rapid reconstruction of pedigrees from genome-wide estimates of identity by descent. *Am. J. Hum. Genet.* **95**, 553–564 (2014).
63. Cadzow, M. *et al.* A bioinformatics workflow for detecting signatures of selection in genomic data. *Front. Genet.* **5**, 293 (2014).
64. Gautier, M. & Vitalis, R. rehh: an R package to detect footprints of selection in genome-wide SNP data from haplotype structure. *Bioinformatics* **28**, 1176–1177 (2012).
65. Sabeti, P.C. *et al.* Detecting recent positive selection in the human genome from haplotype structure. *Nature* **419**, 832–837 (2002).
66. Szpiech, Z.A. & Hernandez, R.D. selscan: an efficient multithreaded program to perform EHH-based scans for positive selection. *Mol. Biol. Evol.* **31**, 2824–2827 (2014).
67. Voight, B.F., Kudaravalli, S., Wen, X. & Pritchard, J.K. A map of recent positive selection in the human genome. *PLoS Biol.* **4**, e72 (2006).
68. Ferrer-Admetlla, A., Liang, M., Korneliussen, T. & Nielsen, R. On detecting incomplete soft or hard selective sweeps using haplotype structure. *Mol. Biol. Evol.* **31**, 1275–1291 (2014).

doi:10.1038/ng.3620

Example qualifying exam (Ph.D.) and comprehensive exam (M.S.) questions pertaining to Peloso et al. (2014) *American Journal of Human Genetics* **94**:223-232.

---

1. Why did authors choose to perform meta-analysis across different parent studies instead of combining data at the level of individual participant and analyzing the entire sample altogether? Discuss both practical and scientific reasons for this approach.

2. The authors performed three gene-based tests (T1, T0.1, and SKAT) for rare variants. What is the rationale for this strategy? Is there any benefit over single-SNP tests?

3. In the "Statistical Significance" sub-section under the "Statistical Analysis" heading, the authors describe the Bonferroni correction they applied in this paper. Would you characterize this approach as conservative or liberal? Would you expect that some of the results they call significant are actually false positives? Would you expect that some true positive signals were missed?

4. Table 1 categories variants on the Exome Array into five types: (1) nonsynonymous, (2) nonsense/splice, (3) synonymous, (4) intronic/intergenic, and (5) other. Why might authors have decided to group nonsense and splice site variants together as a single category? Do you agree with this decision? Why or why not? Same questions for intronic/intergenic variants.

5. Analyses were performed separately in participants of European ancestry (EA) vs. African ancestry (AA)? What is one rationale for this decision?

6. Minor allele frequency thresholds for SNP-based and gene-based tests were different in EA and AA. Explain the authors' reason for this. Do you agree? Why or why not?

7. Authors compare their results to the previous discovery of low frequency variants in *PCSK9*, which lower LDL-C and protect against CHD. Specifically, they query whether the *PCSK9* example represents a paradigm or a fairly unique scenario. How do authors interpret their results in light of the PCSK9 discovery? Do you agree with the authors' interpretation?

8. Authors did not show results for individual samples (they only showed meta-analysis results). What type of plot would have been useful for showing results of the four novel variants across each of the samples? What could be gained from this type of plot?

9. Why is exomic coverage higher in whites compared to blacks?

10. In general, populations of African ancestry are expected to have more low frequency variants than populations of European ancestry. Is Table 1 inconsistent with this expectation? Explain why or why not.

11. The LDL-C phenotype used in this paper was fairly crude (i.e, derived from the Friedewald equation, and adjusted for statin use). How might this affect the statistical analysis, if at all?

ARTICLE

Association of Low-Frequency and Rare Coding-Sequence Variants with Blood Lipids and Coronary Heart Disease in 56,000 Whites and Blacks

Gina M. Peloso,[1,2,3,4] Paul L. Auer,[5,6] Joshua C. Bis,[7] Arend Voorman,[8] Alanna C. Morrison,[9] Nathan O. Stitziel,[10,11] Jennifer A. Brody,[7] Sumeet A. Khetarpal,[12] Jacy R. Crosby,[9,13] Myriam Fornage,[9,14] Aaron Isaacs,[15] Johanna Jakobsdottir,[16] Mary F. Feitosa,[11] Gail Davies,[17,18] Jennifer E. Huffman,[19] Ani Manichaikul,[20] Brian Davis,[9] Kurt Lohman,[21] Aron Y. Joon,[14] Albert V. Smith,[16,22] Megan L. Grove,[9] Paolo Zanoni,[12] Valeska Redon,[12] Serkalem Demissie,[23,24] Kim Lawson,[9] Ulrike Peters,[5] Christopher Carlson,[5] Rebecca D. Jackson,[25] Kelli K. Ryckman,[26] Rachel H. Mackey,[27] Jennifer G. Robinson,[26] David S. Siscovick,[7,28] Pamela J. Schreiner,[29] Josyf C. Mychaleckyj,[20] James S. Pankow,[29] Albert Hofman,[30] Andre G. Uitterlinden,[30] Tamara B. Harris,[31] Kent D. Taylor,[32] Jeanette M. Stafford,[21] Lindsay M. Reynolds,[21] Riccardo E. Marioni,[17,18] Abbas Dehghan,[30] Oscar H. Franco,[30] Aniruddh P. Patel,[1,4,33] Yingchang Lu,[34,35] George Hindy,[36] Omri Gottesman,[34] Erwin P. Bottinger,[34] Olle Melander,[36] Marju Orho-Melander,[37] Ruth J.F. Loos,[34,35,38] Stefano Duga,[39] Piera Angelica Merlini,[40,41] Martin Farrall,[42] Anuj Goel,[42] Rosanna Asselta,[39] Domenico Girelli,[43] Nicola Martinelli,[43] Svati H. Shah,[44,45] William E. Kraus,[45,46] Mingyao Li,[47] Daniel J. Rader,[12] Muredach P. Reilly,[12] Ruth McPherson,[48] Hugh Watkins,[42,49] Diego Ardissino,[40,50] NHLBI GO Exome Sequencing Project, Qunyuan Zhang,[11] Judy Wang,[11] Michael Y. Tsai,[51] Herman A. Taylor,[52,53,54] Adolfo Correa,[54] Michael E. Griswold,[54] Leslie A. Lange,[55] John M. Starr,[17,56] Igor Rudan,[57,58] Gudny Eiriksdottir,[16] Lenore J. Launer,[31] Jose M. Ordovas,[59,60,61] Daniel Levy,[24,62] Y.-D. Ida Chen,[32] Alexander P. Reiner,[5,28] Caroline Hayward,[19] Ozren Polasek,[63] Ian J. Deary,[17,18] Ingrid B. Borecki,[11] Yongmei Liu,[21] Vilmundur Gudnason,[16,22] James G. Wilson,[64] Cornelia M. van Duijn,[15] Charles Kooperberg,[5] Stephen S. Rich,[20] Bruce M. Psaty,[7,28,65,66] Jerome I. Rotter,[32] Christopher J. O'Donnell,[3,24,62,67] Kenneth Rice,[8,69] Eric Boerwinkle,[9,68,69] Sekar Kathiresan,[1,2,3,4,67,69,*] and L. Adrienne Cupples[23,24,69,*]

[1]Center for Human Genetic Research, Massachusetts General Hospital, Boston, MA 02114, USA; [2]Cardiovascular Research Center, Massachusetts General Hospital, Boston, MA 02114, USA; [3]Department of Medicine, Harvard Medical School, Boston, MA 02115, USA; [4]Program in Medical and Population Genetics, Broad Institute, Cambridge, MA 02142, USA; [5]Public Health Sciences Division, Fred Hutchinson Cancer Research Center, Seattle, WA 98109, USA; [6]School of Public Health, University of Wisconsin-Milwaukee, Milwaukee, WI 53201, USA; [7]Cardiovascular Health Research Unit, Department of Medicine, University of Washington, Seattle, WA 98101, USA; [8]Department of Biostatistics, University of Washington, Seattle, WA 98195, USA; [9]Human Genetics Center, School of Public Health, University of Texas Health Science Center at Houston, Houston, TX 77030, USA; [10]Cardiovascular Division, Department of Medicine, Washington University School of Medicine, St. Louis, MO 63110, USA; [11]Division of Statistical Genomics, Department of Genetics, Washington University School of Medicine, St. Louis, MO 63110, USA; [12]Perelman School of Medicine, University of Pennsylvania, Philadelphia, PA 19104, USA; [13]Department of Biostatistics, Bioinformatics, and Systems Biology, The University of Texas Graduate School of Biomedical Sciences at Houston, Houston, TX 77030, USA; [14]Institute of Molecular Medicine, University of Texas Health Science Center at Houston, Houston, TX 77030, USA; [15]Genetic Epidemiology Unit, Department of Epidemiology, Erasmus University Medical Center, Rotterdam 3015CN, the Netherlands; [16]Icelandic Heart Association, Kopavogur 201, Iceland; [17]Centre for Cognitive Ageing and Cognitive Epidemiology, University of Edinburgh, Edinburgh EH8 9JZ, UK; [18]Department of Psychology, University of Edinburgh, Edinburgh EH8 9JZ, UK; [19]MRC Human Genetics, MRC IGMM, University of Edinburgh, Edinburgh EH4 2XU, UK; [20]Center for Public Health Genomics and Department of Public Health Sciences, University of Virginia, Charlottesville, VA 22908, USA; [21]Wake Forest School of Medicine, Winston-Salem, NC 27106, USA; [22]Faculty of Medicine, University of Iceland, Reykjavik 101, Iceland; [23]Department of Biostatistics, Boston University School of Public Health, Boston, MA 02118, USA; [24]National Heart, Lung, and Blood Institute (NHLBI) Framingham Heart Study, Framingham, MA 01702, USA; [25]Division of Endocrinology, Diabetes and Metabolism, Department of Internal Medicine, The Ohio State University, Columbus, OH 43210, USA; [26]Department of Epidemiology, College of Public Health, University of Iowa, Iowa City, IA 52242, USA; [27]Department of Epidemiology, Graduate School of Public Health, University of Pittsburgh, Pittsburgh, PA 15261, USA; [28]Department of Epidemiology, University of Washington, Seattle, WA 98195, USA; [29]Division of Epidemiology and Community Health, School of Public Health, University of Minnesota, Minneapolis, MN 55454, USA; [30]Department of Epidemiology, Erasmus University Medical Center, Rotterdam 3015CN, the Netherlands; [31]National Institute on Aging, NIH, Bethesda, MD 20892, USA; [32]Institute for Translational Genomics and Population Sciences, Los Angeles BioMedical Research Institute at Harbor-UCLA Medical Center, Torrance, CA 90502, USA; [33]School of Medicine, Yale University, New Haven, CT 06510, USA; [34]The Charles Bronfman Institute for Personalized Medicine, The Icahn School of Medicine at Mount Sinai, New York, NY 10029, USA; [35]The Genetics of Obesity and Related Metabolic Traits Program, The Icahn School of Medicine at Mount Sinai, New York, NY 10029, USA; [36]Department of Clinical Sciences in Malmö, Lund University, Clinical Research Center, Malmö 20502, Sweden; [37]Department of Clinical Sciences, Diabetes and Endocrinology, Lund University, University Hospital Malmö, Malmö 20502, Sweden; [38]The Mindich Child Health and Development Institute, The Icahn School of Medicine at Mount Sinai, New York, NY 10029, USA; [39]Dipartimento di Biotecnologie Mediche e Medicina Traslazionale, Università degli Studi di Milano, Milano 20133, Italy; [40]Associazione per lo Studio della Trombosi in Cardiologia (ASTC), Pavia 27100, Italy; [41]Divisione di Cardiologia, Ospedale Niguarda, Milano 20162, Italy; [42]Department of Cardiovascular Medicine, The Wellcome Trust Centre for Human Genetics, University of Oxford, Oxford OX3 7BN, UK; [43]Department of Medicine, University of Verona School of Medicine, Verona 37134, Italy; [44]Department of Obstetrics and Gynecology, Division of Urogynecology, Duke University, Durham, NC 27710, USA; [45]Division of Cardiology, Department of Medicine, Duke University School of Medicine, Durham, NC 27710, USA; [46]Duke Molecular Physiology Institute, Duke University School of Medicine, Durham, NC 27701, USA; [47]Department of Biostatistics and Epidemiology, School of Medicine, University of Pennsylvania, Philadelphia, PA 19104, USA; [48]Atherogenomics Laboratory, Division of Cardiology, University of Ottawa Heart Institute, Ottawa,

Low-frequency coding DNA sequence variants in the proprotein convertase subtilisin/kexin type 9 gene (*PCSK9*) lower plasma low-density lipoprotein cholesterol (LDL-C), protect against risk of coronary heart disease (CHD), and have prompted the development of a new class of therapeutics. It is uncertain whether the *PCSK9* example represents a paradigm or an isolated exception. We used the "Exome Array" to genotype >200,000 low-frequency and rare coding sequence variants across the genome in 56,538 individuals (42,208 European ancestry [EA] and 14,330 African ancestry [AA]) and tested these variants for association with LDL-C, high-density lipoprotein cholesterol (HDL-C), and triglycerides. Although we did not identify new genes associated with LDL-C, we did identify four low-frequency (frequencies between 0.1% and 2%) variants (*ANGPTL8* rs145464906 [c.361C>T; p.Gln121*], *PAFAH1B2* rs186808413 [c.482C>T; p.Ser161Leu], *COL18A1* rs114139997 [c.331G>A; p.Gly111Arg], and *PCSK7* rs142953140 [c.1511G>A; p.Arg504His]) with large effects on HDL-C and/or triglycerides. None of these four variants was associated with risk for CHD, suggesting that examples of low-frequency coding variants with robust effects on *both* lipids and CHD will be limited.

Introduction

Recently, a compelling new therapeutic target for lowering low-density lipoprotein cholesterol (LDL-C) emerged from human genetics: the proprotein convertase subtilisin/kexin type 9 gene (*PCSK9* [MIM 607786]).[1,2] *PCSK9* protein-coding sequence variants that are low in frequency (defined here as allele frequencies from 0.1% to 5%) have been associated with lower plasma LDL-C[3] and reduced risk for coronary heart disease (CHD).[4] With the identification of low-frequency variants that protected against CHD, many pharmaceutical companies have established drug development programs targeting PCSK9. These observations have raised the question of whether the *PCSK9* example is a paradigm for complex diseases like CHD or an exception.[5]

Low-frequency DNA sequence variants and rare alleles (defined here as <0.1% allele frequency) are poorly characterized by earlier generations of genome-wide association study (GWAS) genotyping arrays.[6] Sequencing across the exome or genome can directly assay low-frequency and rare variants but such an approach is currently too costly to study tens of thousands of individuals. One proposed method for testing low-frequency and rare DNA variation is to first sequence the exome to discover variation and, subsequently, to genotype the discovered variants in a larger number of individuals from the same or similar populations to test for association with phenotype. Based on this principle, the Illumina HumanExome genotyping array ("the Exome Array" or "Exome Chip") was designed based on coding sequence variants discovered from sequencing the exomes of ~12,000 individuals.

Here, we set out to address two questions: (1) are there novel low-frequency nonsynonymous and splice site variants associated with lipid levels in the population? and (2) if so, will these coding sequence variants also associate with risk of clinical CHD? To address these questions, we first genotyped and analyzed the Exome Array in 42,208 European ancestry (EA) individuals and 14,330 African ancestry (AA) individuals from 13 cohorts with blood levels of fasting low-density lipoprotein cholesterol (LDL-C), high-density lipoprotein cholesterol (HDL-C), and fasting triglycerides (TG). We subsequently tested validated lipid variants for association with CHD. We discovered four variants associated with HDL-C and/or TG, but these variants did not associate with CHD.

Subjects and Methods

Estimation of Proportion of Variation Captured by Exome Array

We identified EA (n = 3,173) and AA (n = 2,408) participants from the Atherosclerosis Risk in Communities (ARIC) Study with available exome sequence who were not among the ~12,000 individuals utilized to design the Exome Array. Separately by ancestry, we identified all variants with a minor allele frequency (MAF) >0.1% from exome sequencing of these independent ARIC individuals. These variants were compared with the variants available on the Illumina HumanExome v.1.0 array.

Study Participants

Thirteen studies genotyped the Exome Array on a total of 56,538 participants (Table S1 available online). 42,208 individuals were of European ancestry from ARIC, AGES, CHS, FHS, RS, MESA, WHI, CARDIA, Health ABC, FamHS, LBC1936, and Korcula. A total of 14,330 subjects were of African ancestry from ARIC, CHS, MESA, Health ABC, FamHS, JHS, WHI, and CARDIA. All participants provided informed consent and each study was approved by their governing ethics committee.

ON K1Y 4W7, Canada; [49]Merck Sharp & Dohme Corp., Rahway, NJ 07065, USA; [50]Divisione di Cardiologia, Azienda Ospedaliero-Universitaria di Parma, Parma 43100, Italy; [51]Department of Laboratory Medicine and Pathology, University of Minnesota, Minneapolis, MN 55454, USA; [52]Jackson State University, Jackson, MS 39217, USA; [53]Tougaloo College, Tougaloo, MS 39174, USA; [54]Department of Medicine, University of Mississippi Medical Center, Jackson, MS 39216, USA; [55]Department of Genetics, University of North Carolina, Chapel Hill, NC 27599, USA; [56]Alzheimer Scotland Dementia Research Centre, University of Edinburgh, Edinburgh EH8 9JZ, UK; [57]Centre for Population Health Sciences, The University of Edinburgh Medical School, Edinburgh EH8 9AG, UK; [58]Croatian Centre for Global Health, Faculty of Medicine, University of Split, Split 21000, Croatia; [59]Department of Cardiovascular Epidemiology and Population Genetics, National Center for Cardiovascular Investigation, Madrid 28049, Spain; [60]IMDEA-Alimentacion, Madrid 28049, Spain; [61]Nutrition and Genomics Laboratory, Jean Mayer-USDA Human Nutrition Research Center on Aging at Tufts University, Medford, MA 02155, USA; [62]Division of Intramural Research, NHLBI, NIH, Bethesda, MD 20892, USA; [63]Department of Public Health, Faculty of Medicine, University of Split, Split 21000, Croatia; [64]Department of Physiology and Biophysics, University of Mississippi Medical Center, Jackson, MS 39216, USA; [65]Group Health Research Institute, Group Health Cooperative, Seattle, WA 98101, USA; [66]Department of Health Services, University of Washington, Seattle, WA 98195, USA; [67]Cardiology Division, Massachusetts General Hospital, Boston, MA 02114, USA; [68]Human Genome Sequencing Center, Baylor College of Medicine, Houston, TX 77030, USA; [69]These authors contributed equally to this work

*Correspondence: skathiresan@partners.org (S.K.), adrienne@bu.edu (L.A.C.)

http://dx.doi.org/10.1016/j.ajhg.2014.01.009. ©2014 by The American Society of Human Genetics. All rights reserved.

Genotyping and Quality Control

All study participants were genotyped on the HumanExome BeadChip v.1.0 (Illumina). ARIC, AGES, CHS, FHS, RS, MESA, CARDIA, Health ABC, FamHS, and JHS were jointly called[7,8] at the University of Texas Health Science Center at Houston. LBC1936 and Korcula were called in GenomeStudio (Illumina) via the CHARGE Consortium joint calling cluster file. WHI used zCalls.[9] Variant quality control (QC) was performed at the University of Texas Health Science Center and by the individual cohorts. QC involved checking concordance to GWAS data and excluding those individuals missing >5% genotypes, population clustering outliers, individuals with high inbreeding coefficients or heterozygote rates, individuals with gender mismatches, one individual from duplicate pairs, and individuals with an unexpectedly high proportion of identity-by-descent sharing, with consideration for family studies, based on high-quality variants. All contributing studies used an additive coding of variants to the minor allele observed in the jointly called data set.

Phenotypes

Association analyses were performed for three blood lipid traits in mg/dl: LDL-C, HDL-C, and TG. Fasting lipids values were used from the earliest available exam in each study. Studies with only nonfasting lipid levels contributed only to the HDL-C analysis. To account for lipid-lowering therapy in selected participants, we sought to estimate the untreated lipid value in each participant. Such an approach has been demonstrated to perform well in accounting for treatment effects in studies of quantitative traits.[10] Statins are the most widely used treatment to lower plasma lipids and a statin at average dose reduces total cholesterol (TC) by 20% and LDL-C by 30%.[11] Statins became routinely used after the publication of the seminal 4S randomized control trial in 1994.[12]

If the sample was collected after 1994, we accounted for lipid-lowering medication in the following manner: the treated TC value was divided by 0.8. No adjustment was done on data collected before 1994 unless specific information on statin use was available. LDL-C was calculated via the Friedewald equation[13,14] (LDL-C = TC – HDL-C – (TG/5)) for those with TG <400 mg/dl. If TG >400 mg/dl, calculated LDL-C was set to missing. If TC was modified as described above for medication use, the modified total cholesterol was used to calculate LDL-C. If only measured LDL-C was available in a study, we accounted for lipid-lowering medication in the following manner: the treated LDL-C value was divided by 0.7. No adjustments for medication use were made for HDL-C and TG. TG was natural log transformed for analysis.

Statistical Analyses

Single-variant, conditional, and gene-based analyses were conducted with the seqMeta package in R. In brief, seqMeta implements efficient single-variant and gene-based meta-analysis. Each study computes association-specific statistics for each variant and trait assuming an additive model, and genotypic covariance matrices within predefined gene regions. Score statistics and genotypic covariance matrices are combined across studies to obtain an overall score statistic for each variant and a combined covariance matrix across studies. The combined score statistic is used for the single-variant results. For each gene, the score statistics for the variants within the gene along with the combined covariance matrix across those variants are used to construct the gene-based tests. An additive effect of each variant is assumed for individuals carrying more than one rare variant. All analyses were performed separately by race. We chose to meta-analyze EA and AA participants separately to minimize population biases and to increase the number of variants at specific MAF thresholds where there could be vastly different frequencies in the two ancestries.

Single-Variant Analysis

Though we defined low-frequency variants as having a MAF between 0.1% and 5%, we restricted single-variant tests to nonsynonymous and splice site variants with a MAF >0.02% in EA individuals ($n_{\text{variants}} = 54{,}837$) and >0.07% in AA individuals ($n_{\text{variants}} = 90{,}218$), corresponding to approximately 20 copies of the minor allele in each ancestry sample. Twenty copies of the minor allele provided stable estimates of the standard errors of the beta estimates and well-calibrated quantile-quantile plots.

Gene-Based Analysis

We constructed gene-based tests from the cohort-combined variant statistics and LD matrices. We only included nonsynonymous and splice site variants when producing the gene-based statistics. We performed three gene-based tests: (1) T1, where all variants with a MAF <1% were collapsed into gene-based score;[15] (2) T0.1, where all variants with a MAF <0.1% were collapsed into gene-based score; and (3) sequence kernel association test (SKAT)[16] at a MAF <5%. SKAT is more powerful than T1 when there are both protective and deleterious variants with different magnitudes in the same gene whereas T1 and T0.1 are more powerful when the magnitudes and directions of effect for the individual variants in a gene are consistent. We filtered gene-based results with a cumulative MAF <0.05% in the EA individuals and <0.14% in the AA individuals for SKAT analyses, corresponding to approximately 40 copies of the minor allele. For the T1 and T0.1 tests, we used a cumulative MAF >0.04% for the EA individuals and >0.11%, corresponding to 30 copies of the minor allele across all cohorts. Simulations under the null (i.e., no associations) were performed to determine the thresholds to control type I error for the burden tests (results not shown). The gene-based T1 and T0.1 analyses were limited to genes with at least two variants contributing to the test. For EA, T1 analysis included 12,351 genes with a cumulative MAF >0.04% and T0.1 with 8,357 genes; for AA participants, T1 analysis included 13,574 genes with a cumulative MAF >0.11% and T0.1 with 7,579 genes.

All analyses included age, age^2, sex, and up to the first four principal components of ancestry as covariates. Cohort statistics were adjusted for related individuals, where appropriate. Beta coefficients were checked for consistency across the individual studies contributing to the meta-analysis. Hardy-Weinberg equilibrium p values were calculated and cluster plots from the joint calling were verified for the reported associations (Figure S1). Fasting glucose at baseline (between 1987 and 1989) in ARIC EA and exam 5 (between 1991 and 1995) in FHS was tested for association with rs145464906 in *ANGPTL8* by linear regression adjusting for age, sex, and PCs.

Population Structure

Each study identified components to correct for population structure in their study and used these components as covariates in all association analyses.

Conditional Analysis

The allele dosages (0–2 copies) of the top previously identified GWAS variants in each region were used as additional covariates in the association model.

Statistical Significance

For single-variant association, we set the significance threshold to $<3 \times 10^{-8}$, corresponding to a Bonferroni correction for 1,485,864 tests (3 phenotypes × 247,644 variants on the array × 2 ancestries). For the gene-based association, we set the significance threshold to $<2 \times 10^{-7}$, corresponding to a Bonferroni correction for 316,332 tests (3 phenotypes × 17,574 genes on the array × 3 tests × 2 ancestries).

Annotation

We used dbNSFP v.2.0 to annotate the variants.[17]

Clinical CHD Association Analysis

Individuals from AGES, ARIC, CHS, FHS, MESA, Health ABC, RS1, WHI, MDC-CVA, IPM, ATVB/VHS, Ottawa, Procardis, Duke, and Penn contributed to the CHD analysis in EA. Individuals from ARIC, CHS, MESA, Health ABC, WHI, and IPM contributed to the CHD analysis in AA. All individuals were genotyped on the HumanExome BeadChip. Counts of number of CHD events in carriers and noncarriers of the four reported lipid variants were obtained from each available study. A Cochran-Mantel-Haenszel test was performed to associate the four reported lipid variants with CHD by using the R metafor package across the contributing studies.

Power Calculation

Power for the CHD association was calculated via the case-control for discrete traits option in the Genetic Power Calculator.

Mouse Studies Involving PCSK7

We created an adeno-associated virus 8 (AAV8) vector encoding the human *PCSK7* coding region (cDNA) driven by the liver-specific thyroxine-binding globulin (TBG) promoter. An AAV8 vector lacking any transgene was used as a control. Separate groups of 10- to 12-week-old wild-type C57BL/6J male mice (six to seven per group) were injected via the peritoneal route with 1×10^{12} vector genomes/mouse of the relevant vectors. Mice were fed a regular chow diet (Purina LabDiet 5010) throughout the study. Plasma samples after 4 hr of fasting were taken from the mice immediately prior to vector administration, as well as 7 and 14 days after AAV injection for analysis of lipids. Lipid measurements were performed on a Roche Cobas-Mira autoanalyzer (Roche Diagnostic Systems) with Wako Chemicals reagents. Mice were sacrificed at 14 days after AAV administration. All animal procedures were performed according to the regulations of, and with the prior approval of, the University of Pennsylvania Animal Care and Use Committee (IACUC). We repeated this experiment in a separate design comparing plasma lipids at baseline and 14 days after injection of an AAV8 vector encoding the mouse *Pcsk7* cDNA versus control in wild-type C57BL/6J male mice (data not shown).

Results

Coverage of Exome Array

We evaluated the coverage of Exome Array in samples independent from those used to design the array. Based on exome sequences from 3,173 EA and 2,408 AA independent participants, we estimate that the Illumina Exome Array captures 78% of nonsynonymous coding and splice site variation with >1:1,000 allele frequency in EA individuals and 71% in AA individuals. Therefore, the array provides good coverage for low-frequency DNA variation and because of its low cost can be assayed in a large number of individuals.

Exome-sequencing variants not captured by the Exome Array may have been dropped during the design of the array. To address this possibility, we compared the variants discovered from exome sequencing to proposed content of the array (before variants failed design). We estimate that 95% of the variation in EA participants (and 85% of the variation in AA) with frequency >1:1,000 is captured by the proposed content of the array.

Study Participants and Genotypes

Clinical characteristics of the 56,538 analyzed study subjects are summarized in Table S1. Of the 247,644 variants that passed quality control criteria, 85% (n = 209,756) are polymorphic in the EA participants and 82% (n = 202,255) are polymorphic in the AA participants. Approximately 90% (n = 188,480) of the polymorphic variants are annotated[17] as nonsynonymous (nonsense or missense) or splice variants in the EA participants, and 89% (n = 180,908) of the polymorphic variants are annotated as such in the AA participants (Table 1).

Single-Variant Association

We tested each variant individually for association with blood lipid levels separately in each cohort and association summary statistics across cohorts were combined by fixed effects meta-analysis, separately within each ancestry group. There was no evidence of inflation in the association test statistics (Figure S2).

We replicated previously reported associations with common and low-frequency variants (Table 2) in both EA and AA participants. For example, we found that variants in *PCSK9* (c.137G>T [p.Arg46Leu], [rs11591147] in EA and c.2037C>A [p.Cys679*], [rs28362286] in AA) were associated with lower LDL-C (−17 mg/dl; $p = 3 \times 10^{-59}$ and −40 mg/dl; $p = 2 \times 10^{-57}$, respectively).

We discovered four associations of low-frequency variants with either HDL-C and/or TG that met our a priori significance threshold of $p < 3 \times 10^{-8}$ and not previously reported in the literature. Two signals emerged from EA participants and two from AA participants (Table 3). In contrast to HDL-C and TG, we did not discover any new genes where low-frequency or rare DNA sequence variants significantly associated with LDL-C. Below, we describe each of the four new associations.

First, in EA participants, we found an association of blood HDL-C with a 0.1% premature stop codon at the chromosome 19 open reading frame 80 gene (*C19orf80*, aliases include *ANGPTL8*, lipasin, and betatrophin; c.361C>T [p.Gln121*]; rs145464906). Carriers of *ANGPTL8* rs145464906 had 10 mg/dl higher HDL-C ($p = 5 \times 10^{-11}$), lower TG (−15%; p = 0.003), and nonsignificantly lower LDL-C (−5.8 mg/dl; p = 0.13) than did noncarriers of this variant (Table 4). *ANGPTL8* rs145464906 is seen at a 0.01% frequency in AA participants and we were not able to reliably estimate its effect on lipid measures in this group.

Table 1. Number of Exome Array Variants Available for Analysis by Variant Type

Variant Type	All Polymorphic Sites	MAF < 0.1%	MAF 0.1%–5%	MAF > 5%
42,208 European Ancestry Samples				
Nonsynonymous	175,444	130,553	32,501	12,390
Nonsense/splice	13,036	10,694	1,686	656
Synonymous	5,444	3,710	978	756
Intronic/Intergenic	14,205	139	1,186	12,880
Other	1,627	156	199	1,272
14,330 African Ancestry Samples				
Nonsynonymous	169,140	91,083	61,809	16,248
Nonsense/splice	11,768	7,729	3,177	862
Synonymous	5,398	2,341	2,098	959
Intronic/Intergenic	14,169	56	650	13,463
Other	1,780	116	356	1,308

Variant type was determined based on dbNSFP v.2.0 annotations. Abbreviation is as follows: MAF, minor allele frequency. Other category includes variants labeled as downstream (n = 187), ncRNA_exonic (n = 111), ncRNA_intronic (n = 447), ncRNA_splicing (n = 1), ncRNA_UTR3 (n = 8), _UTR5 (n = 1), upstream (n = 181), upstream;downstream (n = 8), UTR3 (n = 518), UTR5 (n = 77).

ANGPTL8 rs145464906 is located in a genomic region previously associated with lipid levels in GWASs (rs737337 at the *DOCK6* [MIM 614194] locus; c.2136A>G [p.(=)]).[18] An analysis conditioning on rs737337 in *DOCK6* revealed rs145464906 to be an independent association ($p_{conditional} = 5.5 \times 10^{-13}$). Another more common coding variant in *ANGPTL8* (8% frequency; rs2278426; c.175C>T [p.Arg59Trp]) has been associated with low LDL-C and low HDL-C.[19] This variant is not present on the exome array, but the correlation between rs2278426 and rs145464906 is low at 0.08 and conditional analyses confirm that rs2278426 and rs145464906 are independent association signals (data not shown).

Angplt8-null mice display lower blood TG and functional studies have suggested that ANGPTL8 may activate ANGPTL3 and thereby regulate lipoprotein metabolism.[19,20] Of note, based on studies in mice, another proposed role for ANGPTL8 is as a hormone that promotes pancreatic β cell proliferation, expands β cell mass, and improves glucose tolerance.[21] These studies raise the hypothesis that loss of ANGPTL8 function might worsen measures of glucose tolerance. We studied the association of ANGPTL8 rs145464906 with fasting plasma glucose levels among 10,642 EA participants in the ARIC study and 3,112 EA participants from FHS and observed no evidence for association in either study. In ARIC, plasma glucose did not differ between the carriers of the rs145464906 allele (n = 23) and noncarriers (n = 10,620) (beta = −3.3 mg/dl; SE = 5.8 mg/dl; p = 0.57). In FHS, carriers of rs145464906 (n = 13) had a mean fasting glucose of 88.2 mg/dl whereas noncarriers had mean glucose of 99.9 mg/dl (p = 0.13).

A second discovery among EA participants is a significant association between a 1% frequency variant in the Platelet-Activating Factor Acetylhydrolase 1b, Catalytic Subunit 2 gene (*PAFAH1B2* [MIM 602508]; c.482C>T [p.Ser161Leu]; rs186808413) and HDL-C. Carriers of rs186808413 had 3 mg/dl higher HDL-C ($p = 2.2 \times 10^{-10}$), lower TG (−10%; $p = 2.3 \times 10^{-9}$), and marginally lower LDL-C (−3 mg/dl; p = 0.01) than did noncarriers (Table 4). In AA participants, the direction of association between HDL-C and *PAFAH1B2* rs186808413 (0.2% frequency in AA participants) was consistent with the EA results, but not significant (1 mg/dl; p = 0.58). *PAFAH1B2* is located near the chromosome 11 gene cluster involving *APOA1/C3/A4/A5*, a region where several genes regulate TG. Conditional analysis adjusting for six previously studied variants in this region (rs964184, rs3135506, rs2266788, rs76353203, rs147210663, rs140621530) showed *PAFAH1B2* rs186808413 to be an independent association signal ($p_{conditional} = 2.1 \times 10^{-11}$). Platelet-activating factor (PAF) is a lipid messenger functioning in many cellular processes.[22] Plasma platelet-activating factor-acetyl hydrolase (PAF-AH) belongs to a subfamily of phospholipases A2 that remove the sn-2 acetyl group and inactivate a number of oxidized lipids,[23,24] but intracellular type I (PAF-AH-Ib) is structurally distinct and may form a part of a signal transduction pathway.[22]

Third, among AA participants, we found an association of blood TG with a 2% frequency variant in the Collagen, Type XVIII, Alpha 1 gene (*COL18A1* [MIM 120328]; c.331G>A [p.Gly111Arg]; rs114139997), where carriers of rs114139997 had 16% lower TG than did noncarriers ($p = 2 \times 10^{-16}$). *COL18A1* rs114139997 was also marginally associated with higher HDL-C (2 mg/dl; $p = 4 \times 10^{-4}$) (Table 4). The frequency of *COL18A1* rs114139997 is 0.003% in EA participants and we were not able to reliably estimate the effect on lipid measures in this group. COL18A1 is a basement membrane proteoglycan with a

Table 2. Top Association Results for Low-Frequency Variants Based on Level of Statistical Significance

Gene	dbSNP ID	Mutation (Substitution)	Chr: Position[a]	MAF[b]	Beta[c]	p Value
HDL-C – EA (n = 42,208)						
ANGPTL4	rs116843064	c.118G>A (p.Glu40Lys)	19: 8,429,323	2.01%	4 mg/dl	1.7×10^{-29}
LIPG	rs77960347	c.1187A>G (p.Asn396Ser)	18: 47,109,955	1.27%	5 mg/dl	5.1×10^{-27}
LPL	rs268	c.953A>G (p.Asn318Ser)	8: 19,813,529	1.78%	−3 mg/dl	2.4×10^{-19}
LDL-C – EA (n = 39,186)						
PCSK9	rs11591147	c.137G>T (p.Arg46Leu)	1: 55,505,647	1.54%	−17 mg/dl	2.7×10^{-59}
APOB	rs5742904	c.10580G>A (p.Arg3527Gln)	2: 21,229,160	0.05%	71 mg/dl	5.6×10^{-34}
CBLC	rs3208856	c.1075C>T (p.His359Tyr)	19: 45,296,806	3.43%	−8 mg/dl	6.2×10^{-30}
Triglycerides – EA (n = 39,859)						
ANGPTL4	rs116843064	c.118G>A (p.Glu40Lys)	19: 8,429,323	2.02%	−15%	2.9×10^{-37}
LPL	rs268	c.953A>G (p.Asn318Ser)	8: 19,813,529	1.76%	14%	1.2×10^{-22}
MAP1A	rs55707100	c.7046C>T (p.Pro2349Leu)	15: 43,820,717	3.25%	9%	1.4×10^{-17}
HDL-C – AA (n = 14,330)						
PCSK7	rs142953140	c.1511G>A (p.Arg504His)	11: 117,089,205	0.2%	17 mg/dl	3.4×10^{-20}
CETP	rs34119551	c.17T>A (p.Val6Asp)	16: 56,995,908	0.24%	16 mg/dl	2.0×10^{-19}
LCAT	rs35673026	c.340G>A (p.Val114Met)	16: 67,976,851	0.34%	10 mg/dl	2.0×10^{-10}
LDL-C – AA (n = 14,227)						
PCSK9	rs28362286	c.2037C>A (p.Cys679*)	1: 55,529,215	0.87%	−40 mg/dl	1.5×10^{-57}
PCSK9	rs67608943	c.426C>G (p.Tyr142*)	1: 55,512,222	0.30%	−35 mg/dl	2.6×10^{-16}
APOE	rs769455	c.487C>T (p.Arg163Cys)	19: 45,412,040	1.93%	−12 mg/dl	3.6×10^{-12}
Triglycerides – AA (n = 14,351)						
APOE	rs769455	c.487C>T (p.Arg163Cys)	19: 45,412,040	1.93%	21%	2.3×10^{-18}
COL18A1	rs114139997	c.331G>A (p.Gly111Arg)	21: 46,875,775	1.93%	−16%	1.6×10^{-11}
ZNF259	rs35120633	c.791C>T (p.Ala264Val)	11: 116,655,600	2.96%	13%	2.7×10^{-12}

Results are based on 42,208 European ancestry (EA) individuals and 14,330 African ancestry (AA) individuals.
[a] Chr: Position is reported in UCSC Genome Browser build hg19.
[b] MAF, minor allele frequency.
[c] Beta is based on the geometric mean for triglycerides.

recently established role in presenting the enzyme lipoprotein lipase to the luminal side of the vascular endothelium.[25] Mice deleted for *Col18a1* (*Col18a1*$^{-/-}$) were shown to have hypertriglyceridemia resulting from decreased lipoprotein lipase activity, and humans with homozygous deficiency of COL18A1 (Knobloch syndrome [MIM 267750]) have been observed to have higher blood TG than do normal individuals.[25]

Finally, in AA participants, we also identified an association of blood HDL-C with a 0.2% frequency variant at the proprotein convertase subtilisin/kexin type 7 serine protease gene (*PCSK7* [MIM 604874]; c.1511G>A [p.Arg504His]; rs142953140). Carriers of the *PCSK7* rs142953140 mutation had 17 mg/dl higher HDL-C levels than did noncarriers ($p = 5 \times 10^{-20}$). *PCSK7* rs142953140 was also associated with lower TG (−30%; $p = 2 \times 10^{-9}$) and nominally associated with lower LDL-C (−11.5 mg/dl; $p = 0.02$) among the AA participants (Table 4). *PCSK7* is located near the chromosome 11 gene cluster involving *APOA1/C3/A4/A5*, a region where several genes regulate HDL-C and TG. Conditional analysis adjusting for six known variants in this region (rs964184, rs3135506, rs2266788, rs76353203, rs147210663, rs140621530) showed *PCSK7* rs142953140 to be an independent association signal ($p_{\text{conditional}} = 3.4 \times 10^{-20}$). *PCSK7* rs142953140 was not polymorphic in individuals of European ancestry. *PCSK7* belongs to the same family of serine proteases as does *PCSK9*, and a putative link between *PCSK7* and lipoprotein metabolism was recently established in vitro.[26,27] In cultured cells, PCSK7 cleaved angiopoietin-like protein 4 (ANGPTL4) and activated its ability to inhibit lipoprotein lipase.

We studied the functional consequence of overexpression of human *PCSK7* in mice and found that mice overexpressing *PCSK7* in liver have lower HDL-C and higher TG compared to controls (Figure 1), suggesting that gain

Table 3. Variant Associations with Blood Lipids that Have Not Been Previously Reported

Trait	Gene	rsID	Mutation (Substitution)	Beta[a]	p Value	Conditional Variants	$p_{conditional}$	EA MAF	AA MAF
Ancestry: EA									
HDL-C	*ANGPTL8*	rs145464906	c.361C>T (p.Gln121*)	10 mg/dl	5.1×10^{-11}	rs737337	5.5×10^{-13}	0.1%	0.01%
HDL-C	*PAFAH1B2*	rs186808413	c.482C>T (p.Ser161Leu)	3 mg/dl	2.2×10^{-10}	rs964184, rs3135506, rs2266788, rs76353203, rs14721066, rs140621530	2.1×10^{-11}	1.1%	0.2%
Ancestry: AA									
TG	*COL18A1*	rs114139997	c.331G>A (p.Gly111Arg)	−16%	1.6×10^{-16}	–	–	0.003%	1.9%
HDL-C	*PCSK7*	rs142953140	c.1511G>A (p.Arg504His)	17 mg/dl	4.9×10^{-20}	rs964184, rs3135506, rs2266788, rs76353203, rs14721066, rs140621530	3.4×10^{-20}	0%	0.2%

Results are based on 42,208 European ancestry (EA) individuals and 14,330 African ancestry (AA) individuals. Abbreviations are as follows: TG, triglycerides; HDL-C, high-density lipoprotein cholesterol; MAF, minor allele frequency.
[a] Effect estimate for triglycerides is based on the geometric mean.

of PCSK7 function decreases HDL-C and increases TG in vivo. Further studies are warranted to determine whether reduction of hepatic PCSK7, for example through *Pcsk7* knockdown in mice, will result in the same lipid profile as that of human subjects with the *PCSK7* rs142953140 mutation.

Gene-Based Association

In contrast to low-frequency variants, the alternative alleles at rare variants occur too infrequently to be analyzed individually and must be evaluated by aggregating into sets. Here, typically, the unit of analysis is a gene. We used two methods to perform gene-based analyses incorporating variants annotated as nonsynonymous or splice site: the sum of the number of minor alleles[15] including variants with a MAF <1% or MAF <0.1% and the sequence kernel association test (SKAT),[16] a test that considers effect sizes in both directions, including variants with a MAF <5%. Gene-based association results were well calibrated (Figure S3). We were able to replicate genes previously reported to be associated with blood lipid levels (Table 5). For example, multiple rare alleles at *LDLR* (MIM 606945) were strongly associated with blood LDL-C ($p = 5 \times 10^{-10}$). No new genetic associations were identified through the gene-based analyses.

Association with CHD

To assess whether the four newly associated low-frequency coding variants also relate to clinical cardiovascular disease, we tested association of each variant with CHD in 63,470 individuals from 15 EA studies and 13,772 individuals from 7 AA studies (Table S2). Of these participants, 14,201 EA and 2,380 AA individuals were affected with CHD.

Table 4. Association Results in Other Lipid Traits for the Reported Associations

Gene	rsID	Trait	EA Beta	EA p Value	AA Beta	AA p Value
ANGPTL8	rs145464906	HDL-C	10 mg/dl	5.1×10^{-11}	–	–
		TG	−15%	0.003	–	–
		LDL-C	−5.8 mg/dl	0.13	–	–
PAFAH1B2	rs186808413	HDL-C	3 mg/dl	2.2×10^{-10}	1 mg/dl	0.58
		TG	−10%	2.3×10^{-09}	−4%	0.48
		LDL-C	−3 mg/dl	0.01	−2.6 md/dl	0.58
COL18A1	rs114139997	HDL-C	–	–	2.2 mg/dl	4.1×10^{-4}
		TG	–	–	−16%	1.6×10^{-16}
		LDL-C	–	–	−2.6 mg/dl	0.12
PCSK7	rs142953140	HDL-C	–	–	17 mg/dl	4.9×10^{-20}
		TG	–	–	−30%	1.5×10^{-09}
		LDL-C	–	–	−11.5 mg/dl	0.02

Abbreviations are as follows: TG, triglycerides; HDL-C, high-density lipoprotein cholesterol; LDL-C, low-density lipoprotein cholesterol; EA, European ancestry; AA, African ancestry; Beta, effect size.

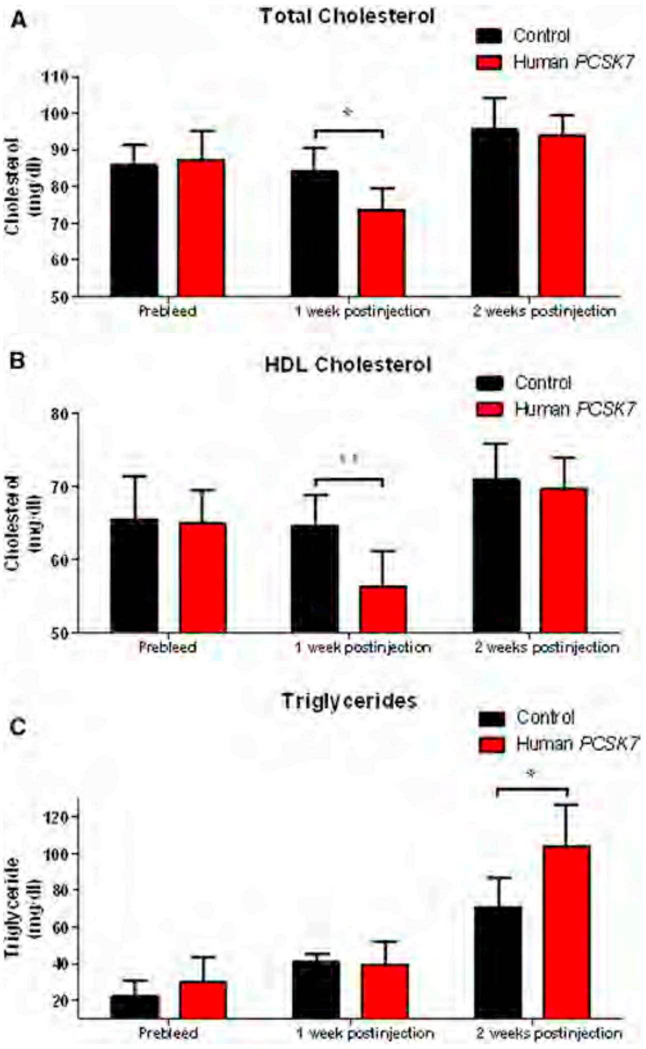

Figure 1. Effects of Human *PCSK7* Overexpression in Mouse Liver on Plasma Lipids
Plasma TC (A), HDL-C (B), and TG (C) were measured at baseline and at 7 and 14 days after injection of the human *PCSK7* or control AAV8 vectors in C57BL/6J male mice. Error bars show standard deviations. $^*p < 0.05$ and $^{**}p < 0.01$, Student's unpaired t test.

As a positive control, we confirmed that the *PCSK9* c.137T (c.137G>T [p.Arg46Leu]; rs11591147) allele leading to lower LDL-C was associated with reduced risk for CHD among EA participants (OR = 0.84, 95% CI = 0.74–0.95, p = 0.007) and *PCSK9* c.2037A (c.2037C>A [p.Cys679*]; rs28362286) allele leading to lower LDL-C was similarly associated with reduced risk for CHD among AA participants (OR = 0.40, 95% CI = 0.23–0.68, $p = 5.4 \times 10^{-4}$).

In contrast to the *PCSK9* variants, none of the four coding sequence variants at *ANGPTL8*, *PAFAH1B2*, *COL18A1*, or *PCSK7* were associated with risk for CHD (Table 6).

Table 5. Top Gene-Based Association Results Based on Level of Statistical Significance

Gene	p Value	Best Test	Beta[a]	SE	CMAF[b]	No. Variants[c]
LDL-EA						
PCSK9	1.81×10^{-62}	SKAT	–	–	0.0626	22
LDLR	4.9×10^{-10}	T1	15.36	2.47	0.0027	28
HDL-EA						
APOC3	3.2×10^{-19}	T1	11.75	1.31	0.0035	4
ANGPTL4	5.41×10^{-30}	SKAT	–	–	0.0283	11
LIPG	2.55×10^{-29}	SKAT	–	–	0.0162	12
LPL	5.76×10^{-29}	SKAT	–	–	0.0372	10
Triglycerides-EA						
APOC3	4.0×10^{-29}	T1	−0.41	0.05	0.0036	4
ANGPTL4	2.70×10^{-37}	SKAT	–	–	0.0286	11
LPL	1.56×10^{-31}	SKAT	–	–	0.037	10
LDL-AA						
PCSK9	1.40×10^{-71}	SKAT	–	–	0.1295	25
APOE	2.65×10^{-12}	SKAT	–	–	0.0205	3
HDL-AA						
APOC3	9.5×10^{-12}	T1	10.14	1.49	0.0055	4
CETP	7.7×10^{-09}	T1	6.18	1.07	0.0065	7
Triglycerides-AA						
APOC3	2.9×10^{-19}	T1	−0.34	0.05	0.0055	4
APOE	2.26×10^{-18}	SKAT	–	–	0.0205	3

Abbreviations are as follows: TG, triglycerides; HDL-C, high-density lipoprotein cholesterol; LDL-C, low-density lipoprotein cholesterol; EA, European ancestry; AA, African ancestry; Beta, effect size; SE, standard error.
[a] Beta is in mg/dl units for LDL and HDL and in percent change for triglycerides.
[b] CMAF, cumulative minor allele frequency of the variants contributing to the test.
[c] No. variants, number of variants contributing to the test.

Discussion

The contribution of low-frequency DNA sequence variation to complex phenotypes such as blood lipids and CHD has been the subject of much debate. Some have argued that low-frequency variants with large effects may be instrumental in discovering genes and that such discoveries can lead to novel therapeutic targets. By using the Exome Array in >42,000 EA individuals and >14,000 AA individuals, we discovered four low-frequency variants with large effects on lipids, but none of these variants associated with risk for CHD.

Several limitations of our study deserve mention. We were not able to evaluate extremely rare variants that may be unique to individuals; exome or whole-genome sequencing is needed to capture this type of variation. As such, it remains possible that a burden of such very rare mutations could contribute to plasma lipid variation. If so, the sample sizes required to yield new rare variant discoveries are likely to be extraordinarily large.

The Exome Array is constrained to the coding and splice site variation observed in the ~12,000 individuals who comprised the initial exome sequencing discovery set.

Table 6. Association of Lipid Variants with Coronary Heart Disease

Gene	Mutation (Substitution)	rsID	Case Frequency	Control Frequency	Odds Ratio	p Value
Ancestry: EA						
ANGPTL8	c.361C>T (p.Gln121*l)	rs145464906	0.29%	0.27%	1.023	0.985
PAFAH1B2	c.482C>T (p.Ser161Leu)	rs186808413	2.05%	2.23%	0.905	0.170
Ancestry: AA						
PCSK7	c.1511G>A (p.Arg504His)	rs142953140	0.53%	0.47%	1.258	0.592
COL18A1	c.331G>A (p.Gly111Arg)	rs114139997	3.39%	3.38%	0.996	0.971

Association with CHD was performed in a total of 63,470 EA individuals and 13,772 AA individuals. 14,201 EA and 2,380 AA individuals developed CHD.

Furthermore, ~20% of the content contributed for design failed to be converted into genotyping assays and thus these variants are not present on the Exome Array.

The lack of significant association of our reported low-frequency variants with CHD may be due to insufficient statistical power. For the CHD association testing among EA participants, we had >80% power at $\alpha = 0.05$ to detect an odds ratio outside the range (0.86, 1.14) with a 2% frequency variant, and an odds ratio outside the range (0.74, 1.29) with a 0.5% frequency variant. Among AA participants, we had >80% power at $\alpha = 0.05$ to detect an odds ratio outside the range (0.69, 1.35) with a 2% frequency variant, and an odds ratio outside the range (0.43, 1.73) with a 0.5% frequency variant.

Of note, all four of our reported loci were associated with HDL-C, which may not be a causal risk factor for clinical CHD, and this observation could explain the lack of association with CHD.[28] Finally, we do not yet fully understand the biologic mechanism by which the genes reported here affect blood lipoproteins.

In summary, by using the Exome Array, we identified four low-frequency coding variants in *ANGPTL8, PAFAH1B2, COL18A1*, and *PCSK7* that altered plasma HDL-C and/or TG but did not affect risk for CHD. These results suggest that the example of *PCSK9* with low-frequency alleles that affect both plasma lipids and CHD is likely to be an exception rather than a paradigm.

Supplemental Data

Supplemental Data include descriptions of study samples, Supplemental Acknowledgments, three figures, and two tables and can be found with this article online at http://www.cell.com/AJHG/.

Acknowledgments

The authors wish to acknowledge the support of the National Heart, Lung, and Blood Institute (NHLBI) and the contributions of the research institutions, study investigators, field staff, and study participants in creating this resource for biomedical research. Funding for GO ESP was provided by NHLBI grants RC2 HL-103010 (HeartGO), RC2 HL-102923 (LungGO), and RC2 HL-102924 (WHISP). The exome sequencing was performed through NHLBI grants RC2 HL-102925 (BroadGO) and RC2 HL-102926 (SeattleGO). Infrastructure for the CHARGE Consortium is supported, in part, by the National Heart, Lung, and Blood Institute (grant HL105756). G.M.P. is supported by award number T32HL007208 from the NHLBI. S.K. is supported by a Research Scholar award from the Massachusetts General Hospital (MGH), the Howard Goodman Fellowship from MGH, the Donovan Family Foundation, R01HL107816, and a grant from Fondation Leducq. Exome Array genotyping in case-control studies of coronary heart disease was supported by NIH RC2 HL-102925 and an investigator-initiated research grant from Merck to S.K. N.O.S. is supported, in part, by a career development award from the NIH/NHLBI K08-HL114642. A.D. is supported by NWO grant (veni, 916.12.154) and the EUR Fellowship. The content is solely the responsibility of the authors and does not necessarily represent the official views of the NHLBI or NIH. A full listing of acknowledgements is provided in Supplemental Data.

Received: November 8, 2013
Accepted: January 9, 2014
Published: February 6, 2014

Web Resources

The URLs for data presented herein are as follows:

dbNSFP v.2.0, https://sites.google.com/site/jpopgen/dbNSFP
Exome Array site information, ftp://share.sph.umich.edu/exomeChip/
Exome Chip Design, http://genome.sph.umich.edu/wiki/Exome_Chip_Design
ExomeChip – Charge Consortium, http://www.chargeconsortium.com/main/exomechip
Genetic Power Calculator, http://pngu.mgh.harvard.edu/~purcell/gpc/
Online Mendelian Inheritance in Man (OMIM), http://www.omim.org/
R metafor package, http://cran.r-project.org/web/packages/metafor/index.html
seqMeta, http://cran.r-project.org/web/packages/seqMeta/
UCSC Genome Browser, http://genome.ucsc.edu

References

1. Stein, E.A., Mellis, S., Yancopoulos, G.D., Stahl, N., Logan, D., Smith, W.B., Lisbon, E., Gutierrez, M., Webb, C., Wu, R., et al. (2012). Effect of a monoclonal antibody to PCSK9 on LDL cholesterol. N. Engl. J. Med. *366*, 1108–1118.

2. Abifadel, M., Varret, M., Rabès, J.P., Allard, D., Ouguerram, K., Devillers, M., Cruaud, C., Benjannet, S., Wickham, L., Erlich, D., et al. (2003). Mutations in PCSK9 cause autosomal dominant hypercholesterolemia. Nat. Genet. *34*, 154–156.
3. Cohen, J., Pertsemlidis, A., Kotowski, I.K., Graham, R., Garcia, C.K., and Hobbs, H.H. (2005). Low LDL cholesterol in individuals of African descent resulting from frequent nonsense mutations in PCSK9. Nat. Genet. *37*, 161–165.
4. Cohen, J.C., Boerwinkle, E., Mosley, T.H., Jr., and Hobbs, H.H. (2006). Sequence variations in PCSK9, low LDL, and protection against coronary heart disease. N. Engl. J. Med. *354*, 1264–1272.
5. Cohen, J.C., and Hobbs, H.H. (2013). Genetics. Simple genetics for a complex disease. Science *340*, 689–690.
6. Kiezun, A., Garimella, K., Do, R., Stitziel, N.O., Neale, B.M., McLaren, P.J., Gupta, N., Sklar, P., Sullivan, P.F., Moran, J.L., et al. (2012). Exome sequencing and the genetic basis of complex traits. Nat. Genet. *44*, 623–630.
7. Psaty, B.M., O'Donnell, C.J., Gudnason, V., Lunetta, K.L., Folsom, A.R., Rotter, J.I., Uitterlinden, A.G., Harris, T.B., Witteman, J.C., and Boerwinkle, E.; CHARGE Consortium (2009). Cohorts for Heart and Aging Research in Genomic Epidemiology (CHARGE) Consortium: Design of prospective meta-analyses of genome-wide association studies from 5 cohorts. Circ Cardiovasc Genet *2*, 73–80.
8. Grove, M.L., Yu, B., Cochran, B.J., Haritunians, T., Bis, J.C., Taylor, K.D., Hansen, M., Borecki, I.B., Cupples, L.A., Fornage, M., et al. (2013). Best practices and joint calling of the HumanExome BeadChip: the CHARGE Consortium. PLoS ONE *8*, e68095.
9. Goldstein, J.I., Crenshaw, A., Carey, J., Grant, G.B., Maguire, J., Fromer, M., O'Dushlaine, C., Moran, J.L., Chambert, K., Stevens, C., et al.; Swedish Schizophrenia Consortium; ARRA Autism Sequencing Consortium (2012). zCall: a rare variant caller for array-based genotyping: genetics and population analysis. Bioinformatics *28*, 2543–2545.
10. Tobin, M.D., Sheehan, N.A., Scurrah, K.J., and Burton, P.R. (2005). Adjusting for treatment effects in studies of quantitative traits: antihypertensive therapy and systolic blood pressure. Stat. Med. *24*, 2911–2935.
11. Baigent, C., Keech, A., Kearney, P.M., Blackwell, L., Buck, G., Pollicino, C., Kirby, A., Sourjina, T., Peto, R., Collins, R., and Simes, R.; Cholesterol Treatment Trialists' (CTT) Collaborators (2005). Efficacy and safety of cholesterol-lowering treatment: prospective meta-analysis of data from 90,056 participants in 14 randomised trials of statins. Lancet *366*, 1267–1278.
12. Scandinavian Simvastatin Survival Study Group (1994). Randomised trial of cholesterol lowering in 4444 patients with coronary heart disease: the Scandinavian Simvastatin Survival Study (4S). Lancet *344*, 1383–1389.
13. Friedewald, W.T., Levy, R.I., and Fredrickson, D.S. (1972). Estimation of the concentration of low-density lipoprotein cholesterol in plasma, without use of the preparative ultracentrifuge. Clin. Chem. *18*, 499–502.
14. Warnick, G.R., Knopp, R.H., Fitzpatrick, V., and Branson, L. (1990). Estimating low-density lipoprotein cholesterol by the Friedewald equation is adequate for classifying patients on the basis of nationally recommended cutpoints. Clin. Chem. *36*, 15–19.
15. Li, B., and Leal, S.M. (2008). Methods for detecting associations with rare variants for common diseases: application to analysis of sequence data. Am. J. Hum. Genet. *83*, 311–321.
16. Wu, M.C., Lee, S., Cai, T., Li, Y., Boehnke, M., and Lin, X. (2011). Rare-variant association testing for sequencing data with the sequence kernel association test. Am. J. Hum. Genet. *89*, 82–93.
17. Liu, X., Jian, X., and Boerwinkle, E. (2013). dbNSFP v2.0: a database of human non-synonymous SNVs and their functional predictions and annotations. Hum. Mutat. *34*, E2393–E2402.
18. Teslovich, T.M., Musunuru, K., Smith, A.V., Edmondson, A.C., Stylianou, I.M., Koseki, M., Pirruccello, J.P., Ripatti, S., Chasman, D.I., Willer, C.J., et al. (2010). Biological, clinical and population relevance of 95 loci for blood lipids. Nature *466*, 707–713.
19. Quagliarini, F., Wang, Y., Kozlitina, J., Grishin, N.V., Hyde, R., Boerwinkle, E., Valenzuela, D.M., Murphy, A.J., Cohen, J.C., and Hobbs, H.H. (2012). Atypical angiopoietin-like protein that regulates ANGPTL3. Proc. Natl. Acad. Sci. USA *109*, 19751–19756.
20. Zhang, R., and Abou-Samra, A.B. (2013). Emerging roles of Lipasin as a critical lipid regulator. Biochem. Biophys. Res. Commun. *432*, 401–405.
21. Yi, P., Park, J.S., and Melton, D.A. (2013). Betatrophin: a hormone that controls pancreatic β cell proliferation. Cell *153*, 747–758.
22. Ho, Y.S., Swenson, L., Derewenda, U., Serre, L., Wei, Y., Dauter, Z., Hattori, M., Adachi, T., Aoki, J., Arai, H., et al. (1997). Brain acetylhydrolase that inactivates platelet-activating factor is a G-protein-like trimer. Nature *385*, 89–93.
23. Stafforini, D.M., McIntyre, T.M., Zimmerman, G.A., and Prescott, S.M. (1997). Platelet-activating factor acetylhydrolases. J. Biol. Chem. *272*, 17895–17898.
24. Derewenda, Z.S., and Derewenda, U. (1998). The structure and function of platelet-activating factor acetylhydrolases. Cell. Mol. Life Sci. *54*, 446–455.
25. Bishop, J.R., Passos-Bueno, M.R., Fong, L., Stanford, K.I., Gonzales, J.C., Yeh, E., Young, S.G., Bensadoun, A., Witztum, J.L., Esko, J.D., and Moulton, K.S. (2010). Deletion of the basement membrane heparan sulfate proteoglycan type XVIII collagen causes hypertriglyceridemia in mice and humans. PLoS ONE *5*, e13919.
26. Oexle, K., Ried, J.S., Hicks, A.A., Tanaka, T., Hayward, C., Bruegel, M., Gögele, M., Lichtner, P., Müller-Myhsok, B., Döring, A., et al. (2011). Novel association to the proprotein convertase PCSK7 gene locus revealed by analysing soluble transferrin receptor (sTfR) levels. Hum. Mol. Genet. *20*, 1042–1047.
27. Seidah, N.G., Khatib, A.M., and Prat, A. (2006). The proprotein convertases and their implication in sterol and/or lipid metabolism. Biol. Chem. *387*, 871–877.
28. Voight, B.F., Peloso, G.M., Orho-Melander, M., Frikke-Schmidt, R., Barbalic, M., Jensen, M.K., Hindy, G., Hólm, H., Ding, E.L., Johnson, T., et al. (2012). Plasma HDL cholesterol and risk of myocardial infarction: a mendelian randomisation study. Lancet *380*, 572–580.

Example qualifying exam (Ph.D.) and comprehensive exam (M.S.) questions pertaining to Gong et al. (2013) *American Journal of Human Genetics*.

---

1. Authors state that "it is still unclear whether these GWAS loci [that were implicated in GWASs of European-ancestry populations] can be generalized to other ethnic groups, such as African Americans." Do you agree or disagree with this assertion? Explain why or why not.

2. Studies have shown that obesity is highly genetic, with heritability estimates ranging from 40-70%. Furthermore, the prevalence of worldwide obesity has increased sharply over recent decades. Are these two observations conflicting? Does the recent increase in obesity indicate recent changes in the genetic composition of the human population, worldwide?

3. Investigators performed genetic imputation for the WHI SHARe cohort. In brief, 1,962 women serving as a reference panel were genotyped for both (1) the Metabochip custom panel of SNPs at putative BMI loci, and (2) the (less-dense) Affymetrix 6.0 platform. Another 6,326 women were genotyped only for the Affymetrix platform. Imputation of the Metbochip SNPs was performed for the 6,326 women. Explain the logical basis of imputation, what the investigators stood to gain from this analysis, and whether you think this was a good approach? What could the investigators have done to assess the accuracy of the imputed genotypes?

4. Authors used the p-value threshold of 5.8×10^{-5} for statistical significance. This is a considerably smaller p-value threshold than 0.05. Explain why investigators used the stricter p-value threshold.

5. Authors were careful to model population structure (i.e., principal components of ancestry). Given that their samples were all African American, do you think this approach was necessary?

6. The investigators claim that differences in the linkage disequilibrium patterns between European ancestry and African ancestry population can aid in narrowing the association signals. Explain the logic behind this approach. What is the purpose of narrowing the association signal? Were investigators successful in this effort?

7. The investigators repeated their analysis in sex-stratified samples. Why did they do this?

ARTICLE

Fine Mapping and Identification of BMI Loci in African Americans

Jian Gong,[1,*] Fredrick Schumacher,[9] Unhee Lim,[8] Lucia A. Hindorff,[10] Jeff Haessler,[1] Steven Buyske,[4,5] Christopher S. Carlson,[1] Stephanie Rosse,[1] Petra Bůžková,[19] Myriam Fornage,[23] Myron Gross,[24] Nathan Pankratz,[24] James S. Pankow,[25] Pamela J. Schreiner,[25] Richard Cooper,[13] Georg Ehret,[11,12] C. Charles Gu,[17] Denise Houston,[18] Marguerite R. Irvin,[16] Rebecca Jackson,[6] Lew Kuller,[7] Brian Henderson,[9] Iona Cheng,[27] Lynne Wilkens,[8] Mark Leppert,[15] Cora E. Lewis,[14] Rongling Li,[10] Khanh-Dung H. Nguyen,[11] Robert Goodloe,[22] Eric Farber-Eger,[22] Jonathan Boston,[22] Holli H. Dilks,[22] Marylyn D. Ritchie,[20] Jay Fowke,[21,22] Loreall Pooler,[9] Misa Graff,[3] Lindsay Fernandez-Rhodes,[3] Barbara Cochrane,[26] Eric Boerwinkle,[23] Charles Kooperberg,[1] Tara C. Matise,[4] Loic Le Marchand,[8] Dana C. Crawford,[22] Christopher A. Haiman,[9] Kari E. North,[2,3] and Ulrike Peters[1,*]

Genome-wide association studies (GWASs) primarily performed in European-ancestry (EA) populations have identified numerous loci associated with body mass index (BMI). However, it is still unclear whether these GWAS loci can be generalized to other ethnic groups, such as African Americans (AAs). Furthermore, the putative functional variant or variants in these loci mostly remain under investigation. The overall lower linkage disequilibrium in AA compared to EA populations provides the opportunity to narrow in or fine-map these BMI-related loci. Therefore, we used the Metabochip to densely genotype and evaluate 21 BMI GWAS loci identified in EA studies in 29,151 AAs from the Population Architecture using Genomics and Epidemiology (PAGE) study. Eight of the 21 loci (*SEC16B, TMEM18, ETV5, GNPDA2, TFAP2B, BDNF, FTO*, and *MC4R*) were found to be associated with BMI in AAs at 5.8×10^{-5}. Within seven out of these eight loci, we found that, on average, a substantially smaller number of variants was correlated ($r^2 > 0.5$) with the most significant SNP in AA than in EA populations (16 versus 55). Conditional analyses revealed *GNPDA2* harboring a potential additional independent signal. Moreover, Metabochip-wide discovery analyses revealed two BMI-related loci, *BRE* (rs116612809, $p = 3.6 \times 10^{-8}$) and *DHX34* (rs4802349, $p = 1.2 \times 10^{-7}$), which were significant when adjustment was made for the total number of SNPs tested across the chip. These results demonstrate that fine mapping in AAs is a powerful approach for both narrowing in on the underlying causal variants in known loci and discovering BMI-related loci.

Introduction

Obesity (MIM 601665) is a major risk factor for a number of chronic diseases, such as type 2 diabetes (MIM 125853), hyperlipidemia (MIM 144250), cardiovascular diseases, and several cancer types.[1,2] Worldwide obesity prevalence has nearly doubled since 1980, and in 2008 more than 1.4 billion adults worldwide were obese. In the United States, more than one-third of adults (35.7%) were obese in 2010.

Studies have shown that obesity is highly heritable; heritability is estimated to fall in the range of 40%–70%.[3,4] Genome-wide association studies (GWAS) have identified numerous loci associated with body mass index (BMI),[5–7] a common measure of obesity. However, most of these studies were performed among European-ancestry (EA) populations. It is still unclear whether previously identified GWAS loci are population specific or whether they can be generalized to other ethnic groups, such as African Americans (AAs). Furthermore, the overall lower linkage disequilibrium (LD) patterns in AA compared to EA populations can offer opportunities to narrow in or fine-map BMI-related loci.[8] This will help to reduce the number of variants for functional follow-up studies, which tend to

[1] Division of Public Health Sciences, Fred Hutchinson Cancer Research Center, Seattle, WA 98109, USA; [2] Carolina Center for Genome Sciences, University of North Carolina, Chapel Hill, NC 27514, USA; [3] Department of Epidemiology, School of Public Health, University of North Carolina at Chapel Hill, Chapel Hill, NC 27514, USA; [4] Department of Genetics, Rutgers University, Piscataway, NJ 08854, USA; [5] Department of Statistics and Biostatistics, Rutgers University, Piscataway, NJ 08854, USA; [6] Department of Internal Medicine, Ohio State Medical Center, Columbus, OH 43210, USA; [7] Department of Medicine, University of Pittsburgh, Pittsburgh, PA 15261, USA; [8] Epidemiology Program, University of Hawaii Cancer Center, Honolulu, HI 96813, USA; [9] Department of Preventive Medicine, Norris Comprehensive Cancer Center, Keck School of Medicine, University of Southern California, Los Angeles, CA 90089, USA; [10] Division of Genomic Medicine, National Human Genome Research Institute, National Institutes of Health, Bethesda, MD 20892, USA; [11] Center for Complex Disease Genomics, McKusick-Nathans Institute of Genetic Medicine, Johns Hopkins University School of Medicine, Baltimore, MD 21205, USA; [12] Division of Cardiology, Geneva University Hospital, Geneva, OH 44041, Switzerland; [13] Preventive Medicine and Epidemiology, Loyola University, Chicago, IL 60153, USA; [14] Department of Medicine, University of Alabama, Birmingham, AL 35294, USA; [15] Department of Human Genetics, University of Utah, Salt Lake City, UT 84112, USA; [16] Department of Biostatistics, University of Alabama, Birmingham, AL 35294, USA; [17] Department of Biostatistics, Washington University, St. Louis, MO 63110, USA; [18] Wake Forest University School of Medicine, Winston-Salem, NC 27157, USA; [19] Department of Biostatistics, University of Washington, Seattle, WA 98195, USA; [20] Pennsylvania State University, State College, PA 16801, USA; [21] Vanderbilt Epidemiology Center, Vanderbilt University Medical Center, Nashville, TN 37203, USA; [22] Center for Human Genetics Research, Vanderbilt University Medical Center, Nashville, TN, 37203, USA; [23] The Human Genetics Center and Institute of Molecular Medicine, The University of Texas Health Science Center at Houston, Houston, TX 77030, USA; [24] Masonic Cancer Center, University of Minnesota, Minneapolis, MN 55455, USA; [25] Division of Epidemiology & Community Health, School of Public Health, University of Minnesota, Minneapolis, MN 55455, USA; [26] Baylor College of Medicine, Houston, TX 77030, USA; [27] Cancer Prevention Institute of California, Fremont, CA 94538, USA

*Correspondence: jgong@fhcrc.org (J.G.), upeters@fhcrc.org (U.P.)

http://dx.doi.org/10.1016/j.ajhg.2013.08.012. ©2013 by The American Society of Human Genetics. All rights reserved.

be time and labor intensive. In addition, dense genotyping of the GWAS loci could aid the discovery of additional independent signals within the GWAS loci.

In this study, we densely genotyped 21 BMI loci identified in EA studies in 29,151 AAs from the Population Architecture using Genomics and Epidemiology (PAGE) consortium by using the Metabochip.[9] We aimed to fine-map the 21 known BMI loci in the AA population and search for additional independent signals associated with BMI. For validated loci in AAs, we evaluated whether weaker LD patterns in AAs can help narrow in on the underlying potential causal variants. In addition, because Metabochip was developed to test putative association signals for BMI and many obesity-related metabolic and cardiovascular traits and to fine-map established loci,[9] we also conducted a Metabochip-wide discovery-oriented analysis to search for potential BMI-associated loci.

Subjects and Methods

Study Population

The National Human Genome Research Institute funds the PAGE consortium to investigate the epidemiologic architecture of well-replicated genetic variants associated with human diseases or traits.[10] PAGE consists of a coordinating center and four consortia, Epidemiologic Architecture for Genes Linked to Environment (EAGLE), which is uses data from Vanderbilt University Medical Center's biorepository and links it to deidentified electronic medical records (BioVU); the Multiethnic Cohort Study (MEC); the Women's Health Initiative (WHI); and Causal Variants Across the Life Course (CALiCo), itself a consortium of five cohort studies—the Atherosclerosis Risk in Communities (ARIC) study, Coronary Artery Risk Development in Young Adults (CARDIA), the Cardiovascular Health Study (CHS), the Hispanic Community Health Study/Study of Latinos, and the Strong Heart Study.[10]

This PAGE Metabochip study included AA participants from the ARIC, BioVU, CHS, CARDIA, MEC, and WHI studies and from extended collaborations to two additional studies – GenNet and the Hypertension Genetic Epidemiology Network (HyperGen) (Table S1, in the Supplemental Data available with this article online). The detailed description of each study can be found in the Supplemental Data. We excluded underweight (BMI $<$ 18.5 kg/m^2) and extremely overweight (BMI $>$ 70 kg/m^2) individuals under the assumption that these extremes could be attributable to data-coding errors or an underlying rare condition outside the scope of this investigation. We also limited analysis to adults (defined as having an age $>$ 20 years). The CARDIA participants are young, and the BMI $<$ 18.5 exclusion criterion was not applied in this cohort. All studies were approved by institutional review boards at their respective sites, and all study participants provided informed consent.

Anthropometric Measurements

For individuals from the ARIC, CHS, CARDIA, HyperGEN, GenNet, and WHI studies, BMI was calculated from height and weight measured at the time of study enrollment. For individuals from BioVU, the median height and weight across all visit years were used in BMI calculations. For individuals from MEC, self-reported height and weight were used for calculations of baseline BMI. A validation study within MEC has shown high validity of self-reported height and weight. Specifically, this study showed that BMI was underestimated on the basis of self-reports versus measured weight, but the difference was small ($<$ 1 BMI unit) and was comparable to the findings from national surveys.[11]

Genotyping and Quality Control

Genotyping was performed with the Metabochip, whose design has been described elsewhere.[9] In brief, the Metabochip, a custom Illumina iSelect genotyping array of nearly 200,000 SNP markers, is designed to cost-effectively analyze putative association signals identified through GWAS meta-analyses of many obesity-related metabolic and cardiovascular traits and to fine-map established loci.[9] Metabochip SNPs were selected from the catalogs developed by the International HapMap and 1000 Genomes projects.[9] More than 122,000 SNPs were included for fine mapping of 257 GWAS loci of 23 traits (including 21 BMI loci).[9] For determination of the boundaries around each GWAS index SNP, all SNPs with $r^2 \geq 0.5$ with the index SNP were identified, and then initial boundaries were expanded by 0.02 cM in either direction through use of the HapMap-based genetic map. SNPs were excluded if (1) the Illumina design score was $<$0.5 or (2) SNPs within 15 bp in both directions of the SNP of interest could be found with an allele frequency of $>$0.02 among Europeans (CEU). SNPs annotated as nonsynonymous, essential splice site, or stop codon were included regardless of allele frequency, design score, or nearby SNPs in the primer.[9] Twenty-one BMI GWAS loci identified at the time at which the Metabochip was designed were represented for signal fine mapping (Table S2).

Samples were genotyped at the Human Genetics Center of the University of Texas, Houston (ARIC, CHS, CARDIA, GenNet, and HyperGEN), the Vanderbilt DNA Resources Core in Nashville (BioVU), the University of Southern California Epigenome Center (MEC), and the Translational Genomics Research Institute (WHI). Each center genotyped the same 90 HapMap YRI (Yoruba in Ibadan, Nigeria) samples to facilitate cross-study quality control (QC), as well as 2%–3% study-specific blinded replicates to assess genotyping quality. Genotypes were called separately for each study via GenomeStudio with the GenCall 2.0 algorithm. Study-specific cluster definitions (based on samples with call rate $>$ 95%; ARIC, BioVU, CHS, CARDIA, MEC, and WHI) or cluster definitions provided by Illumina (GenNet and HyperGEN) were used for sample calling, and samples were kept in the analysis if the call rate was $>$95%. We excluded SNPs with a GenTrain score $<$0.6 (ARIC, BioVU, CHS, CARDIA, MEC, and WHI) or $<$0.7 (GenNet and HyperGEN), a cluster separation score $<$0.4, a call rate $<$0.95, and a Hardy-Weinberg equilibrium p $< 1 \times 10^{-6}$. We utilized the common 90 YRI samples and excluded any SNP that had more than 1 Mendelian error (in 30 YRI trios), any SNP that had more than two replication errors with discordant calls when comparisons were made across studies in 90 YRI samples, and any SNP that had more than three discordant calls for 90 YRI genotyped in PAGE versus the HapMap database. SNPs were excluded from the meta-analyses if they were present in less than three studies.

For ARIC, BioVU, CHS, CARDIA, MEC, and WHI combined we identified related individuals by using PLINK to estimate identical-by-descent (IBD) statistics for all pairs. When apparent pairs of first-degree relatives were identified, we excluded from each pair the member with the lower call rate. We excluded from further analysis samples with an inbreeding coefficient (F) above

0.15 (ARIC, BioVU, CHS, CARDIA, MEC, and WHI).[12] We determined principal components of ancestry in each study separately by using EIGENSOFT[13,14] and excluded apparent ancestral outliers from further analysis as described elsewhere.[15]

WHI SHARe Imputation

Of the WHI women genotyped on the Metabochip, 1,962 women were part of the group of 8,288 WHI subjects genotyped for the WHI SNP Health Association Resource (SHARe) GWAS via the Affymetrix 6.0 platform. To improve statistical power, we imputed the Metabochip SNPs in the remaining 6,326 SHARe subjects with Affymetrix 6.0 data. Details can be found elsewhere.[16] In brief, we first merged genotypes for the 1,962 subjects genotyped on both the Affymetrix 6.0 platform and the Metabochip and constructed haplotypes (study-specific reference panel). We then phased the haplotypes for samples genotyped on the Affymetrix 6.0 platform only and performed a haplotype-to-haplotype imputation on Metabochip SNPs for the 6,326 target individuals to estimate genotypes (as allele dosages). We used MACH for phasing and Minimac for final imputation. To evaluate the quality of each imputed SNP, we calculated the dosage r^2. We excluded imputed SNPs with $r^2 < 0.5$ for SNPs with allele frequency < 1% and with $r^2 < 0.3$ for SNPs with allele frequency > 1%. Given the large reference panel and strict QC criteria, this resulted in high imputation quality.[16]

Statistical Analysis

In each study, we evaluated the association between natural-log-transformed BMI and each SNP. Because the distribution of BMI was not normal (it was skewed toward higher BMI), we used natural-log-transformed BMI,[17] which reduces the influence of potential outlying observations on the analyses. Except for GenNet and HyperGen, linear regression models were used under the assumption of an additive genetic model and with the adjustment for age, sex, study site (as applicable), and ancestry principal components in each study. All models (except WHI) included the interaction term of sex and age so that possible effect modification by sex was accounted for. Family data from GenNet and HyperGen were analyzed with linear mixed models so that relatedness was accounted for. We used fixed-effect models with inverse variance weighting to pool the study-specific association results as implemented in METAL.[18] We used Q-statistics and I^2 to measure heterogeneity across studies. To determine whether the 21 previously identified GWAS loci were significantly associated with BMI in AA, we used the p value threshold 5.8×10^{-5} as an approximate correction for an average of 866 SNPs at each locus (i.e., 0.05/866 SNPs).[19] To identify additional independent signals in any of the loci that were significantly associated with BMI in our study, we conducted conditional analyses. We performed linear regression models that included the most significant SNP (i.e., lead SNP) as a covariate and each of the other SNPs at the same locus (two SNPs in each model) to search for additional independent signals. If, after adjustment for the lead SNP, any SNP remained significant at the locus-specific Bonferroni-corrected significance level (i.e., 0.05/number of SNPs tested at a given locus), we defined the SNP as an additional independent signal. When testing all other SNPs on the Metabochip, we used a Bonferroni-adjusted significance level based on the total number of SNPs on the chip, 2.5×10^{-7} (0.05/200,000 SNPs), to declare a BMI-associated SNP. No inflation was observed in any analysis (the inflation factor $\lambda = 1.00$) in our Metabochip-wide analysis. For sex-stratified analysis, GenNet and HyperGen were excluded because of the family-study design.

LD in the AA sample was calculated in 500 kb sliding windows via PLINK.[20] Likewise, the Malmo Diet and Cancer Study on 2,143 controls from a Swedish population[21] provided Metabochip LD and frequency information in Europeans to facilitate the LD pattern comparisons between AA and EA populations. We used LocusZoom plots[22] to graphically display the fine-mapping results. SNP positions from NCBI build 37 were used, and recombination rates were estimated from 1000 Genomes Project data.

Functional Annotation

To inform the discussion about the underlying potential functional variants, we made functional hypotheses for each of our most significantly BMI-associated variants by compiling a list of correlated SNPs ($r^2 > 0.5$) genotyped in our AA study populations and annotating each list for potential regulatory evidence consistent with enhancers, promoters, insulators, silencers and other effects related to gene expression. Because our lead SNPs and the SNPs in strong LD with our lead SNPs were in noncoding regions, we hypothesized that the underlying biology behind the signal was likely to impact gene expression through some unknown regulatory mechanism. For each list we aligned correlated SNPs with a combined browser view of all currently available ENCODE tracks in the UCSC Genome Browser and compared each allelic region for altered transcription factor binding site (TFBS) motifs by using JASPAR and ConSite. Given that methylation patterns are highly variable, it is useful to look for, in addition to BMI-relevant tissues, histone modifications in many cell lines to identify regions that are actively regulated, meaning that histone marks are present in some but not all cell lines. Thus, in addition to adipocytes, hepatocytes, and neurons, we used ENCODE's histone modification tracks to query a wide variety of cell lines for all available histone marks to identify SNPs falling in various regulatory regions. The DNase hypersensitivity track provided a more precise demarcation of open chromatin loci, and the ChIP-Seq TFBS track provided evidence for the binding of specific proteins. Although less specific than ChIP-Seq, JASPAR, ConSite, and HaploReg databases were used for querying a larger number of conserved TFBS and predicting alterations in predicted motifs between reference and alternate alleles. A 46-way PhastCons track in the UCSC Genome Browser was used as secondary evidence for a regulatory region, but lack of conservation did not rule out a functional candidate. The most likely functional-candidate SNPs for each locus were evaluated for statistical significance in association with BMI. The detailed list of functional annotation data sets we used is shown in Table S3.

Results

This study consisted of 29,151 AAs from eight studies. Study participants had an average age of 51.2 years (Table S1). Approximately 80% of study participants were women. Within and across studies, men tended to have a lower mean BMI than women. The obesity rate (BMI ≥ 30 kg/m^2) ranged from 16%–46% in men and 26%–64% in women. After quality control, we tested 18,187 genetic variants across 21 BMI loci and 177,663 variants across the Metabochip.

Table 1. Association Results for the Most Significant SNP and All Previously Identified GWAS SNPs for Eight BMI-Related Loci with Significant[a] Results in African Americans

Region	Lead AA SNP on Metabochip	GWAS Index SNP	Position	Number of SNPs	Candidate Gene	R^2 Lead SNP with GWAS SNP in AAs	R^2 Lead SNP with GWAS SNP in EA Populations	CA[b]	CAF[c] in AAs	CAF in EA Populations	Effect	p Value	Rsq[d]	Het P [e]	I^2
1q25.2	rs543874	rs543874	177889480	765	*SEC16B*	-	-	T	0.75	0.81	−0.0110	2.4×10^{-9}	NA	0.04	0.52
2p25.3	rs6548240	-	636929	1,123	*TMEM18*	-	-	A	0.87	0.83	0.0130	1.1×10^{-7}	0.98	0.96	0
-	-	rs6548238	634905	-	*TMEM18*	0.86	0.99	A	0.12	0.17	−0.0128	3.8×10^{-7}	1.00	0.82	0
-	-	rs2867125	622827	-	*TMEM18*	0.80	0.96	A	0.12	0.17	−0.0114	5.6×10^{-6}	1.00	0.79	0
-	-	rs7561317	644953	-	*TMEM18*	0.49	0.99	A	0.24	0.17	−0.0054	4.8×10^{-3}	1.00	0.89	0
3q27.2	rs7647305	rs7647305	185834290	369	*ETV5*	-	-	A	0.41	0.23	−0.0069	3.2×10^{-5}	0.95	0.29	0.18
-	-	rs9816226	185834499	-	*ETV5*	0.37	0.85	A	0.80	0.81	0.0067	9.1×10^{-4}	0.96	0.57	0
4p12	rs10938397	rs10938397	45182527	342	*GNPDA2*	-	-	A	0.75	0.57	−0.0099	1.7×10^{-7}	0.99	0.24	0.23
6p12.3	rs2744475	-	50784880	1,685	*TFAP2B*	-	-	C	0.67	0.71	−0.0082	2.8×10^{-6}	0.98	0.39	0.05
-	-	rs987237	50803050	-	*TFAP2B*	0.23	0.50	A	0.90	0.82	−0.0093	5.2×10^{-4}	NA	0.07	0.46
11p14.1	rs1519480	-	27675712	688	*BDNF*	-	-	A	0.25	0.68	−0.0095	7.8×10^{-7}	1.00	0.90	0
-	-	rs6265	27667202	-	*BDNF*	0.14	0.12	A	0.05	0.18	−0.0172	1.8×10^{-5}	NA	0.64	0
-	-	rs925946	27679916	-	*BDNF*	0.12	0.97	T	0.27	0.30	−0.0005	7.9×10^{-1}	1.00	0.23	0.24
-	-	rs10767664[f]	27724745	-	*BDNF*	0.12	0.13	C	0.93	0.76	0.0111	3.7×10^{-4}	0.99	0.28	0.18
16q12.2	rs62048402	-	53803223	1,814	*FTO*	-	-	A	0.11	0.41	0.0120	5.1×10^{-6}	1.00	0.14	0.34
-	-	rs1421085	53800954	-	*FTO*	1.00	1.00	T	0.89	0.59	−0.0119	6.5×10^{-6}	NA	0.15	0.33
-	-	rs9930506	53830465	-	*FTO*	0.44	0.81	T	0.79	0.57	−0.0082	3.9×10^{-5}	NA	0.21	0.27
-	-	rs9941349	53825488	-	*FTO*	0.52	0.91[g]	A	0.19	0.41	0.0082	1.1×10^{-4}	NA	0.56	0
-	-	rs1558902	53803574	-	*FTO*	0.98	1.00	A	0.88	0.58	−0.0132	4.5×10^{-4}	1.00	0.43	0
-	-	rs8050136	53816275	-	*FTO*	0.15	0.94	A	0.43	0.41	0.0027	1.0×10^{-1}	NA	0.05	0.48
-	-	rs9939609	53820527	-	*FTO*	0.13	0.94	A	0.47	0.41	0.0027	1.0×10^{-1}	1.00	0.10	0.40
-	-	rs1121980	53809247	-	*FTO*	0.14	0.90	T	0.47	0.43	0.0021	1.9×10^{-1}	NA	0.26	0.21
-	-	rs6499640	53769677	-	*FTO*	0.00	0.09	A	0.65	0.60	−0.0013	4.6×10^{-1}	1.00	0.52	0
18q21.32	rs6567160	-	57829135	1275	*MC4R*	-	-	A	0.81	0.75	−0.0096	4.7×10^{-6}	0.98	0.03	0.52
-	-	rs17782313	57851097	-	*MC4R*	0.06	0.99	T	0.72	0.77	−0.0068	1.5×10^{-4}	1.00	0.50	0
-	-	rs10871777	57851763	-	*MC4R*	0.05	0.97	A	0.71	0.75	−0.0061	6.7×10^{-4}	1.00	0.40	0.04

(*Continued on next page*)

Table 1. *Continued*

-	rs12970134	57884750	-	*MC4R*	0.24	0.77	A	0.14	0.28	0.0065	5.9×10^{-3}	1.00	0.21	0.26
-	rs571312	57839769	-	*MC4R*	0.03	0.99	A	0.34	0.25	0.0009	6.1×10^{-1}	NA	0.99	0

Results for all 21 loci are shown in Table S2.
[a] Significance level: 0.05 divided by 866 (average number of SNPs across 21 BMI loci).
[b] CA: coded allele.
[c] CAF: coded allele frequency.
[d] Measurement of imputation accuracy, ranging from 0 (low) to 1 (high); NA indicates that there was no imputation in a subset of 6,326 WHI samples and that all other samples have directly genotyped data.
[e] Het p: heterogeneity test p value.
[f] SNP failed in quality control; SNP proxy (rs988748, LD $r^2 = 1.0$ in HapMap YRI) was substituted.
[g] SNP failed in genotyping in our EA population, and r^2 is calculated from 1000 Genomes Project European populations.

Fine Mapping BMI Loci

Among the 21 BMI GWAS loci identified in EA studies, eight loci (*SEC16B* [MIM 612855], *TMEM18* [MIM 613220], *ETV5* [MIM 601600], *GNPDA2* [MIM 613222], *TFAP2B* [MIM 601601], *BDNF* [MIM 113505], *FTO* [MIM 610966], and *MC4R* [MIM 155541]) displayed SNPs with significant evidence of association (Table 1; see also Table S2). The lead SNP (the most significant SNP in AAs) in each of these eight loci had a minor-allele frequency >0.05 and showed little evidence of heterogeneity. In these eight loci most GWAS index SNPs previously identified in EA GWASs (20 out of 23) had a consistent direction of the effects reported in original EA studies. Because the results of the *FTO* locus have been described previously,[23] we focused on the other seven regions. Among those seven loci, the lead SNPs, rs543874 in *SEC16B* ($p = 1.5 \times 10^{-9}$), rs7647305 in *ETV5* ($p = 3.2 \times 10^{-5}$), and rs10938397 in *GNPDA2* ($p = 1.7 \times 10^{-7}$), were consistent with the previously identified GWAS SNP (the most significant SNP highlighted in the previous GWAS) in EA populations. For rs543874 and rs10938397, the observed effects on BMI were slightly stronger in AAs than in EA individuals (change in BMI per coded allele: 1.1% in AAs and 0.9% in EA individuals for rs543874; 1.0% in AAs and 0.8% in EAs for rs10938397[5]), whereas they were slightly weaker in AAs than in EA individuals for rs7647305 (change in BMI per coded allele: 0.7% in AAs and 0.9% in EA individuals[6]). The minor-allele frequency (MAF) was higher for rs543874 and rs7647305 and lower for rs10938397 in AAs than in EA individuals (Table 1). In the other four loci, the lead SNPs in AAs differed from the GWAS SNPs from EA populations. The lead SNPs in all four loci (rs6548240 in *TMEM18*, rs2744475 in *TFAP2B*, rs1519480 in *BDNF*, and rs6567160 in *MC4R*) were modestly to strongly correlated (r^2 ranged from 0.5–1.0) with at least one of the GWAS SNPs on the basis of LD in EA populations. However, when LD was based on AA populations, the correlation was weaker, in several cases substantially weaker (Table 1). For the 13 BMI loci that did not replicate in our AA analysis, most GWAS index SNPs (13 out of 17) from previous GWASs involving EA individuals showed effects in the same direction when results from our AA samples were compared with results from the previous EA studies.

We investigated the question of whether LD patterns in AA studies can narrow previous association signals from EA studies and found that at seven out of the eight significant loci, AA LD patterns assisted with narrowing association signals (Table 2; see also Figure S1). One of the most extreme examples was for *MC4R*. Among EA individuals, 107 and 119 SNPs were correlated ($r^2 > 0.5$) with the lead SNP in our analysis (rs6567160) and with the GWAS index SNPs, respectively; these SNPs represent a region spanning 184 kb and 230 kb, respectively. However, among AAs only five SNPs were correlated with rs6567160 at $r^2 > 0.5$, and these SNPs represented a region spanning 71 kb. In *SEC16B*, *ETV5*, *TFAP2B*, *BDNF*, and *FTO*, the number of

Table 2. **Comparison of Correlation between African American and European Populations for Eight BMI-Related Loci that had Significant[a] Lead SNPs**

					AA Populations		EA Populations			
Region	**Gene**	**Lead SNP in AAs of PAGE**	**Region Size**	**Number of SNPs**	**Number of SNPs with $r^2 > 0.5$ with Lead SNP**	**Region size for SNPs with $r^2 > 0.5$ with Lead SNP (bp)**	**Number of SNPs with $r^2 > 0.5$ with Lead SNP**	**Region Size for SNPs with $r^2 > 0.5$ with Lead SNP (bp)**	**Number of SNPs with $r^2 > 0.5$ with GWAS Index SNPs**	**Region size for SNPs r^2>0.5 with GWAS index SNPs (bp)**
1q25.2	*SEC16B*	rs543874	180 kb	765	2	4,242	39	95,660	39	95,660
2p25.3	*TMEM18*	rs6548240	250 kb	1,123	81	40,820	104	53,290	106	75,430
3q27.2	*ETV5*	rs7647305	110 kb	369	5	10,348	28	49,410	29	49,620
4p12	*GNPDA2*	rs10938397	90 kb	342	6	20,482	5	20,482	5	20,482
6p12.3	*TFAP2B*	rs2744475	560 kb	1,685	1	1,128	44	15,320	29	152,570
11p14.1	*BDNF*	rs1519480	300 kb	688	7	21,942	42	22,4200	42[b]	224,200[b]
16q12.2	*FTO*	rs62048402	650 kb	1,814	19	44,529	74	47,575	76[c]	73,850[c]
18q21.32	*MC4R*	rs6567160	360 kb	1,275	5	71,160	107	183,730	119	229610
Average for number of SNPs or region size					16	26,831	55	86,208	56	115,178

[a] Significance level: 0.05 divided by 866 (average number of SNPs across 21 BMI loci).

[b] Only included the GWAS index SNP rs925946 because the other two GWAS SNPs, rs10767664 and rs6265, have $r^2 < 0.15$ with the lead SNP and rs925946 in AA and EA populations.

[c] GWAS index SNP rs6499640 was not included because it has $r^2 < 0.1$ with the lead SNP and the other GWAS index SNPs in AA and EA populations.

SNPs correlated at r^2>0.5 with the lead SNP and the spanning region size were also substantially reduced and to a limited degree for *TMEM18* (Table 2). Only for *GNPDA2* did the number of correlated SNPs and the spanning region size not reduce, but the number of correlated SNPs in Europeans was already small.

To further refine the regions associated with BMI in AAs, we performed conditional analyses for each of the eight significant loci by including the lead SNP in a locus as a covariate to search for additional independent signals. rs186117327 in *GNPDA2* was borderline significantly associated with BMI when the locus-specific significance level was taken into account (Table 3). No evidence of heterogeneity was observed across studies. In *GNPDA2*, rs186117327 was significantly associated with BMI in the marginal analysis ($p = 3.7 \times 10^{-7}$),; this association became less significant but remained marginally so when adjustment was made for the lead SNP ($p = 1.7 \times 10^{-4}$). rs186117327 was weakly correlated with the lead SNP (rs10938397) as well as with the GWAS SNP at this locus ($r^2 = 0.11$ in AAs; 0.16 in EA individuals).

Identification of Two BMI-Related Loci in AAs by Metabochip-wide Analysis

In the Metabochip-wide analysis (excluding the SNPs in the 21 BMI-related loci), we identified five SNPs in two loci (these SNPs were rs116612809, rs114584581, rs74941130, and rs79329695 in 2p23.2/*BRE* [MIM 610497] and rs4802349 in 19q13.32/*DHX34*) as being associated with BMI in AAs at a Metabochip-wide significance level ($p < 2.5 \times 10^{-7}$). Two of the SNPs in 2p23.2/*BRE* (rs116612809 and rs79329695) reached the conventional genome-wide significance level ($p < 5.0 \times 10^{-8}$) (Table 4 and Figure 1). Furthermore, with $p = 3.7 \times 10^{-7}$, rs57813622 at the 7p21.2/*DGKB* [MIM 604070] locus approached the Metabochip-wide significance level.

In 2p23.2/*BRE*, all four SNPs are rare variants in Europeans (MAF = 0.1% in the 1000 Genomes Project) but common in AAs (MAF = 10%). The most significant SNP, rs116612809, is located in the intronic region of *BRE* and is highly correlated with the three other significant SNPs (r^2 ranges from 0.98–1.00, Figure 2). In the conditional analysis for all other SNPs at the *BRE* locus, we did not observe evidence for an additional independent signal associated with BMI after conditioning on rs116612809, suggesting that all four SNPs point to the same functional variant. The 2p23.2/*BRE* was included on the Metabochip as a part of a ~1.3-Mb-long region so that a GWAS locus associated with blood triglyceride (TG) concentrations could be fine-mapped.[24,25] Within this region, the four BMI-associated SNPs were more than 500 kb away from the TG GWAS index SNPs (rs1260326, rs1260333, rs780093, and rs780094; r^2 ranged from 0.02–0.05 in AAs). To examine the association between rs116612809 and blood TG concentrations in our population, we used ARIC and WHI, for which the TG individual data were available (n = 11,680). We did not observe a significant

Table 3. Conditional Analysis Showing a Locus with Evidence of Second Independent BMI Association Signals in African Americans

							Marginal Results[a]			Conditional Results[b]			
Region	**Gene**	**SNP**	**Position**	**Number of Tested SNPs**	**Coded Allele**	**CAF**	**Effect**	**p Value**	**Het p[d]**	**Effect**	**p Value**	**Het p**	**r^2 with Lead SNP in AAs**
4p12	*GNPDA2*	rs186117327	45,101,187	285	A	0.75	−0.0095	3.7×10^{-7}	0.54	−0.0074	1.7×10^{-4}	0.91	0.11
-	-	rs10938397[c]	45,182,527	-	A	0.75	−0.0099	1.7×10^{-7}	0.24	−0.0068	1.6×10^{-3}	0.37	-

[a] Marginal results represent results when only the single variant was in the model.
[b] Conditional analysis represents the result for the SNP when adjustment was made for the most significant lead SNP and vice versa.
[c] The most significant SNP in a locus.
[d] Het p: heterogeneity-test p value.

Table 4. Two BMI Loci Identified in African Americans on the Basis of Metabochip-wide Analysis

Region	SNP	Position	Candidate Gene	Coded Allele	CAF in AAs	CAF in EA Individuals	Effect	p value	Rsq[a]	Het p	r^2 with Lead SNP in AAs
2p23.2	rs116612809	28,301,171	*BRE*	A	0.90	0.001	−0.0151	3.6×10^{-8}	0.99	0.48	-
-	rs114584581	28,304,380	*BRE*	A	0.10	0.001	0.0148	5.9×10^{-8}	0.99	0.43	0.98
-	rs74941130	28,306,293	*BRE*	A	0.10	0.001	0.0148	6.9×10^{-8}	0.99	0.44	1.00
-	rs79329695	28,319,874	*BRE*	A	0.10	0.001	0.0151	3.7×10^{-8}	0.99	0.56	0.99
19q13.32	rs4802349	47,874,510	*DHX34*	A	0.48	0.12	−0.0087	1.2×10^{-7}	1.00	0.46	-

[a] Measurement of imputation accuracy, ranging from 0 (low) to 1 (high).

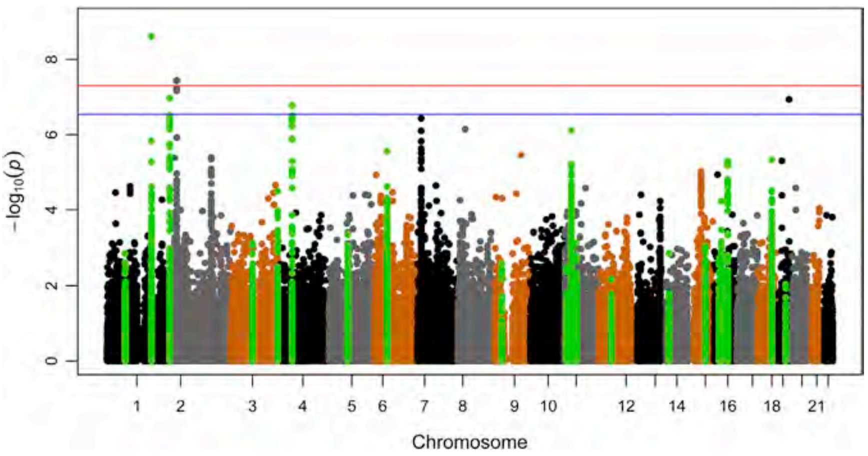

Figure 1. Manhattan Plot for Metabochip-Wide Analysis of BMI in African Americans

The –log10 of p values for each SNP on the Metabochip is plotted against physical chromosomal positions. Green dots represent the SNPs in 21 BMI-related loci that were previously identified in European populations and fine-mapped on the Metabochip. Blue line: $p = 2.5 \times 10^{-7}$; red line: $p = 5 \times 10^{-8}$.

association (p = 0.71) with blood TG concentrations, which did not change after adjustment for BMI. Furthermore, the association between rs116612809 and BMI did not change after adjustment for TG (Table S4).

In 19q13.32/*DHX34*, rs4802349 is located in an intron of *DHX34* and has a MAF of 0.48 in AAs and 0.12 in EA individuals. Only ten SNPs surrounding rs4802349 (±200 kb) were genotyped; none was correlated with rs4802349 in Aas, and none was associated with BMI. Previously, rs4802349 was reported to be a putative association signal for high-density lipoprotein (HDL) cholesterol at a moderate p value of 0.005.[26] We examined the association between rs4802349 and blood HDL concentrations with and without BMI adjustment in ARIC and WHI (n = 11,680). We observed that the p value changed from 0.25 to 0.04 after BMI adjustment. Furthermore, the association between rs4802349 and BMI did not change after adjustment for HDL (Table S4).

Sex-Stratification Analyses

We did not observe any additional loci when we stratified the analysis by sex (Tables S5 and S6 and Figures S2 and S3). Also, the results for the SNPs that were significant in the fine-mapping analyses and the two BMI loci results were consistent across sex (p-heterogeneity ≥ 0.29, Table S7). However, as a result of the relatively small sample of men in this study, we have limited power to detect a difference-of-sex effect.

Functional Annotation

In silico analysis assessed whether each BMI-associated locus was in an “open,” transcriptionally permissive conformation, as would be expected of a functional locus. Using ENCODE data sets, we found each signal to be in a region consistent with regulatory evidence, such as active histone marks, open chromatin structure (DNase hypersensitivity), or regions experimentally shown to bind one or more transcription factors (Table S8). Bioinformatics analyses revealed that the lead SNP, rs6548240 in the *TMEM18* locus, was the strongest functional candidate. rs6548240 is in a region of open chromatin that binds multiple transcription factors, and elevated levels of active histone marks associated with promoters were detected in several cell lines (Figure S4). The functional properties of TMEM18 are obscure, although a recent study indicated that TMEM18 plays a regulatory role in adipocyte differentiation and biology.[27] For *GNPDA2*, the potential additional independent signal rs186117327 could be tagging rs7659184 (r^2 = 0.6 with rs186117327 in AAs), which falls in a region of open chromatin, and relative to the reference allele, the alternate allele reduces the binding affinity of GATA2 and EN1 transcription factors. In 2p23.2/*BRE,* bioinformatics analyses indicated that the lead SNP, rs116612809, tags another intronic SNP, rs78003529 (r^2 = 0.65 in AAs), which falls in a region of open chromatin with elevated enhancer histone marks and is in a region that binds both Pol2 and c-Jun. Furthermore, evidence from scans of positional weight matrices (PWMs) suggests that the alternate allele of rs78003527 has a much higher binding affinity for Nkx3 and Nkx2. In 19q13.32/*DHX34*, the *DHX34* signal rs4802349 and two SNPs highly correlated with it are located within putative regulatory regions. rs4802349 falls within histone-modification marks associated with enhancer activity and alters the Mtf1 transcription-factor binding motif. In addition, two other functional candidates, rs2547369 and rs2341878 (r^2 = 0.7 and 0.6, respectively in African populations) were highly correlated with this signal and fall in regions of open chromatin having methylation patterns associated with promoter or enhancer activity. Furthermore, rs25476369 (r^2 = 0.65 with rs4802349 in African populations) falls in a region that binds six transcription factors, whereas rs2341878 is of particular interest because it falls in a strong promoter region in a number of relevant tissues. The function of GNPDA2, BRE, and DHX34 is unknown, which makes it difficult to link the underlying biological mechanisms of these genetic variants to BMI.

Discussion

In this study, encompassing close to 30,000 AAs, we used the Metabochip to systematically evaluate 21 BMI loci

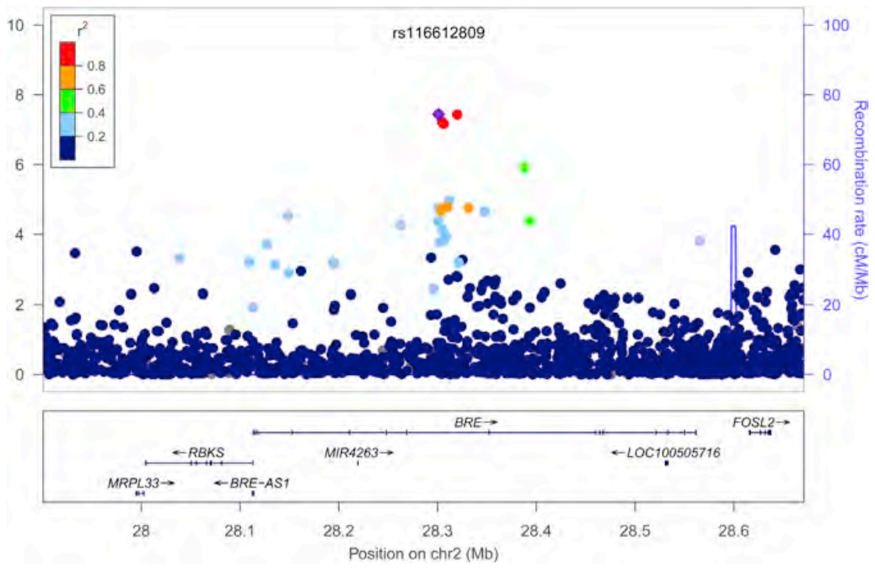

Figure 2. Regional-Association Plot for the New BMI-Related Locus at 2p23.2/*BRE*
The –log10 of p values (left *y* axis) is plotted against the SNP genomic position based on NCBI build 37 (*x* axis); the estimated recombination rate from the 1000 Genomes Project for African populations is on the right *y* axis and is plotted in blue. The most significant SNP is denoted with a purple diamond. SNPs are colored to reflect correlation with the most significant SNP. Gene annotations are from the UCSC Genome Browser.

discovered among European descent populations in previous GWASs and to search for potential BMI loci. Eight of the 21 loci (*SEC16B*, *TMEM18*, *ETV5*, *GNPDA2*, *TFAP2B*, *BDNF*, *FTO*, and *MC4R*) were found to be associated with BMI in our AA study population. Further conditional analyses indicated that *GNPDA2* contained an additional independent signal. Moreover, Metabochip-wide analyses revealed two BMI-associated loci: the *BRE* locus at genome-wide significance ($p < 5 \times 10^{-8}$) and the *DHX34* locus at Metabochip-wide significance ($p < 2.5 \times 10^{-7}$).

Among the eight BMI loci that were significant in the AA population, the lead SNPs in *SEC16B, ETV5*, and *GNPDA2* were the same as the GWAS SNPs identified in previous EA studies, which provided further support for the idea that the three SNPs (rs543874, rs7647305, and rs10938397) are proxies of causal variants influencing BMI. The most significant (lead) SNPs in the other five loci differed from the previously reported GWAS SNPs, although, as expected, all were moderately to highly correlated with the GWAS SNPs in European populations (r^2 ranged from 0.5 to 1.0). In *TFAP2B* and *MC4R*, the GWAS SNPs were not significantly associated with BMI in AAs, suggesting that the lead SNPs in these two loci are better proxies for the underlying functional variants. We showed that the weaker LD patterns in AA populations than in EA populations substantially reduced the number of functional-variant proxies in six of the eight BMI loci that were significant in AAs (and to a limited extent in *TMEM18*). Our results illustrate the important contribution of AAs to systematic fine-mapping of GWAS loci originally reported in EA populations. In addition, the lead SNPs that were either consistent or correlated with the GWAS SNPs at these replicated loci in EA populations might indicate that EA populations and AA populations share the underlying causal variants at these loci.

Bioinformatics analyses revealed that the lead SNP, rs6548240 in the *TMEM18* locus, was the strongest functional candidate. Although rs6548240 is located in an intergenic region 31 kb downstream of *TMEM18*, ChIP-seq evidence indicates that CTCF looping might anchor this distant putative enhancer to the promoter of *TMEM18*. Taken together, these pieces of evidence make rs6548240 an interesting functional candidate for future laboratory follow-up. This example shows that combining fine mapping with bioinformatics analysis can help to narrow in on the putative functional variants for further follow-up studies.

There are multiple reasons that 13 BMI loci originally identified in EA populations were not significantly associated with BMI in this sample of AAs. Limited statistical power could be an important reason for this observation. Statistical power is impacted by the variance of BMI, MAF, effect size, and sample size. Compared to populations in some large European-focused studies, our AA population had larger variance in BMI[7] (standard deviation: 6.2 kg/m^2 versus 4.2 kg/m^2), which reduces the statistical power. Also compared with primarily very large European-focused studies with sample sizes from ~90,000 to ~250,000,[5–7] our study was relatively small. Nonreplication might arise because of different causal variants between EA individuals and AAs, a weak AA LD pattern, which leads to weak correlation between causal variants and marker SNPs on the Metabochip, and limited statistical power. All of this might explain that we did not observe all loci significantly associated with BMI in AAs, and it emphasizes the need for a larger sample size. We used a uniform p value threshold of 5.8×10^{-5} (0.05/average number of SNPs per locus) as an approximate correction for the average of 866 SNPs across these loci. However, if we use Bonferroni correction (i.e., 0.05/the number of SNPs at a given locus) or correction by the effective number of SNPs at each locus after accounting for LD patterns, one more locus, *SH2B1* [MIM 608937], would be indicated to be significant in AAs (Table S2).

Conditional analysis indicated that the *GNPDA2* locus contained a potential additional independent signal. The potential additional independent signal, rs186117327, is physically relatively close (80 kb) to the lead SNP, rs10938397, but is only weakly correlated ($r^2 = 0.11$) with it.

We identified two BMI-related loci, 2p23.2/*BRE* and 19p13.32/*DHX34*, in the Metabochip-wide analysis. We evaluated whether African ancestry plays role in these two BMI-related loci among 8,310 AAs from a GWAS in WHI. We didn't observe a significant effect of ancestry at these two loci ($p > 0.5$; Table S9). At 2p23.3/*BRE*, the most significant SNP, rs116612809, reached the conventional genome-wide significance level (5×10^{-8}) and was surrounded (3–18 kb) by three highly correlated SNPs ($r^2 = 0.98$–1.00) showing very similar results. All four SNPs are common (MAF = 0.1), but they all are rare variants in EA populations (MAF = 0.001)[28] and hence it is unlikely that these SNPs would be identified in EA GWASs unless they have much stronger effects than the moderate effects observed in our study or are tested in very large sample sets. The lead SNP in 2p23.3/*BRE* (rs116612809) is located within an intron of *BRE*, which is stress responsive and highly expressed in brain and reproductive organs.[29] No previous study reported an association with BMI or any other trait; however, in support of our finding, the GIANT consortium reported that 82 of 200 SNPs within *BRE* had a p value < 0.05 (min. $p = 2.5 \times 10^{-4}$) for a BMI association in EA populations.[5] Accordingly, our results showed that varying allele frequency in different ancestral groups significantly contributes to the statistical power and that studying different ancestral groups helps to identify potentially functional loci.[30]

We found another potential BMI-related locus at 19q13.32/*DHX34*. The SNP rs4802349, located in an intron *DHX34*, was marginally significantly associated with BMI at a Metabochip-wide significance level ($p = 1.2 \times 10^{-7}$), but because the finding did not reach the conventional genome-wide significance level of 5×10^{-8}, additional replication studies in AAs are warranted. *DHX34* is a putative RNA helicase and has not been reported to be associated with any diseases or traits in humans before, except for a suggestive association with HDL cholesterol ($p = 0.005$).[26] A recent GWAS in EA populations showed an association with BMI in a neighboring region, 19q13.32/*ZC3H4*; rs3810291 was the most significant SNP.5 However, rs4802349 is physically 300 kb away from rs3810291, and a recombination hotspot lies between *ZC3H4* and *DHX34* in AAs and Europeans (HapMap phase II YRI and CEU), resulting in a low correlation between both SNPs in African populations ($r^2 = 0.04$) and Europeans ($r^2 < 0.001$). This observation suggests that these two associations are independent from each other. Our results along with the evidence from functional annotation warrant additional validation studies for this locus.

In conclusion, we observed that eight BMI-associated GWAS loci identified from EA populations were significantly associated with BMI in AAs and identified a potential additional independent signal in one locus. In addition, we discovered two potential BMI-related loci through Metabochip-wide analysis; one of these loci which reached the conventional genome-wide significance level. Importantly, our study demonstrated that fine mapping in AA populations in combination with bioinformatics analyses is a valuable and effective way to narrow in on the underlying causal variants in GWAS loci discovered in EA populations and that studying minority populations can contribute to loci discovery.

Supplemental Data

Supplemental data include four figures, nine tables, and supplemental text, including acknowledgments and can be found with this article online at http://www.cell.com/AJHG/.

Acknowledgments

See Supplemental Data.

Received: May 6, 2013
Revised: August 7, 2013
Accepted: August 16, 2013
Published: October 3, 2013

Web Resources

The URLs for data presented herein are as follows:

Center for Disease Control and Prevention (CDC), Adult Obesity Facts, http://www.cdc.gov/obesity/data/adult.html

GIANT consortium data files, http://www.broadinstitute.org/collaboration/giant/index.php/GIANT_consortium_data_files

MACH, http://www.sph.umich.edu/csg/abecasis/mach

Minimac, http://genome.sph.umich.edu/wiki/Minimac

Online Mendelian Inheritance in Man (OMIM), http://www.omim.org

The Population Architecture using Genomics and Epidemiology (PAGE) Study, http://www.pagestudy.org

World Health Organization (WHO) (2011) Obesity and Overweight Fact Sheet, http://www.who.int/mediacentre/factsheets/fs311/en/index.html

References

1. Kopelman, P.G. (2000). Obesity as a medical problem. Nature *404*, 635–643.
2. Miller, W.M., Nori-Janosz, K.E., Lillystone, M., Yanez, J., and McCullough, P.A. (2005). Obesity and lipids. Curr. Cardiol. Rep. *7*, 465–470.
3. Maes, H.H., Neale, M.C., and Eaves, L.J. (1997). Genetic and environmental factors in relative body weight and human adiposity. Behav. Genet. *27*, 325–351.
4. Hjelmborg, Jv., Fagnani, C., Silventoinen, K., McGue, M., Korkeila, M., Christensen, K., Rissanen, A., and Kaprio, J. (2008). Genetic influences on growth traits of BMI: a longitudinal study of adult twins. Obesity (Silver Spring) *16*, 847–852.
5. Speliotes, E.K., Willer, C.J., Berndt, S.I., Monda, K.L., Thorleifsson, G., Jackson, A.U., Lango Allen, H., Lindgren, C.M., Luan, J., Mägi, R., et al.; MAGIC; Procardis Consortium. (2010). Association analyses of 249,796 individuals reveal 18 new loci associated with body mass index. Nat. Genet. *42*, 937–948.

6. Thorleifsson, G., Walters, G.B., Gudbjartsson, D.F., Steinthorsdottir, V., Sulem, P., Helgadottir, A., Styrkarsdottir, U., Gretarsdottir, S., Thorlacius, S., Jonsdottir, I., et al. (2009). Genome-wide association yields new sequence variants at seven loci that associate with measures of obesity. Nat. Genet. *41*, 18–24.
7. Willer, C.J., Speliotes, E.K., Loos, R.J., Li, S., Lindgren, C.M., Heid, I.M., Berndt, S.I., Elliott, A.L., Jackson, A.U., Lamina, C., et al.; Wellcome Trust Case Control Consortium; Genetic Investigation of ANthropometric Traits Consortium. (2009). Six new loci associated with body mass index highlight a neuronal influence on body weight regulation. Nat. Genet. *41*, 25–34.
8. McCarthy, M.I., and Hirschhorn, J.N. (2008). Genome-wide association studies: potential next steps on a genetic journey. Hum. Mol. Genet. *17*(R2), R156–R165.
9. Voight, B.F., Kang, H.M., Ding, J., Palmer, C.D., Sidore, C., Chines, P.S., Burtt, N.P., Fuchsberger, C., Li, Y., Erdmann, J., et al. (2012). The metabochip, a custom genotyping array for genetic studies of metabolic, cardiovascular, and anthropometric traits. PLoS Genet. *8*, e1002793.
10. Matise, T.C., Ambite, J.L., Buyske, S., Carlson, C.S., Cole, S.A., Crawford, D.C., Haiman, C.A., Heiss, G., Kooperberg, C., Marchand, L.L., et al.; PAGE Study. (2011). The Next PAGE in understanding complex traits: design for the analysis of Population Architecture Using Genetics and Epidemiology (PAGE) Study. Am. J. Epidemiol. *174*, 849–859.
11. Connor Gorber, S., and Tremblay, M.S. (2010). The bias in self-reported obesity from 1976 to 2005: a Canada-US comparison. Obesity (Silver Spring) *18*, 354–361.
12. Weale, M.E. (2010). Quality control for genome-wide association studies. Methods Mol. Biol. *628*, 341–372.
13. Patterson, N., Price, A.L., and Reich, D. (2006). Population structure and eigenanalysis. PLoS Genet. *2*, e190.
14. Price, A.L., Patterson, N.J., Plenge, R.M., Weinblatt, M.E., Shadick, N.A., and Reich, D. (2006). Principal components analysis corrects for stratification in genome-wide association studies. Nat. Genet. *38*, 904–909.
15. Buyske, S., Wu, Y., Carty, C.L., Cheng, I., Assimes, T.L., Dumitrescu, L., Hindorff, L.A., Mitchell, S., Ambite, J.L., Boerwinkle, E., et al. (2012). Evaluation of the metabochip genotyping array in African Americans and implications for fine mapping of GWAS-identified loci: the PAGE study. PLoS ONE *7*, e35651.
16. Liu, E.Y., Buyske, S., Aragaki, A.K., Peters, U., Boerwinkle, E., Carlson, C., Carty, C., Crawford, D.C., Haessler, J., Hindorff, L.A., et al. (2012). Genotype imputation of Metabochip SNPs using a study-specific reference panel of ~4,000 haplotypes in African Americans from the Women's Health Initiative. Genet. Epidemiol. *36*, 107–117.
17. Fesinmeyer, M.D., North, K.E., Ritchie, M.D., Lim, U., Franceschini, N., Wilkens, L.R., Gross, M.D., Bůžková, P., Glenn, K., Quibrera, P.M., et al. (2013). Genetic risk factors for BMI and obesity in an ethnically diverse population: results from the population architecture using genomics and epidemiology (PAGE) study. Obesity (Silver Spring) *21*, 835–846.
18. Willer, C.J., Li, Y., and Abecasis, G.R. (2010). METAL: fast and efficient meta-analysis of genomewide association scans. Bioinformatics *26*, 2190–2191.
19. Wu, Y., Waite, L.L., Jackson, A.U., Sheu, W.H., Buyske, S., Absher, D., Arnett, D.K., Boerwinkle, E., Bonnycastle, L.L., Carty, C.L., et al. (2013). Trans-ethnic fine-mapping of lipid loci identifies population-specific signals and allelic heterogeneity that increases the trait variance explained. PLoS Genet. *9*, e1003379.
20. Purcell, S., Neale, B., Todd-Brown, K., Thomas, L., Ferreira, M.A., Bender, D., Maller, J., Sklar, P., de Bakker, P.I., Daly, M.J., and Sham, P.C. (2007). PLINK: a tool set for whole-genome association and population-based linkage analyses. Am. J. Hum. Genet. *81*, 559–575.
21. Berglund, G., Elmstähl, S., Janzon, L., and Larsson, S.A. (1993). The Malmo Diet and Cancer Study. Design and feasibility. J. Intern. Med. *233*, 45–51.
22. Pruim, R.J., Welch, R.P., Sanna, S., Teslovich, T.M., Chines, P.S., Gliedt, T.P., Boehnke, M., Abecasis, G.R., and Willer, C.J. (2010). LocusZoom: regional visualization of genome-wide association scan results. Bioinformatics *26*, 2336–2337.
23. Peters, U., North, K.E., Sethupathy, P., Buyske, S., Haessler, J., Jiao, S., Fesinmeyer, M.D., Jackson, R.D., Kuller, L.H., Rajkovic, A., et al. (2013). A systematic mapping approach of 16q12.2/FTO and BMI in more than 20,000 African Americans narrows in on the underlying functional variation: results from the Population Architecture using Genomics and Epidemiology (PAGE) study. PLoS Genet. *9*, e1003171.
24. Kathiresan, S., Willer, C.J., Peloso, G.M., Demissie, S., Musunuru, K., Schadt, E.E., Kaplan, L., Bennett, D., Li, Y., Tanaka, T., et al. (2009). Common variants at 30 loci contribute to polygenic dyslipidemia. Nat. Genet. *41*, 56–65.
25. Aulchenko, Y.S., Ripatti, S., Lindqvist, I., Boomsma, D., Heid, I.M., Pramstaller, P.P., Penninx, B.W., Janssens, A.C., Wilson, J.F., Spector, T., et al.; ENGAGE Consortium. (2009). Loci influencing lipid levels and coronary heart disease risk in 16 European population cohorts. Nat. Genet. *41*, 47–55.
26. Teslovich, T.M., Musunuru, K., Smith, A.V., Edmondson, A.C., Stylianou, I.M., Koseki, M., Pirruccello, J.P., Ripatti, S., Chasman, D.I., Willer, C.J., et al. (2010). Biological, clinical and population relevance of 95 loci for blood lipids. Nature *466*, 707–713.
27. Bernhard, F., Landgraf, K., Klöting, N., Berthold, A., Büttner, P., Friebe, D., Kiess, W., Kovacs, P., Blüher, M., and Körner, A. (2013). Functional relevance of genes implicated by obesity genome-wide association study signals for human adipocyte biology. Diabetologia *56*, 311–322.
28. Abecasis, G.R., Auton, A., Brooks, L.D., DePristo, M.A., Durbin, R.M., Handsaker, R.E., Kang, H.M., Marth, G.T., and McVean, G.A.; 1000 Genomes Project Consortium. (2012). An integrated map of genetic variation from 1,092 human genomes. Nature *491*, 56–65.
29. Gu, C., Castellino, A., Chan, J.Y., and Chao, M.V. (1998). BRE: A modulator of TNF-alpha action. FASEB J. *12*, 1101–1108.
30. Pulit, S.L., Voight, B.F., and de Bakker, P.I. (2010). Multiethnic genetic association studies improve power for locus discovery. PLoS ONE *5*, e12600.

Example qualifying exam (Ph.D.) and comprehensive exam (M.S.) questions pertaining to Jordan et al. (2012) *American Journal of Human Genetics*.

1. The burden test and variable threshold test (both of which collapse information on rare variants across a genomic region) were used to test rare variants in CARD14 exons for association with psoriasis. What is the rationale for such tests? Why did investigators not test each rare variant individually?

2. The common variant rs11652075 (see Figure 2A) was tested for genetic association with psoriasis in six individual cohorts, as well as across all six cohorts simultaneously using meta-analysis. The odds ratios in the individual cohorts ranged from moderately protective (OR=0.66) to weakly harmful (OR=1.09) and associations were statistically significant in some, but not all, cohorts. However, the odds ratio of the meta-analysis was protective (OR=0.87) and very significant (p=0.000002). Interpret the meta-analysis results in light of the findings from individual cohorts. Is the meta-analysis inconsistent with the individual cohorts? Why or why not?

3. Consider the "common disease, common variant" hypothesis. What is the premise of this hypothesis, and do the results from this paper support or refute this hypothesis an explanation for genetic nature of psoriasis?

4. Consider Table 2, which shows for each CARD14 coding variant (1) the bioinformatically-predicted effect on protein function, (2) the effect on NF-kB activation, and (3) the allele frequencies in cases and controls. Suppose that the bioinformatics prediction of variant's function was "benign" and that this prediction was accurate. What would you expect for the variant's effect on NF-kB activation? What would you expect for the relative allele frequencies in cases and controls?

Suppose instead that the bioinformatics prediction of a variant's function was "damaging" and that this prediction was accurate. What would you expect for the variant's effect on NF-kB activation? What would you expect for the relative allele frequencies in cases and controls?

Scanning Table 2, are there any coding variants for which functional prediction is inconsistent with effect of NF-kB activation, or relative allele frequencies in cases vs. controls, or both?

5. The effect of CARD14 variants on NF-kB activity was measured both with and without TNF-alpha stimulation. Explain the rationale for this.

Rare and Common Variants in *CARD14*, Encoding an Epidermal Regulator of NF-kappaB, in Psoriasis

Catherine T. Jordan,[1] Li Cao,[1] Elisha D.O. Roberson,[1] Shenghui Duan,[1] Cynthia A. Helms,[1] Rajan P. Nair,[2] Kristina Callis Duffin,[3] Philip E. Stuart,[2] David Goldgar,[3] Genki Hayashi,[4] Emily H. Olfson,[1] Bing-Jian Feng,[3] Clive R. Pullinger,[5] John P. Kane,[6] Carol A. Wise,[7] Raphaela Goldbach-Mansky,[8] Michelle A. Lowes,[9] Lynette Peddle,[10] Vinod Chandran,[11] Wilson Liao,[4] Proton Rahman,[10] Gerald G. Krueger,[3] Dafna Gladman,[11] James T. Elder,[2] Alan Menter,[12] and Anne M. Bowcock[1,*]

Psoriasis is a common inflammatory disorder of the skin and other organs. We have determined that mutations in *CARD14*, encoding a nuclear factor of kappa light chain enhancer in B cells (NF-kB) activator within skin epidermis, account for PSORS2. Here, we describe fifteen additional rare missense variants in *CARD14,* their distribution in seven psoriasis cohorts (>6,000 cases and >4,000 controls), and their effects on NF-kB activation and the transcriptome of keratinocytes. There were more *CARD14* rare variants in cases than in controls (burden test p value = 0.0015). Some variants were only seen in a single case, and these included putative pathogenic mutations (c.424G>A [p.Glu142Lys] and c.425A>G [p.Glu142Gly]) and the generalized-pustular-psoriasis mutation, c.413A>C (p.Glu138Ala); these three mutations lie within the coiled-coil domain of *CARD14*. The c.349G>A (p.Gly117Ser) familial-psoriasis mutation was present at a frequency of 0.0005 in cases of European ancestry. CARD14 variants led to a range of NF-kB activities; in particular, putative pathogenic variants led to levels >2.5× higher than did wild-type CARD14. Two variants (c.511C>A [p.His171Asn] and c.536G>A [p.Arg179His]) required stimulation with tumor necrosis factor alpha (TNF-α) to achieve significant increases in NF-kB levels. Transcriptome profiling of wild-type and variant CARD14 transfectants in keratinocytes differentiated probably pathogenic mutations from neutral variants such as polymorphisms. Over 20 *CARD14* polymorphisms were also genotyped, and meta-analysis revealed an association between psoriasis and rs11652075 (c.2458C>T [p.Arg820Trp]; p value = 2.1×10^{-6}). In the two largest psoriasis cohorts, evidence for association increased when rs11652075 was conditioned on *HLA-Cw*0602* (PSORS1). These studies contribute to our understanding of the genetic basis of psoriasis and illustrate the challenges faced in identifying pathogenic variants in common disease.

Introduction

Psoriasis is a chronic, inflammatory disease of the skin and other organs. It affects approximately 2% of individuals of European descent,[1] and in up to 30% of cases, it is associated with chronic inflammatory psoriatic arthritis.[2] Genome-wide association studies (GWASs) have identified over 20 susceptibility loci for psoriasis.[3–11] However, with the exception of psoriasis susceptibility locus 1 (PSORS1 [MIM 177900]), for which the odds ratio (OR) is approximately 3.0,[12,13] risk conferred by these loci is generally small (ORs $\leq$ 1.5). Moreover, less than 20% of disease variance has been explained.[14,15] This implies that additional low-risk loci, genetic interactions, or rare variants of large effect account for the remaining variance.

In our accompanying paper, we identified rare, gain-of-function mutations in caspase recruitment domain family, member 14 (*CARD14* [MIM 607211])[16] in two large multiplex families affected by Mendelian forms of psoriasis and psoriatic arthritis (see the accompanying paper[17] in this issue of AJHG). We also identified a de novo mutation in *CARD14* in a child with early-onset, severe pustular psoriasis (PSORP [MIM 614204]). These mutations are responsible for the elusive psoriasis susceptibility locus 2 (PSORS2 [MIM 602723]) in chromosomal region 17q25. These results led us to hypothesize that additional rare and common variants in *CARD14* might contribute to psoriasis and/or psoriatic arthritis in the general population.

Here, we identify and characterize 15 additional rare missense variants within *CARD14* and determine their frequencies in a large cohort of approximately 6,000 psoriasis cases and 4,000 controls. Statistical analyses revealed an excess of rare variants in psoriasis cases relative to controls. The potential pathogenicity of variants was demonstrated by their ability to increase transcriptional activation by nuclear factor of kappa light chain enhancer in B cells (NF-kB) and to enhance production of a subset of psoriasis-associated transcripts. A common missense

[1] Division of Human Genetics, Department of Genetics, Washington University School of Medicine, St. Louis, MO 63110, USA; [2] Department of Dermatology, University of Michigan, Ann Arbor, MI 48109, USA; [3] Department of Dermatology, University of Utah School of Medicine, Salt Lake City, UT 84132, USA; [4] Department of Dermatology, University of California, San Francisco, San Francisco, CA 94115, USA; [5] Cardiovascular Research Institute and Department of Physiological Nursing, University of California, San Francisco, San Francisco, CA 94143, USA; [6] Cardiovascular Research Institute, Department of Medicine, and Department of Biochemistry and Biophysics, University of California, San Francisco, San Francisco, CA 94143, USA; [7] Sarah M. and Charles E. Seay Center for Musculoskeletal Research, Texas Scottish Rite Hospital for Children, Dallas, TX 75219, USA; [8] National Institute of Arthritis and Musculoskeletal and Skin Diseases, National Institutes of Health, Bethesda, MD 20892, USA; [9] Laboratory for Investigative Dermatology, The Rockefeller University, New York, NY 10065, USA; [10] Department of Medicine, Division of Rheumatology, Memorial University of Newfoundland, St. John's, NL A1C 5S7, Canada; [11] University of Toronto and Toronto Western Hospital, Toronto, ON M5T 2S8, Canada; [12] Psoriasis Research Institute, Baylor University Medical Center, Dallas, TX 75246, USA
*Correspondence: bowcock@genetics.wustl.edu

DOI 10.1016/j.ajhg.2012.03.013. ©2012 by The American Society of Human Genetics. All rights reserved.

variant within *CARD14* was also associated with psoriasis, and that evidence for association increased when this locus was conditioned on the presence of PSORS1. Our findings indicate that a range of NF-kB responses in the skin are mediated by CARD14 and that a subset of rare CARD14 variants leads to psoriasis and psoriatic arthritis.

Subjects and Methods

Subjects

Cases and controls for sequencing and genotyping were recruited from multiple institutions. Samples were organized into cohorts as shown in Table 1. There were six cohorts of European ancestry and one of Asian ancestry. Referring to Table 1, European cases in cohort A were recruited from either Washington University in St. Louis or the Department of Dermatology at the University of California, San Francisco (UCSF). Controls in cohort A were unaffected individuals who were over 20 years of age and who had no family history of psoriasis; they were recruited from the Texas Scottish Rite Hospital for Children or from the Cardiovascular Research Institute and Center for Human Genetics at the University of California, San Francisco or they were CEU (Utah residents with Northern and Western European ancestry from the CEPH collection) grandparents. Cohort B samples were from the National Psoriasis Foundation Victor Henschel Tissue Repository (NPF). Cases and controls in cohort C were recruited from the Department of Dermatology at the University of Utah. For cohorts A–C, psoriasis was diagnosed by a dermatologist.

Cohort D samples were recruited from the Department of Dermatology at the University of Michigan. Cases had at least two psoriatic plaques or a single plaque occupying at least 1% of the total body surface outside the scalp. Individuals presenting with only palmoplantar psoriasis, inverse psoriasis, or sebopsoriasis were excluded. Controls were at least 18 years of age and had no personal or family history of psoriasis.

Cohort E samples were gathered from the University of Toronto and Toronto Western Hospital. Cohort F samples were gathered from the Department of Medicine, Division of Rheumatology, Memorial University of Newfoundland. Psoriasis was diagnosed by a dermatologist. When psoriatic arthritis was suspected, cases were evaluated according to clinical history and rheumatologic and radiologic evaluation. Control individuals showed no evidence of psoriasis, psoriatic arthritis, or any other autoimmune disease.

Asian samples in Cohort G were recruited from the Cardiovascular Research Institute and Center for Human Genetics at the University of California, San Francisco, from the University of Toronto and Toronto Western Hospital and the Department of Medicine, or from the NPF.

DNA was isolated from whole blood or saliva by standard methods. Protocols were approved by local institutional review boards. All subjects or their parents (if the subjects were minors) provided informed consent.

Sanger Resequencing and Genotyping

As a first pass, all coding exons of *CARD14* (full-length, *CARD14fl*) were resequenced in 192 psoriasis cases and 96 controls of European ancestry. Exons in which rare missense mutations were identified were resequenced in 95 more controls of European ancestry. Exon 4 of *CARD14* was resequenced in an additional 1,856 cases and 882 controls of European ancestry. Primers are available upon request. Samples were genotyped with the Sequenom MassARRAY at Washington University and by TaqMan at the University of Michigan (Table S2, available online). All samples from the NPF were genotyped, but only samples of known ethnicity were included in statistical analyses.

Table 1. Psoriasis Cases and Controls Included in this Study

Cohort	Cohort Description	Cases	Controls
A	St. Louis/Dallas/UCSF	676	570
B	NPF (European)	486	154
C	Utah	931	236
D	Michigan	2,768	2,749
E	Toronto	981	483
F	Newfoundland	340	379
G	Asians	194	193
H	Combined European (rows A–F)	6,182	4,571
I	NPF (all samples)	976	758

Individuals were recruited from multiple institutions and organized into cohorts, as shown in this table. Cohorts A–F are independent case/control cohorts of Northern European ancestry. Cohort G includes samples of Asian ancestry from the St. Louis/Dallas/UCSF (University of California, San Francisco) and the NPF (National Psoriasis Foundation Victor Henschel Tissue Repository) cohorts (cohorts A and B, respectively). Cohorts A–G include samples of known ancestry. Cohort H lists all cases and controls contributed by the NPF, including those of unknown ancestry. Demographic data were available only for approximately half of the NPF samples.

Expression Plasmids

Full-length *CARD14sh* (GenBank BC018142, coding for 740 amino acids) and *CARD14cl* (RefSeq NM_052819, coding for 434 amino acids) were cloned into pReceiver-M11 (Capital Biosciences). The *CARD14sh* construct was subjected to in vitro mutagenesis with the QuikChange Site-Directed Mutagenesis Kit (Stratagene). The numbering of all *CARD14* mutations in this manuscript is based on RefSeq NM_024110.3. For rare, nonannotated missense variants, constructs were generated with the mutant allele. For polymorphisms (rare and common), constructs were generated as follows (the allele and amino acid used are listed in parentheses): rs115582620 (c.185A [p.Gln185]), p.Ser200Asn (c.599A [p.Asn200]), rs146214639 (c.449G [p.Arg150]), rs144475004 (c.526C [p.His176]), rs2066964 (c.930C [p.Ser547]), rs34367357 (c.1042A [p.Ile585]), rs117918077 (c.2044T [p.Trp682]), and rs151150961 (c.2140A [p.Ser714]). Full-length *CARD14fl* was not available for subcloning. As a result, constructs could not be created for rs144285237 (c.2919C>G [p.Asp973Gln]) or rs11652075 (c.2458C>T [p.Arg820Trp]).

NF-kB Luciferase Reporter Assay

The NF-kB luciferase reporter assay was performed with the pNFkB-luc system (Clontech) as described in our accompanying manuscript.[17] The *CARD14cl* clone was used as a negative control in this assay because it lacks the sequence encoding the CARD domain, which is necessary for CARD14-induced NF-kB activation.

Expression Profiling and qRT-PCR

HEK 001 cells (human-papillomavirus-16-transformed keratinocytes) were transfected with wild-type CARD14sh or expression constructs encoding CARD14sh substitutions. Cells were cultured for 24 hr, and then RNA was isolated with the miRNeasy kit (QIAGEN). Global expression profiling of RNA from cells was performed with the HumanHT-12 v4 Expression BeadChip (Illumina). Experiments were conducted in compliance with MIAME (minimum information about a microarray experiment) guidelines. Raw and normalized expression data are deposited in the National Center for Biotechnology Information (NCBI) Gene Expression Omnibus (GEO) as series GSE36381. 100 ng to 1 μg of randomly primed total RNA was used for quantitative RT-PCR (qRT-PCR) according to standard procedures. Expression levels were normalized to 18S rRNA. Relative expression levels were calculated as follows: $2 \times 10^{6((\mathrm{Ct\ 18S})-(\mathrm{Ct\ CARD14}))}$. We also normalized expression levels in transfected cells to levels of FLAG to correct for differences in transfection efficiency.

Clustering of Variants on the Basis of Expression Levels in Keratinocytes

On the basis of the NF-kB reporter assays, a subset of CARD14 variants were classified as (1) leading to enhanced basal NF-kB activation when they were compared to the effects of wild-type CARD14sh (these are c.349G>A [p.Gly117Ser], c.413A>C [p.Glu138Ala], c.424G>A [p.Glu142Lys], and c.425A>G [p.Glu142Gly]), (2) leading to downregulation of NF-kB activation (c.112C>T [p.Arg38Cys]), or (3) having no effect on NF-kB activation (these are c.185G>A [p.Arg62Gln] [rs115582620], c.930G>C [p.Arg547Ser] [rs2066964], c.449T>G [p.Leu150Arg] [rs146214639], c.854A>G [p.Asp285Gly], c.1778T>A [p.Ile593Asn], c.2044C>T [p.Arg682Trp] [rs117918077], and c.2140G>A [p.Gly714Ser] [rs151150961]). After performing mRNA transcriptome analysis on cells that were transfected with either wild-type CARD14sh or CARD14 variants, we found that 1,531 transcripts had at least a 2-fold change (up or down) in expression as well as a significant p value in transfectants with the CARD14 variants causing enhanced NF-kB activation relative to transfectants with wild-type CARD14sh. The variants were then clustered with the use of the reduced probe set and the R (v2.10.1) randomForest package (v4.6-2). Random forests were generated with 500 trees and unweighted classes, and importance was calculated for a total of 10,000,000 forests. The probes were then ranked from highest to lowest mean decrease in Gini. A heat map of the clustering of the full set of variants was generated with the top 30 probes.

Pathway Analysis of the "CARD14 Pathogenic Keratinocyte Signature"

A list was generated of genes differentially expressed as a consequence of the introduction of CARD14 psoriasis-specific alterations into HEK 001 cells as described above. We obtained this list, termed the "CARD14 pathogenic keratinocyte signature," by comparing the global transcriptomes of keratinocyte transfectants with overtly pathogenic CARD14 substitutions (p.Gly117Ser, p.Glu138Ala, p.Gly142Lys, and p.Glu142Gly) to those with nonpathogenic substitutions (p.Leu150Arg [rs146214639], p.Val191Leu, p.Asp285Gly, and wild-type CARD14sh). Expression data from each sample were quantile normalized, log2 transformed, and fitted to linear models in R (R v2.13.1; Biobase v2.12.2; BeadArray v2.2.0; and limma v3.8.3). The contrast was defined as "pathogenic versus nonpathogenic," and the t tests, fold changes, and false-discovery-rate-corrected p values were calculated with ImFit and eBayes. Given the overexpression of the constructs, larger sample sizes would be required for the detection of significant group-wise effects. However, by taking the genes with a nominal group-wise p value of 0.05 and ranking them by fold change, we generated a list of the top 200 upregulated and top 200 downregulated genes. This list was analyzed with Ingenuity pathway analysis (IPA).

Statistical Analysis

Analysis of variants was performed with PLINK.[18] The variable threshold test[19] and a straightforward burden test for association of rare variants with disease were performed with PLINK/SEQ version 0.05. For both tests, we included *CARD14* variants with minor allele frequencies of less than or equal to 0.01 among our controls of northern European ancestry. This included the following 16 variants: c.112C>T (p.Arg38Cys), c.185G>A (p.Arg62Gln) (rs115582620), c.349G>A (p.Gly117Ser) (altered in family PS1[17]), c.413A>C (p.Glu138Ala) (altered in generalized pustular psoriasis[17]), c.424G>A (p.Glu142Lys), c.425A>G (p.Glu142Gly), c.449T>G (p.Leu150Arg) (rs146214639), c.511C>A (p.His171Asn), c.526G>C (p.Asp176His) (rs144475004), c.536G>A (p.Arg179His), c.571G>T (p.Val191Leu), c.599G>A (p.Ser200Asn), c.854A>G (p.Asp285Gly), c.1778T>A (p.Ile593Asn), c.2140G>A (p.Gly714Ser) (rs151150961), and c.2919C>G (p.Asp973Gly) (rs144285237). Meta-analysis of polymorphisms and generation of forest plots were performed with R version 2.12.2[20] with the rmeta package.

Results

Rare-Variant Screening

In our accompanying manuscript, we identified rare gain-of-function *CARD14* mutations that lead to psoriasis.[17] These included the familial c.349G>A (p.Gly117Ser) mutation in family PS1, affected by multiple cases of psoriasis and psoriatic arthritis,[21] and the de novo c.413A>C (p.Glu138Ala) germline mutation in a case of childhood generalized pustular psoriasis. To determine whether there were additional rare variants predisposing to psoriasis in *CARD14*, we resequenced all coding exons of *CARD14* (full-length, *CARD14fl*) in over 192 psoriasis cases and 96 controls (see Subjects and Methods). This revealed ten rare missense mutations in *CARD14* (Figure 1, Table 2, and Table S1): c.112C>T (p.Arg38Cys), c.185G>A (p.Arg62Gln) (rs115582620), c.425A>G (p.Glu142Gly), c.449T>G (p.Leu150Arg) (rs146214639), c.599G>A (p.Ser200Asn), c.854A>G (p.Asp285Gly), c.1778T>A (p.Ile593Asn), c.2044C>T (p.Arg682Trp) (rs117918077), c.2140G>A (p.Gly714Ser) (rs151150961), and c.2919C>G (p.Asp973Gln) (rs144285237). On the basis of the observation that several rare mutations were clustered in exon 4, which encodes part of the critical coiled-coil domain, we reasoned that it might be a mutation hotspot and resequenced an additional 1,800 cases and 900 controls for that exon. This revealed five additional rare variants within *CARD14*: c.424G>A (p.Glu142Lys), c.511C>A (p.His171Asn), c.526G>C

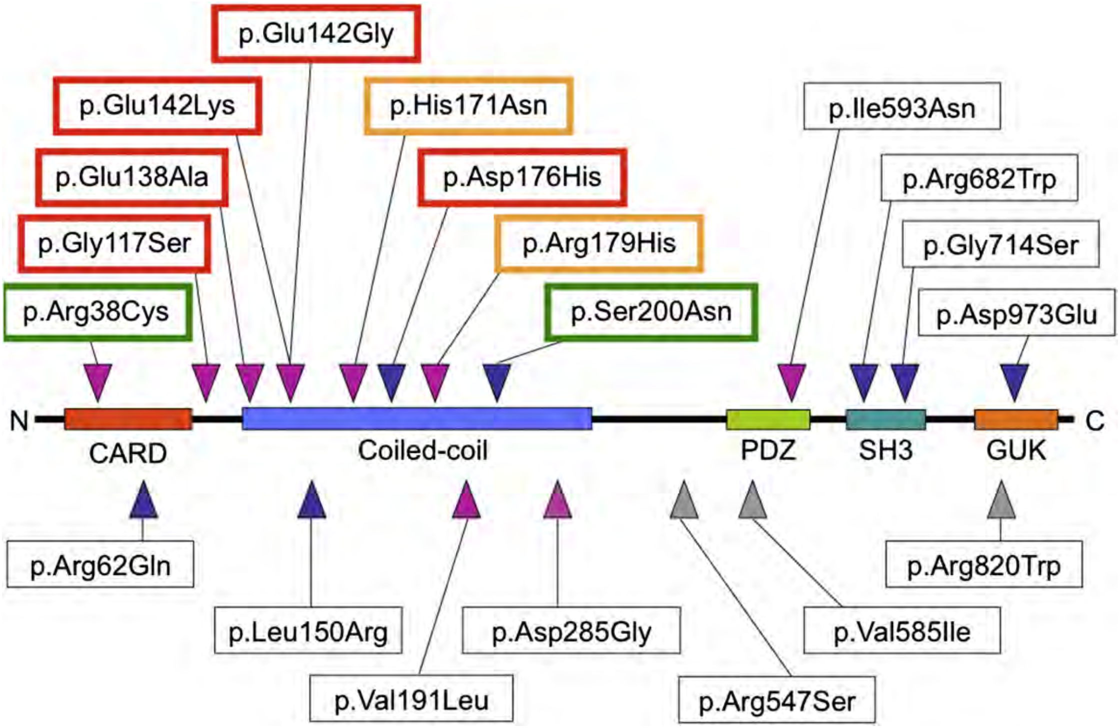

Figure 1. CARD14 Protein Domains and Locations of Amino Acid Substitutions

Missense variants identified in CARD14 by resequencing are shown relative to key protein domains. Red outlining indicates increased NF-kB activation by a variant (relative to wild-type); green outlining indicates reduced activation. Gold outlining indicates variants that showed increased NF-kB activation only in response to TNF-α stimulation. SNPs and variants also identified in dbSNP135, which includes data from the 1,000 Genomes Project and the National Heart, Lung, and Blood Institute (NHLBI) and National Human Genome Research Institute (NHGRI) Exome Project, are indicated with blue triangles. A polymorphism, rs114688446, was observed at the same site as p.Ser200Asn, but a different substitution, p.Ser200Ile, was detected. SNPs used for meta-analysis are indicated with gray triangles.

(p.Asp176His) (rs144475004), c.536G>A (p.Arg179His), and c.571G>T (p.Val191Leu) (Figure 1, Table 2, and Table S1). A search in dbSNP135 revealed that 8 of the 15 identified rare variants have not been previously annotated; these eight are c.112C>T (p.Arg38Cys), c.424G>A (p.Glu142Lys), c.425A>G (p.Glu142Gly), c.511C>A (p.His171Asn), c.536G>A (p.Arg179His), c.571G>T (p.Val191Leu), c.599G>A (p.Ser200Asn), c.854A>G (p.Asp285Gly), and c.1778T>A (p.Ile593Asn). Furthermore, this search revealed that the c.349G>A (p.Gly117Ser) and c.413A>C (p.Glu138Ala) mutations have also not been previously annotated.

Population-Based Frequency Estimates of Rare Variants

We determined the frequencies of all rare *CARD14* variants, including those encoding the familial p.Gly117Ser alteration (causing psoriasis and/or psoriatic arthritis) and the p.Glu138Ala alteration (causing generalized pustular psoriasis), by high-throughput genotyping seven independent case/control cohorts (>10,000 individuals; Tables 1 and 2 and Tables S1 and S2). This revealed two other unrelated psoriasis cases with the *CARD14* c.349G>A (p.Gly117Ser) mutation; one woman was from the NPF repository and was diagnosed with psoriasis at 10 years old and psoriatic arthritis at 20 years old, and another woman was from Utah and had a history of psoriasis, which was diagnosed at 65 years old. This latter woman transmitted the mutation to her daughter, who developed psoriasis at age 32. This mutation was also detected in a male NPF control for whom additional data (e.g., ethnicity, age, and family history of psoriasis) were not available. None of these individuals harbored the *SLC26A11*[22] (solute carrier family 26, member 11, [SLC26A11 (MIM 610117)]) c.365A>G (p.Tyr122Cys) mutation, which cosegregated with c.349G>A (p.Gly117Ser) in family PS1,[17] providing evidence that these variants can arise independently. Numbering of the *SLC26A11* mutation is based on RefSeq NM_001166347.1. In total, the frequency of the *CARD14* c.349G>A (p.Gly117Ser) mutation in cases of European ancestry was 0.0005. The *CARD14* c.349+5G>A mutation, which segregated with psoriasis in a large multiply affected Taiwanese family,[17] was not detected in any other cases or controls. However, given the relatively small number of Asian samples screened, we were not well powered to detect variants at low frequencies in that population. The mutation encoding p.Glu138Ala seen in the single pustular psoriasis case was also not seen in any other cases or controls.

Five rare *CARD14* variants (encoding p.Arg38Cys, p.Glu142Gly, p.Glu142Lys, p.Val191Leu, and p.Asp285Gly; Figure 1 and Tables S1 and S2) were seen in only one case and

Table 2. Characteristics and Frequencies of *CARD14* Coding Variants

CARD14 Exon	cDNA Mutation and Corresponding Protein Change	Protein Domain	PolyPhen2[27]-Predicted Effect on Protein Function	Effect on NF-kB Activation (FC versus Wild-Type CARD14sh)	Allele Frequency in Cases (Number Sampled)	Allele Frequency in Controls (Number Sampled)
2	c.112C>T (p.Arg38Cys)	CARD	probably damaging	0.11	0.00019 (2,691)	0 (1,271)
2	c.185G>A (p.Arg62Gln) (rs115582620)	CARD	benign	1.06	0.0014 (3,284)	0.00084 (1,797)
3	c.349G>A (p.Gly117Ser)	none	possibly damaging	3.71	0.00023 (6,630)	0 (4,731)
3	c.349+5G>A	none	NA	ND	0 (2,871)	0 (1,339)
4	c.413A>C (p.Glu138Ala)	coiled-coil	probably damaging	8.95	0.00015 (3,488)	0 (1,902)
4	c.424G>A (p.Glu142Lys)	coiled-coil	probably damaging	4.03	0.00012 (4,107)	0 (1,874)
4	c.425A>G (p.Glu142Gly)	coiled-coil	probably damaging	5.00	0.00019 (2,848)	0 (1,451)
4	c.449T>G (p.Leu150Arg) (rs146214639)	coiled-coil	probably damaging	1.79	0.0025 (6,140)	0.0016 (4,614)
4	c.511C>A (p.His171Asn)	coiled-coil	benign	0.68 (5.95 with TNF-α stimulation)	0.00025 (4,077)	0 (1,858)
4	c.526G>C (p.Asp176His) (rs144475004)	coiled-coil	probably damaging	2.78	0.00056 (3,575)	0.00062 (1,609)
4	c.536G>A (p.Arg179His)	coiled-coil	probably damaging	1.38 (2.19 with TNF-α stimulation)	0.00025 (4,061)	0.00027 (1,848)
4	c.571G>T (p.Val191Leu)	coiled-coil	benign	1.02	0.00014 (3,575)	0 (1,613)
4	c.599G>A (p.Ser200Asn)	coiled-coil[a]	benign	0.67	0.011 (6,163)	0.0084 (4,624)
6	c.854A>G (p.Asp285Gly)	none	possibly damaging	1.14	0.00019 (2,673)	0 (1,467)
13	c.1778T>A (p.Ile593Asn)	PDZ	probably damaging	1.30	0.00024 (2,049)	0.00048 (1,039)
15	c.2044C>T (p.Arg682Trp) (rs117918077)	SH3	probably damaging	0.95	0.013 (2,169)	0.012 (1,042)
15	c.2140G>A (p.Gly714Ser) (rs151150961)	SH3	benign	1.02	0.0021 (2,105)	0.0014 (1,038)
21	c.2919C>G (p.Asp973Glu) (rs144285237)	GUK	benign	ND[b]	0.0024 (5,177)	0.0015 (4,099)

CARD14 missense variants are listed with details on their locations in critical CARD14 protein domains, their predicted effect on protein function from PolyPhen2,[27] their effect on NF-kB activation (fold change compared to unstimulated wild-type CARD14sh; see also Figure 3), and frequencies in unrelated cases and controls of European ancestry. The number of individuals screened is in parenthesis. The following abbreviations are used: FC, fold change; and ND, not done.

[a] The p.Ser200 residue lies within a 6 bp sequence separating two predicted coiled-coil regions and thus could be considered part of an overarching coiled-coil domain. Also, variant rs114688446 was identified at this location in dbSNP, but the amino acid change (p.Ser200Ile) was different.

[b] The impact of p.Asp973Glu on NF-kB activation could not be tested because it is exclusive to CARD14fl, for which a full-length cDNA clone was unavailable. Additional data on these variants are presented in Table S1.

in no controls. The variant encoding p.His171Asn was only seen in two psoriasis- and psoriatic-arthritis-affected cases from Newfoundland and in no controls. We performed a simple burden test and a variable threshold test[19] to compare the distribution of rare variants in cases and controls. These tests provided evidence of an excess of rare *CARD14* variants in cases versus controls (burden test p value = 0.0015; variable threshold test p value = 0.0053).

Common-Variant Association Tests

Resequencing validated several common missense polymorphisms described in dbSNP: rs2066964, rs34367357, and rs11652075. We genotyped these and 20 other previously described SNPs in our seven psoriasis case/control cohorts (Table S2) and looked for association with psoriasis. Most variants were present at similar frequencies in cases and controls. However, three missense SNPs (rs2066964, rs34367357, and rs11562075) within *CARD14* and rare variant c.599G>A (p.Ser200Asn) provided evidence of association with psoriasis in some of the cohorts (Table S2). A meta-analysis of these four missense variants was performed for the six cohorts of European ancestry (Figure 2 and Figure S1). This revealed further evidence of association between psoriasis and rs11652075 (c.2458C>T [p.Arg820Trp]) (fixed effects p value = 2.1×10^{-6}, OR = 0.87 [0.83–0.92]; random effects p value = 0.031, OR = 0.86 [0.75–0.99]); c.2458C was the risk allele (Figures 2A and 2B). This SNP, as well as the same risk allele, was also associated with psoriasis in Asians (p value = 0.0029, OR = 0.64 [0.48–0.86]). The meta-analysis also revealed evidence of association with p.Ser200Asn (fixed and random effects p values = 0.05, OR = 1

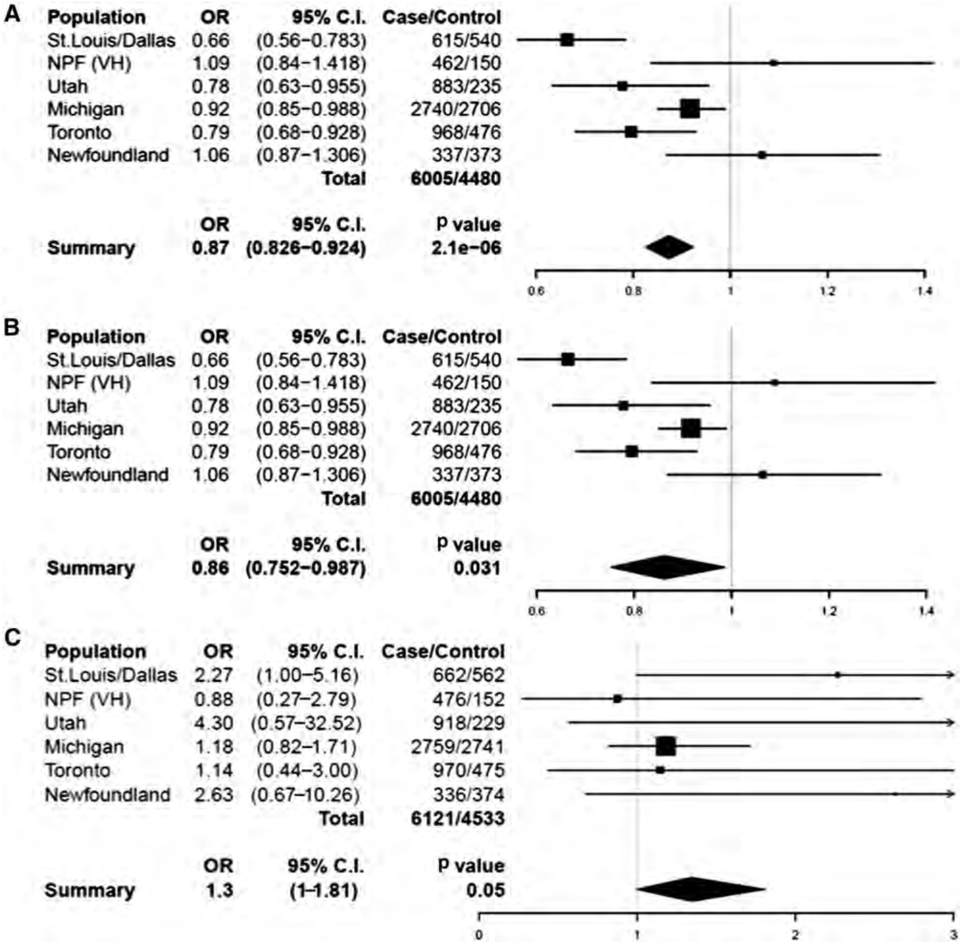

A

Population	OR	95% C.I.	Case/Control
St.Louis/Dallas	0.66	(0.56–0.783)	615/540
NPF (VH)	1.09	(0.84–1.418)	462/150
Utah	0.78	(0.63–0.955)	883/235
Michigan	0.92	(0.85–0.988)	2740/2706
Toronto	0.79	(0.68–0.928)	968/476
Newfoundland	1.06	(0.87–1.306)	337/373
		Total	**6005/4480**

	OR	95% C.I.	p value
Summary	**0.87**	**(0.826–0.924)**	**2.1e-06**

B

Population	OR	95% C.I.	Case/Control
St.Louis/Dallas	0.66	(0.56–0.783)	615/540
NPF (VH)	1.09	(0.84–1.418)	462/150
Utah	0.78	(0.63–0.955)	883/235
Michigan	0.92	(0.85–0.988)	2740/2706
Toronto	0.79	(0.68–0.928)	968/476
Newfoundland	1.06	(0.87–1.306)	337/373
		Total	**6005/4480**

	OR	95% C.I.	p value
Summary	**0.86**	**(0.752–0.987)**	**0.031**

C

Population	OR	95% C.I.	Case/Control
St.Louis/Dallas	2.27	(1.00–5.16)	662/562
NPF (VH)	0.88	(0.27–2.79)	476/152
Utah	4.30	(0.57–32.52)	918/229
Michigan	1.18	(0.82–1.71)	2759/2741
Toronto	1.14	(0.44–3.00)	970/475
Newfoundland	2.63	(0.67–10.26)	336/374
		Total	**6121/4533**

	OR	95% C.I.	p value
Summary	**1.3**	**(1–1.81)**	**0.05**

Figure 2. Meta-Analyses of rs11652075 and p.Ser200Asn across Six Case/Control Cohorts of European Ancestry
The results of the fixed- (A) and random-effects (B) meta-analyses for rs11652075 (c.2458C>T [p.Arg820Trp]) and the fixed-effects meta-analysis for p.Ser200Asn (c.599G>A) (C) are shown. The random-effects meta-analysis for p.Ser200Asn was identical to that of the fixed-effects meta-analysis and is therefore not pictured. Forest plots indicate the direction of effect, relative weight, and confidence interval for the odds ratio of this SNP in each cohort. The number of cases and controls successfully genotyped in each cohort is shown, and the meta-analysis OR and p value are listed below each plot. The following abbreviations are used: OR, odds ratio; and C.I., confidence interval.

[1.3–1.82]); the rare c.599A allele increased psoriasis risk (Figure 2C). However, this would not be significant if it were adjusted for multiple testing.

Because of the large effect of *HLA-Cw*0602* from the major histocompatibility complex (MHC) class I region (PSORS1),[12,13] we investigated its connection with the four *CARD14* variants described above. In the Michigan and Utah psoriasis cohorts, rs11652075 was found to have a higher association with psoriasis when it was conditioned on *HLA-Cw*0602* (p value of rs11652075 alone = 0.023 (Michigan), 0.017 (Utah); stratified on *HLA-Cw*0602*, p value = 0.0021 (Michigan), 0.0086 (Utah); Table S3). No such evidence was observed with the other variants.

Effect of Variants on CARD14 Function In Vitro

CARD14 encodes a 1,004 amino acid protein that activates NF-kB.[16] In our companion paper, we observed that compared to wild-type CARD14, the familial p.Gly117Ser and de novo p.Glu138Ala substitutions lead to enhanced NF-kB activation (3.71- and 8.95-fold enhancement, respectively). To test the effect of rare variants described here on this activity, we again used an NF-kB luciferase reporter assay. Several rare variants (p.Glu142Lys, p.Glu142Gly, and p.Asp176His [rs144475004]) in the coiled-coiled domain increased NF-kB activation two to five times more than did wild-type CARD14sh (Table 2, Figure 3A). The p.Arg38Cys, p.His171Asn, and p.Ser200Asn substitutions led to less NF-kB activation than did CARD14sh, but compared to wild-type CARD14sh, other rare variants and the CARD14 missense polymorphisms (p.Arg62Gln [rs115582620], p.Arg547Ser [rs2066964], p.Arg682Trp [rs117918077]) did not significantly alter NF-kB activation levels (Table 2, Figure 3A). As discussed below, variants that increased NF-kB activation at least 2.5× more than that seen with CARD14sh also induced greater upregulation of psoriasis-associated genes. Relative to wild-type CARD14sh, variants that resulted in a more

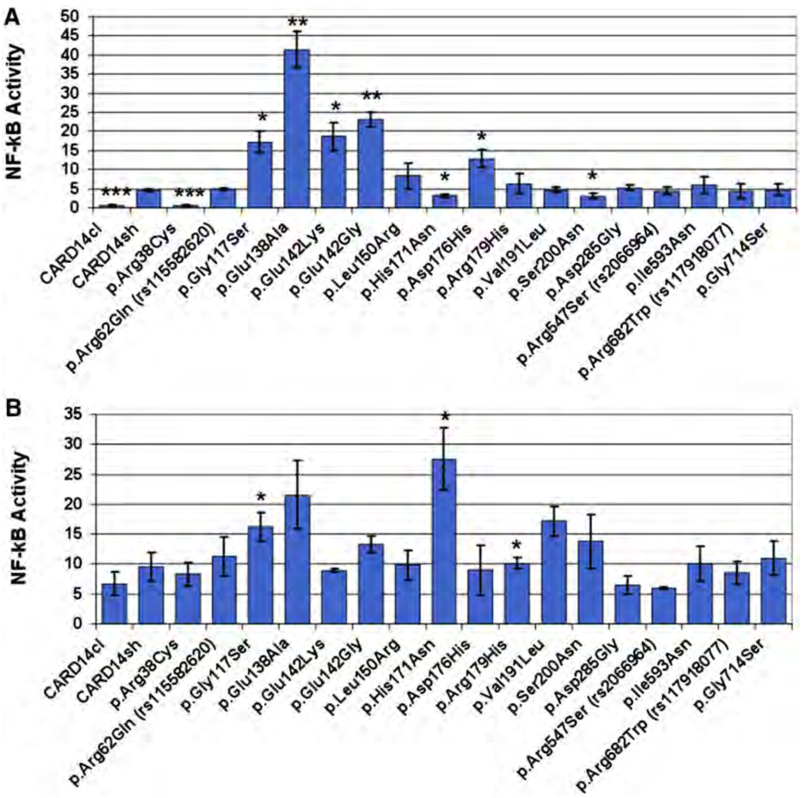

Figure 3. Effect of Wild-Type and Altered CARD14 on NF-kB Activation

HEK 293 cells were transfected with the construct that codes for CARD14sh, the same construct harboring one of the rare variants shown, or a construct that codes for CARD14cl and lacks the CARD domain. NF-kB activity was determined by measuring relative luciferase activity. Transfection efficiency was controlled for by first normalizing all values to *Renilla* expression, and activity of the empty background vector, pTAL-luc, was controlled for by adjusting the values. Change in NF-kB activity relative to the background vector was determined for each variant (*y* axis, NF-kB activity). Every data point represents the average value of three replicates. Error bars represent the standard deviation of replicates. For experiments involving TNF-α stimulation, treated cells were exposed to 20 ng/ml TNF-α in culture media for 24 hr. Asterisks show results from two-tailed, unpaired student's t tests comparing NF-kB activation induced by the indicated variant to either that of unstimulated cells with CARD14sh (A) or that of TNF-α-stimulated cells with CARD14sh (B). $^*p \leq 0.05$, $^{**}p \leq 0.01$, and $^{***}p \leq 0.001$.

modest increase in NF-kB activation, those that reduced NF-kB activation, and those that did not change it did not induce upregulation of those genes to the same degree. Therefore, when compared with the level of NF-kB activation caused by wild-type CARD14, a 2.5× or greater increase in NF-kB activation is predictive of putative pathogenic CARD14 amino acid substitutions.

Onset of psoriatic lesions is thought to be triggered by an inflammatory stimulus. We therefore examined the effects of wild-type and variant CARD14 on NF-kB activation after stimulation with tumor necrosis factor alpha (TNF-α). Compared with unstimulated CARD14sh, TNF-α-stimulated p.His171Asn and p.Arg179His resulted in a 5.95- and a 2.95-fold increase in NF-kB activation, respectively; compared with TNF-α-stimulated CARD14sh, TNF-α-stimulated p.His171Asn and p.Arg179His resulted in a 2.87- and a 1.06-fold increase in NF-kB activation, respectively (Table 2 and Figure 3B, discussed further below).

Effect of CARD14 Substitutions on Keratinocyte Gene Expression

We have shown that CARD14 is localized in keratinocytes and that the familial and pustular-psoriasis variants (p.Gly117Ser and p.Glu138Ala, respectively) lead to enhanced production of some chemokines and other transcripts that are upregulated in psoriatic skin.[17] To evaluate the effect of the additional rare variants on transcription in keratinocytes, we transfected all altered constructs into the keratinocyte cell line HEK 001. The transcriptome of each transfectant was then evaluated after 24 hr by interrogation with Illumina bead arrays. A heat map with 30 probes (see Subjects and Methods, random forest classification) revealed clustering of the p.Glu142Lys and p.Glu142Gly transfectants with those with the p.Gly117Ser and p.Glu138Ala alterations (Figure 4). The p.Glu138Ala substitution clustered at the extreme end of other pathogenic variants and on its own branch of the tree. This might be expected given the severity of the disease in the child (who has generalized pustular psoriasis) in whom it was found.

Within this heat map, the following 13 genes were upregulated in keratinocytes transfected with pathogenic substitutions: superoxide dismutase 2, mitochondrial (*SOD2* [MIM 147460]); interleukin 6 (interferon, beta 2 [*IL6* (MIM 147620)]); colony stimulating factor 2 (granulocyte-macrophage [*CSF2* (MIM 138960)]); interleukin 8 (*IL8* [MIM 146930]); matrix metallopeptidase 9 (gelatinase B, 92kDa gelatinase, 92kDa type IV collagenase [*MMP9* (MIM 120361)]); BRF2, subunit of RNA polymerase III transcription initiation factor, BRF1-like (*BRF2* [MIM 607013]); chemokine (C-C motif) ligand 20 (*CCL20* [MIM 601960]); solute carrier family 7 (cationic amino acid transporter, y+ system), member 2 (*SLC7A2* [MIM 601872]); oxidized low density lipoprotein (lectin-like) receptor 1 (*OLR1* [MIM 602601]); interleukin 36, gamma (*IL36G* [MIM 605542]); guanylate binding protein 2, interferon-inducible (*GBP2* [MIM 600412]); tumor necrosis factor, alpha-induced protein 2 (*TNFAIP2* [MIM 603300]); and tumor necrosis factor (*TNF* [MIM 191160]). We used g:Profiler[23] to look for specific functions of these genes. The most significant Gene Ontology[24] terms associated with this group of genes included: immune-system process/development, hematopoietic- or lymphoid-organ

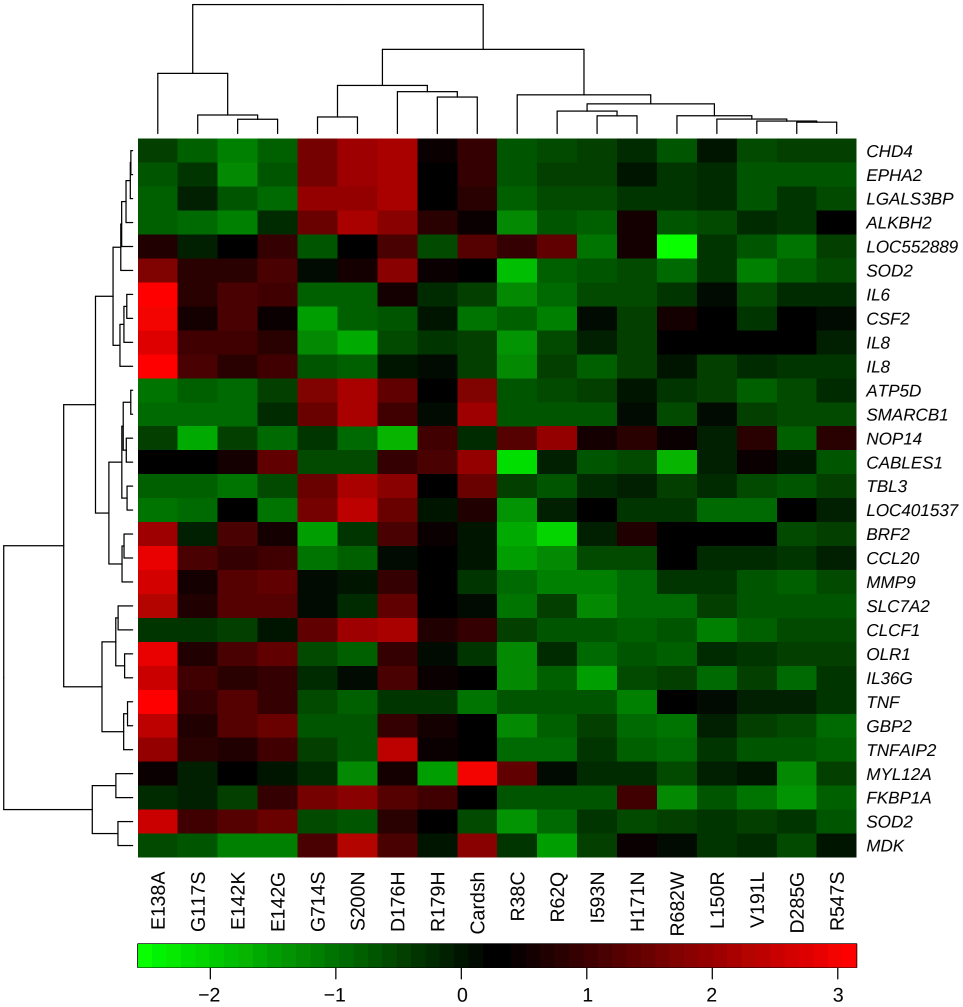

Figure 4. Heat Map Generated after Transcriptome Analysis of Wild-Type and Mutant CARD14 Transfectants
Cells were transfected with CARD14cl, wild-type CARD14sh, or variant CARD14 expression constructs. After 24 hr, RNA was extracted and used for the interrogation of Illumina bead arrays. A subset of differentially expressed genes was used for clustering of CARD14 variants (see Subjects and Methods).

development, and response to lipopolysaccharide/bacterium/molecule of bacterial origin. *IL6, MMP9*, and *BRF2* have also been implicated in cell migration and could mediate immune cell infiltration into the skin. *CSF2*, *IL8*, and *SLC7A2* have been specifically implicated in myeloid leukocyte activation. Psoriasis is a disease of keratinocyte and immune cell proliferation, and genes involved in cell proliferation include *SOD2, IL6, CSF2*, and *IL8*. Other terms included response to wounding (*SOD2, IL6, IL8, CCL20, SLC7A2*, and *OLR1*), nitric oxide biosynthetic process (*SOD2, IL6*, and *SLC7A2*), and antiapoptosis (*SOD2, IL6*, and *CSF2*). *IL6* and *CSF2* are implicated in the regulation of the JAK-STAT pathway, and *IL6, IL8*, and *MMP9* are implicated in angiogenesis. Genes involved in the response to biotic stimuli include *SOD2, IL6, IL8, MMP9*, and *CCL20*. Psoriasis increases risk of cardiovascular disease,[25,26] and five of these genes have been implicated in the development of the cardiovascular system (*SOD2, IL6, IL6, MMP9,* and *TNFAIP2*). Upregulation of these thirteen genes thus constitutes a pathogenic psoriatic signature.

Two variants clustered together: c.526G>C (p.Asp176His) (rs144475004) and c.536G>A (p.Arg179His). Both amino acid substitutions were predicted to be damaging by PolyPhen2,[27] and both lead to upregulation of NF-kB activation (2.78- and 1.38-fold increases, respectively). In the case of p.Arg179His, TNF-α was required for NF-kB activation to achieve pathogenic levels; compared with unstimulated CARD14sh and TNF-α-stimulated CARD14sh, TNF-α-stimulated p.Arg179His produced a 2.95- and a 1.06-fold increase, respectively. Both variants were seen in a small number of cases and controls (4:2 and 2:1, respectively).

Three other constructs clustered in the same branch with p.Asp176His (rs144475004) and p.Arg179His. These included wild-type CARD14sh, c.2140G>A (p.Gly714Ser) (rs151150961), and c.599G>A (p.Ser200Asn). However, the latter three did not induce expression of the pathogenic psoriatic signature described above to the same degree as the overtly pathogenic variants. One noteworthy example of this is that the *IL8* expression produced by these three constructs was much lower than that seen with the pathogenic variants. Moreover, clustering of these constructs was due to other transcripts that are not considered part of the pathogenic signature. Other variants exhibited reduced levels of genes in this psoriasis signature, even when compared to wild-type CARD14sh.

We confirmed altered expression of all thirteen transcripts (*SOD2*, *IL6*, *CSF2*, *BRF2*, *MMP9*, *IL8*, *CCL20*, *SLC7A2*, *OLR1*, *IL36G*, *GBP2*, *TNFAIP1*, and *TNF*) by qRT-PCR (Figure S2).

We also performed a group-wise comparison of the global expression profiles of the overtly pathogenic substitutions (p.Gly117Ser, p.Glu138Ala, p.Glu142Lys, and p.Glu142Gly) and several nonpathogenic variants (p.Leu150Arg [rs146214639], p.Val191Leu, p.Asp285Gly, and wild-type CARD14sh). The top 200 upregulated and top 200 downregulated genes were identified (see Subjects and Methods), and pathway analysis was performed with IPA (Table S4). A number of cytokine signaling pathways were significant (including IL-17 signaling, IL-6 signaling, and TNFR2 signaling). Also significant were communication between innate and adaptive immune cells, dendritic cell maturation, mTOR signaling, notch signaling, and atherosclerosis signaling pathways. This latter pathway is interesting given the association between psoriasis and other systemic comorbidities, including cardiovascular disease.[25,26]

A comparison of these results with a published psoriasis transcriptome[28] revealed that a number of these pathways are significantly represented in both groups. For example, the atherosclerosis signaling pathway, the NF-kB signaling pathway, and many of the cytokine signaling pathways were significant in both the published psoriasis transcriptome and the CARD14 pathogenic keratinocyte signature (Table S4). These results indicate that some of the pathways upregulated in keratinocytes in which CARD14 harbors a pathogenic substitution are also upregulated in classic psoriatic skin. This suggests that altered keratinocyte activation might significantly contribute to the transcriptome signatures in classic psoriasis lesions.

Discussion

Here, we describe a spectrum of rare and common variation within CARD14, an activator of NF-kB[16] in skin epidermis, and we demonstrate enrichment of rare variants in cases by using two independent statistical tests. The burden test, which performs a straightforward comparison of the number, or "burden," of rare variants in cases and controls, provided a p value of 0.0015. The variable threshold test,[19] which compares rare variants subject to a variable allele-frequency threshold in cases and controls, gave a p value of 0.0053. We also demonstrate that pathogenic alterations were enriched in the coiled-coil domain of CARD14. This domain is predicted to be involved in the oligomerization of CARD14 with other proteins and the formation of its active conformation.[29,30] Interestingly, although some of the rare variants we identified have been annotated in dbSNP135, none of the putative pathogenic alterations are annotated. A coding polymorphism in CARD14, rs11652075 (p.Arg820Trp), and c.599G>A (p.Ser200Asn) were also associated with psoriasis in several large cohorts. In the two largest psoriasis cohorts, evidence of association between psoriasis and rs11652075 increased when rs11652075 was conditioned on PSORS1.

Two rare variants, c.424G>A (p.Glu142Lys) and c.425A>G (p.Glu142Gly), were identified in cases but not in controls and manifested as overtly causing of disease. Compared with wild-type CARD14sh, they significantly enhanced NF-kB activation (4.03- and 5.00-fold enhancement, respectively), and they clustered with p.G117Ser and p.Glu138Ala after transfection into the keratinocyte line HEK 001 and global expression profiling. The c.424G>A (p.Glu142Lys) variant was identified in a Caucasian male who was diagnosed with psoriasis at 42 years of age and who responded well to treatment with UV light and a topical mixture of corticosteroid and a vitamin D analog. The c.425A>G (p.Glu142Gly) variant was found in a Caucasian male who was diagnosed with psoriasis in infancy and whose father also had psoriasis. He experienced a partial remission of psoriasis with methotrexate treatment. It is noteworthy that after these variants were stimulated with TNF-α, levels of NF-kB activation induced by these variants and the pustular-psoriasis substitution, p.Glu138Ala, decreased at the 24 hr mark. This suggests that at this time, downregulation of the NF-kB response might have been initiated in our cell-culture system, which merits further study. Both of these variants lie in the coiled-coil domain of CARD14, as does the de novo pustular-psoriasis substitution, p.Glu138Ala.

Compared with wild-type CARD14sh, a third variant, p.Asp176His (rs144475004), leads to enhanced NF-kB activation. However, its frequency was similar in cases and controls, and it didn't increase NF-kB activity in vitro as much as other variants did. Hence, it might lie below the NF-kB-activation threshold required for disease. Alternatively, disease might require a specific stimulus or interaction with a second genetic factor. Other variants such as p.Arg38Cys and p.Ser200Asn exhibited significantly less NF-kB activation than did wild-type CARD14sh. Previous studies have shown that decreased activation of NF-kB, much like increased activation, can induce inflammation and epidermal hyperplasia.[31,32] It might be interesting to examine clinical features, such as inflammation after skin wounding, of individuals with these variants. However, it should be noted that the p.Arg38Cys and p.Ser200Asn substitutions did not induce expression of the pathogenic psoriasis signature when transfected into keratinocytes. Thus, although we cannot completely rule out a role for these variants in some aspects of disease, they are neither overtly pathogenic nor likely to be causative for initiation of psoriasis.

Two variants, p.His171Asn and p.Arg179His, required stimulation with TNF-α to achieve maximal levels of NF-kB activation. The p.Arg179His substitution was observed in two unrelated cases from Toronto and one control. The cases included a female who was diagnosed with psoriasis at 40 years of age and a male who was diagnosed with psoriasis at 64 years of age and who had a family history of psoriasis. The female responded well to oral and topical steroids, but the male was not treated.

The p.His171Asn alteration was seen in two unrelated psoriasis- and psoriatic-arthritis-affected individuals from Newfoundland and was not seen in controls. One individual was diagnosed with psoriasis at 40 years of age and psoriatic arthritis at 41 years of age and had a family history of psoriasis. The second individual was diagnosed with psoriasis at 55 years of age after being diagnosed with psoriatic arthritis at 53 years of age. The identification of the c.511C>A (p.His171Asn) variant in only the Newfoundland population suggests that it arose as a result of a founder effect in this population, but confirming this will require further studies. Inspection of the genotypes of 13 polymorphisms in a 75 kb region harboring *CARD14* revealed a shared haplotype that is common in cases and controls from the Newfoundland cohort and our other case/control cohorts from the United States (e.g., St. Louis/Dallas/UCSF, Michigan, and Utah). Therefore, further evidence of a founder effect for the p.His171Asn substitution seen in these two cases was not possible.

The altered transcriptome signature with pathologic substitutions included upregulation of psoriasis-specific transcripts *SOD2*, *IL6*, *CSF2*, *IL8*, *MMP9*, *BRF2*, *CCL20*, *SLC7A2*, *OLR1*, *IL36G*, *GBP2*, *TNFAIP2*, and *TNF*. Expression of these molecules is expected to be an early event in the pathogenesis of psoriasis. Many of these genes have been implicated in immune-system development. However, BRF2 is implicated in the development of squamous cell carcinoma of the lung.[33] This suggests that it might have global effects on the transcriptional profile of squamous cell epithelia in general and might help elicit a wound-healing or regenerative response in psoriatic keratinocytes.

Despite the dramatic effects of some CARD14 variants as keratinocyte transfectants, there was a wide range of phenotypes, even among individuals who carried the same substitution. This suggests that in many instances, the variable phenotypes are likely to be due to genetic background and/or environmental factors. For example, affected members of family PS1 all harbor the c.349G>A (p.Gly117Ser) mutation, but they have variable ages of onset (ranging from infancy to 83 years of age) and variable levels of disease severity, including the presence of psoriatic arthritis. Similarly, age of onset and response to treatment differed among individuals with the putative pathogenic variants from the coiled-coil domain (p.Glu142Lys, p.Glu142Gly, and p.Glu138Ala).

However, there might be some genotype-phenotype correlations because the pustular-psoriasis substitution, p.Glu138Ala, led to the most severe phenotype (in terms of both clinical presentation and increased NF-kB activation) relative to that produced by wild-type CARD14sh. The child with this alteration presented with a spectrum of plaque-type lesions, but she mostly presented with pustular lesions. This implies that some forms of plaque psoriasis might be pathogenetically linked to pustular psoriasis at the severe end of the disease spectrum. The child's lesions also exhibited a pronounced infiltration of neutrophils. Interestingly, in keratinocyte transfectants with this CARD14 substitution, there was a higher level of *IL8* than there was with other variants, which could lead to higher levels of neutrophil infiltration. The observation that the p.Glu138Ala alteration led to the most severe clinical phenotype and induced the greatest increase in NF-kB activation and upregulation of psoriasis-associated transcripts suggests that the phenotype of psoriasis could, in some cases, be predicted by the detection of pathogenically increased levels of NF-kB activation and signaling. How the CARD14 substitutions translate to variable levels of chemokine activation and how genetic background and environment trigger variable phenotypes are important areas for further study.

CARD14 missense variants rs11652075 (c.2458C>T [p.Arg820Trp]) and c.599G>A (p.Ser200Asn) were associated with psoriasis in cohorts of European ancestry. In the Asian cohort, the c.2458T>C polymorphism was also associated with psoriasis, but c.599G was monomorphic. *CARD14* was not shown to be associated with psoriasis in a previous GWAS.[8] However, none of the polymorphisms with evidence of association with psoriasis in this study were included in that GWAS and would not have been likely to exceed genome-wide significance if they had been. From the PSORS2 region of linkage, the SNP with the most significant p value in the GWAS was rs7216577 (p value = 0.00261).[8] That SNP is located within an intron of *SLC26A11* and might regulate levels of *CARD14* mRNAs in the skin. However, rs11652075, although not on the Perlegen microarray in the CASP-GWAS,[8] was part of the HapMap-based imputed dataset that was used for the association analyses in that study. Its association p value was of nominal significance (p = 0.039, OR = 1.10 for the C risk allele reported here) and would not have been reported because it was considerably below the threshold for genome-wide significant association.

PSORS2 was originally identified by linkage,[21,34] and our studies with a common missense SNP (rs11652075) also indicate that it can be associated with psoriasis. Linkage and association have also been seen in some genes for other common diseases, e.g., *NOD2* (nucleotide-binding oligomerization domain containing 2, [MIM 605956] in inflammatory bowel disease (IBD1 [MIM 266600])[35–37] and *CFH* (complement factor H, [CFH (MIM 134370)]) in age-related macular degeneration (ARMD1 [MIM 603075]).[38,39]

In two cohorts of European ancestry, evidence of association between psoriasis and rs11652075 increased when the PSORS1 variant *HLA-Cw*0602* was included as a covariate, suggesting a genetic connection between PSORS1 and PSORS2. This variant resides in the CARD14fl C-terminal GUK domain, which is predicted to relay external signals to the cellular milieu.[16] This could explain the possible genetic connection because antigen stimulation via PSORS1 might increase the risk of psoriasis by upregulating signaling through the CARD14 pathway. This is consistent with the fact that CARD14 affects signaling downstream of antigen stimulation. However, it is important to note that the PSORS1 risk variant, *HLA-Cw*0602*[40], was not present in the affected members of the 17q-linked multiplex families, the pustular-psoriasis case described previously,[17] or the cases with the p.Glu142Lys or p.Glu142Gly variants, indicating that rare CARD14 variants can be sufficient to lead to disease.

Our study illustrates some of the difficulties in searching for rare variants associated with common disease, even with an established gene. For example, it is not always easy to differentiate pathogenic rare variants from others when their numbers are very small. This also has an impact on the detection of gene-gene or gene-environment interactions. Moreover, it is sometimes necessary to recreate the cellular milieu (e.g., an inflammatory stimulus in the case of CARD14) when one attempts to differentiate disease-causing variants from neutral variants through functional studies. Nevertheless, our findings provide evidence that some rare CARD14 variants predispose to psoriasis and, possibly, to psoriatic arthritis, and they suggest that common variants in this region might also predispose to disease. They illustrate the challenges faced in identifying truly pathogenic rare variants in common disease and contribute to our understanding of the genetic basis of psoriasis.

Supplemental Data

Supplemental Data include two figures and three tables and can be found with this article online at http://www.cell.com/AJHG.

Acknowledgments

This work was supported by grants from the National Institutes of Health (NIH): AR050266 and 5RC1AR058681 (A.M.B.), T32AR007279 (E.D.O.R.), T32HL083822 and T32 GM07200 (C.T.J), AR060222 (M.A.L), T32HG000045 (C.E.J), and K08AR057763 (W.L.). J.T.E., R.N., and P.S. were supported by NIH grants R01 AR042742, R01 AR050511, and AR054966 and by the Babcock Memorial Trust. J.T.E. is supported by the Ann Arbor Veterans Affairs Hospital. R.G.M. is supported by the Intramural Research Programs of the National Institute of Arthritis and Musculoskeletal and Skin Diseases. Additional funding came from the Arthritis Society of Canada, the Atlantic Innovation Fund, the Canadian Institute of Health Research, the Arthritis Society, the Dana Foundation, and the Academia Sinica and National Science Council (National Clinical Core, National Genotyping Core) of Taiwan. The authors thank the many individuals with psoriasis and the controls who participated in this study. We thank Linus Schwantes-An, Weimin Duan, and Nancy Saccone for advice on statistical analyses. We also thank Mayte Suarez-Farinas for biostatistical assistance, Haoyan Chen, Olivia Lai, Fawnda Pellet, and M.J. Malloy for assembling the control population, Pui-Yan Kwok for sample procurement, Trilokraj Tejasvi for clinical evaluation of study subjects, Nikki Plass for patient scheduling and study logistics, Damaris Garcia for the management of samples, and Debbie Stone and Dawn Chapelle for patient care. Mike Lovett provided helpful comments on the manuscript. The authors are indebted to the National Psoriasis Foundation for continuing support during the course of this study.

Received: December 27, 2011
Revised: February 29, 2012
Accepted: March 13, 2012
Published online: April 19, 2012

Web Resources

The URLs for data presented herein are as follows:

1,000 Genomes Project, http://www.1000genomes.org
dbSNP135, http://www.ncbi.nlm.nih.gov/projects/SNP/
g:Profiler, http://biit.cs.ut.ee/gprofiler/index.cgi
Gene Ontology, http://www.geneontology.com
Ingenuity Pathway Analysis (IPA), http://www.ingenuity.com/
Microarray Gene Expression Data Society (MIAME), http://www.mged.org/Workgroups/MIAME/miame_checklist.html
NCBI Gene Expression Omnibus (GEO), http://www.ncbi.nlm.nih.gov/geo/
NCBI Reference Sequence (RefSeq), http://www.ncbi.nlm.nih.gov/RefSeq/
NHLBI/NHGRI Exome Project, http://exome.gs.washington.edu/
Online Mendelian Inheritance in Man (OMIM), http://omim.org
PLINK, http://pngu.mgh.harvard.edu/purcell/plink/
PLINK/SEQ version 0.05, http://atgu.mgh.harvard.edu/plinkseq/
PolyPhen-2.0, http://genetics.bwh.harvard.edu/pph2/
R, http://www.R-project.org
rmeta, http://cran.r-project.org/web/packages/rmeta/index.html
SequenomARRAY, http://hg.wustl.edu/info/Sequenom_description.html
SIFT, http://sift.jcvi.org/

References

1. Lowes, M.A., Bowcock, A.M., and Krueger, J.G. (2007). Pathogenesis and therapy of psoriasis. Nature *445*, 866–873.
2. Nograles, K.E., Brasington, R.D., and Bowcock, A.M. (2009). New insights into the pathogenesis and genetics of psoriatic arthritis. Nat. Clin. Pract. Rheumatol. *5*, 83–91.
3. Capon, F., Bijlmakers, M.J., Wolf, N., Quaranta, M., Huffmeier, U., Allen, M., Timms, K., Abkevich, V., Gutin, A., Smith, R., et al. (2008). Identification of ZNF313/RNF114 as a novel psoriasis susceptibility gene. Hum. Mol. Genet. *17*, 1938–1945.
4. Cargill, M., Schrodi, S.J., Chang, M., Garcia, V.E., Brandon, R., Callis, K.P., Matsunami, N., Ardlie, K.G., Civello, D., Catanese,

J.J., et al. (2007). A large-scale genetic association study confirms IL12B and leads to the identification of IL23R as psoriasis-risk genes. Am. J. Hum. Genet. *80*, 273–290.

5. Ellinghaus, E., Ellinghaus, D., Stuart, P.E., Nair, R.P., Debrus, S., Raelson, J.V., Belouchi, M., Fournier, H., Reinhard, C., Ding, J., et al. (2010). Genome-wide association study identifies a psoriasis susceptibility locus at TRAF3IP2. Nat. Genet. *42*, 991–995.
6. Hüffmeier, U., Uebe, S., Ekici, A.B., Bowes, J., Giardina, E., Korendowych, E., Juneblad, K., Apel, M., McManus, R., Ho, P., et al. (2010). Common variants at TRAF3IP2 are associated with susceptibility to psoriatic arthritis and psoriasis. Nat. Genet. *42*, 996–999.
7. Liu, Y., Helms, C., Liao, W., Zaba, L.C., Duan, S., Gardner, J., Wise, C., Miner, A., Malloy, M.J., Pullinger, C.R., et al. (2008). A genome-wide association study of psoriasis and psoriatic arthritis identifies new disease loci. PLoS Genet. *4*, e1000041.
8. Nair, R.P., Duffin, K.C., Helms, C., Ding, J., Stuart, P.E., Goldgar, D., Gudjonsson, J.E., Li, Y., Tejasvi, T., Feng, B.J., et al; Collaborative Association Study of Psoriasis. (2009). Genome-wide scan reveals association of psoriasis with IL-23 and NF-kappaB pathways. Nat. Genet. *41*, 199–204.
9. Strange, A., Capon, F., Spencer, C.C., Knight, J., Weale, M.E., Allen, M.H., Barton, A., Band, G., Bellenguez, C., Bergboer, J.G., et al; Genetic Analysis of Psoriasis Consortium & the Wellcome Trust Case Control Consortium 2. (2010). A genome-wide association study identifies new psoriasis susceptibility loci and an interaction between HLA-C and ERAP1. Nat. Genet. *42*, 985–990.
10. Stuart, P.E., Nair, R.P., Ellinghaus, E., Ding, J., Tejasvi, T., Gudjonsson, J.E., Li, Y., Weidinger, S., Eberlein, B., Gieger, C., et al. (2010). Genome-wide association analysis identifies three psoriasis susceptibility loci. Nat. Genet. *42*, 1000–1004.
11. Sun, L.D., Cheng, H., Wang, Z.X., Zhang, A.P., Wang, P.G., Xu, J.H., Zhu, Q.X., Zhou, H.S., Ellinghaus, E., Zhang, F.R., et al. (2010). Association analyses identify six new psoriasis susceptibility loci in the Chinese population. Nat. Genet. *42*, 1005–1009.
12. Elder, J.T. (2006). PSORS1: Linking genetics and immunology. J. Invest. Dermatol. *126*, 1205–1206.
13. Nair, R.P., Stuart, P.E., Nistor, I., Hiremagalore, R., Chia, N.V., Jenisch, S., Weichenthal, M., Abecasis, G.R., Lim, H.W., Christophers, E., et al. (2006). Sequence and haplotype analysis supports HLA-C as the psoriasis susceptibility 1 gene. Am. J. Hum. Genet. *78*, 827–851.
14. Vineis, P., and E Pearce, N. (2011). Genome-wide association studies may be misinterpreted: Genes versus heritability. Carcinogenesis *32*, 1295–1298.
15. Chen, H., Poon, A., Yeung, C., Helms, C., Pons, J., Bowcock, A.M., Kwok, P.Y., and Liao, W. (2011). A genetic risk score combining ten psoriasis risk loci improves disease prediction. PLoS ONE *6*, e19454.
16. Bertin, J., Wang, L., Guo, Y., Jacobson, M.D., Poyet, J.L., Srinivasula, S.M., Merriam, S., DiStefano, P.S., and Alnemri, E.S. (2001). CARD11 and CARD14 are novel caspase recruitment domain (CARD)/membrane-associated guanylate kinase (MAGUK) family members that interact with BCL10 and activate NF-kappa B. J. Biol. Chem. *276*, 11877–11882.
17. Jordan, C.T., Cao, L., Roberson, E.D.O., Pierson, K.C., Yang, C.-F., Joyce, C.E., Ryan, C., Duan, S., Helms, C.A., Liu, Y., et al. (2012). PSORS2 is Due to Mutations in *CARD14*. Am. J. Hum. Genet. *90*, in press. Published online April 19, 2012. 10.1016/j.ajhg.2012.03.012.
18. Purcell, S., Neale, B., Todd-Brown, K., Thomas, L., Ferreira, M.A., Bender, D., Maller, J., Sklar, P., de Bakker, P.I., Daly, M.J., and Sham, P.C. (2007). PLINK: A tool set for whole-genome association and population-based linkage analyses. Am. J. Hum. Genet. *81*, 559–575.
19. Price, A.L., Kryukov, G.V., de Bakker, P.I., Purcell, S.M., Staples, J., Wei, L.J., and Sunyaev, S.R. (2010). Pooled association tests for rare variants in exon-resequencing studies. Am. J. Hum. Genet. *86*, 832–838.
20. R Development Core Team. (2011). R: A language and environment for statistical computing. R Foundation for Statistical Computing, Vienna, Austria. http://www.R-project.org.
21. Tomfohrde, J., Silverman, A., Barnes, R., Fernandez-Vina, M.A., Young, M., Lory, D., Morris, L., Wuepper, K.D., Stastny, P., Menter, A., et al. (1994). Gene for familial psoriasis susceptibility mapped to the distal end of human chromosome 17q. Science *264*, 1141–1145.
22. Vincourt, J.B., Jullien, D., Amalric, F., and Girard, J.P. (2003). Molecular and functional characterization of SLC26A11, a sodium-independent sulfate transporter from high endothelial venules. FASEB J. *17*, 890–892.
23. Reimand, J., Kull, M., Peterson, H., Hansen, J., and Vilo, J. (2007). g:Profiler—a web-based toolset for functional profiling of gene lists from large-scale experiments. Nucleic Acids Res. *35* (Web Server issue), W193–200.
24. Ashburner, M., Ball, C.A., Blake, J.A., Botstein, D., Butler, H., Cherry, J.M., Davis, A.P., Dolinski, K., Dwight, S.S., Eppig, J.T., et al; The Gene Ontology Consortium. (2000). Gene ontology: Tool for the unification of biology. Nat. Genet. *25*, 25–29.
25. Mehta, N.N., Yu, Y., Pinnelas, R., Krishnamoorthy, P., Shin, D.B., Troxel, A.B., and Gelfand, J.M. (2011). Attributable risk estimate of severe psoriasis on major cardiovascular events. Am J Med. *124*, 775e1–775e6.
26. Davidovici, B.B., Sattar, N., Prinz, J.C., Puig, L., Emery, P., Barker, J.N., van de Kerkhof, P., Ståhle, M., Nestle, F.O., Girolomoni, G., and Krueger, J.G. (2010). Psoriasis and systemic inflammatory diseases: Potential mechanistic links between skin disease and co-morbid conditions. J. Invest. Dermatol. *130*, 1785–1796.
27. Adzhubei, I.A., Schmidt, S., Peshkin, L., Ramensky, V.E., Gerasimova, A., Bork, P., Kondrashov, A.S., and Sunyaev, S.R. (2010). A method and server for predicting damaging missense mutations. Nat. Methods *7*, 248–249.
28. Suárez-Fariñas, M., Lowes, M.A., Zaba, L.C., and Krueger, J.G. (2010). Evaluation of the psoriasis transcriptome across different studies by gene set enrichment analysis (GSEA). PLoS ONE *5*, e10247.
29. Moreno-García, M.E., Sommer, K., Shinohara, H., Bandaranayake, A.D., Kurosaki, T., and Rawlings, D.J. (2010). MAGUK-controlled ubiquitination of CARMA1 modulates lymphocyte NF-kappaB activity. Mol. Cell. Biol. *30*, 922–934.
30. Thome, M., Charton, J.E., Pelzer, C., and Hailfinger, S. (2010). Antigen receptor signaling to NF-kappaB via CARMA1, BCL10, and MALT1. Cold Spring Harb Perspect Biol *2*, a003004.
31. Pasparakis, M. (2009). Regulation of tissue homeostasis by NF-kappaB signalling: Implications for inflammatory diseases. Nat. Rev. Immunol. *9*, 778–788.
32. Wullaert, A., Bonnet, M.C., and Pasparakis, M. (2011). NF-κB in the regulation of epithelial homeostasis and inflammation. Cell Res. *21*, 146–158.

33. Lockwood, W.W., Chari, R., Coe, B.P., Thu, K.L., Garnis, C., Malloff, C.A., Campbell, J., Williams, A.C., Hwang, D., Zhu, C.Q., et al. (2010). Integrative genomic analyses identify BRF2 as a novel lineage-specific oncogene in lung squamous cell carcinoma. PLoS Med. *7*, e1000315.

34. Hwu, W.L., Yang, C.F., Fann, C.S., Chen, C.L., Tsai, T.F., Chien, Y.H., Chiang, S.C., Chen, C.H., Hung, S.I., Wu, J.Y., and Chen, Y.T. (2005). Mapping of psoriasis to 17q terminus. J. Med. Genet. *42*, 152–158.

35. Ogura, Y., Bonen, D.K., Inohara, N., Nicolae, D.L., Chen, F.F., Ramos, R., Britton, H., Moran, T., Karaliuskas, R., Duerr, R.H., et al. (2001). A frameshift mutation in NOD2 associated with susceptibility to Crohn's disease. Nature *411*, 603–606.

36. Hugot, J.P., Laurent-Puig, P., Gower-Rousseau, C., Olson, J.M., Lee, J.C., Beaugerie, L., Naom, I., Dupas, J.L., Van Gossum, A., Orholm, M., et al. (1996). Mapping of a susceptibility locus for Crohn's disease on chromosome 16. Nature *379*, 821–823.

37. van Heel, D.A., Fisher, S.A., Kirby, A., Daly, M.J., Rioux, J.D., and Lewis, C.M.; Genome Scan Meta-Analysis Group of the IBD International Genetics Consortium. (2004). Inflammatory bowel disease susceptibility loci defined by genome scan meta-analysis of 1952 affected relative pairs. Hum. Mol. Genet. *13*, 763–770.

38. Fisher, S.A., Abecasis, G.R., Yashar, B.M., Zareparsi, S., Swaroop, A., Iyengar, S.K., Klein, B.E., Klein, R., Lee, K.E., Majewski, J., et al. (2005). Meta-analysis of genome scans of age-related macular degeneration. Hum. Mol. Genet. *14*, 2257–2264.

39. Raychaudhuri, S., Iartchouk, O., Chin, K., Tan, P.L., Tai, A.K., Ripke, S., Gowrisankar, S., Vemuri, S., Montgomery, K., Yu, Y., et al. (2011). A rare penetrant mutation in CFH confers high risk of age-related macular degeneration. Nat. Genet. *43*, 1232–1236.

40. Elder, J.T.; Cluster 17 Collaboration. (2005). Fine mapping of the psoriasis susceptibility gene PSORS1: A reassessment of risk associated with a putative risk haplotype lacking HLA-Cw6. J. Invest. Dermatol. *124*, 921–930.

Example qualifying exam (Ph.D.) and comprehensive exam (M.S.) questions pertaining to Albersen et al. (2012) *PLoS ONE*.

---

1. Why would investigators perform a GWAS of endometriosis when many previous candidate gene studies have been reported?

2. Surgically-confirmed cases of endometriosis were compared to controls. Given that endometriosis is a common gynecological condition and that diagnosis is typically delayed 7-10 years from onset, do you expect that some control participants may actually be undiagnosed cases? How would the presence of cryptic endometriosis cases in the control sample effect this study? Comment on how this scenario would impact the reported odds ratios.

3. Previous twin studies have estimated that the narrow-sense heritability of endometriosis is 51%, 75%, and 87%. Do you interpret these three estimates as consistent with each other? If so, explain why. If not, explain possible reasons for this inconsistency. What additional pieces of information could help you jointly interpret these results?

4. Genomic data were used to test for unknown relatedness among participants, and if detected, related samples were excluded from analysis. Why did the investigators do this?

5. Genomic data were used to determine genetic ancestry, and only samples of 95% or more European ancestry were included in statistical analysis. Why did the investigators do this?

6. Numerous genotyped and imputed SNPs in the chromosomal 1 region containing WNT4, CDC42, and HSPC157 showed evidence of genetic association (Figure 1). Based on these associated SNPs, is it possible to determine how many causal alleles are in this region? Are variants in all three genes causal? What additional information could help answers these questions?

Genome-Wide Association Study Link Novel Loci to Endometriosis

Hans M. Albertsen, Rakesh Chettier, Pamela Farrington, Kenneth Ward*

Juneau Biosciences, LLC, Salt Lake City, Utah, United States of America

Abstract

Endometriosis is a common gynecological condition with complex etiology defined by the presence of endometrial glands and stroma outside the womb. Endometriosis is a common cause of both cyclic and chronic pelvic pain, reduced fertility, and reduced quality-of-life. Diagnosis and treatment of endometriosis is, on average, delayed by 7–10 years from the onset of symptoms. Absence of a timely and non-invasive diagnostic tool is presently the greatest barrier to the identification and treatment of endometriosis. Twin and family studies have documented an increased relative risk in families. To identify genetic factors that contribute to endometriosis we conducted a two-stage genome-wide association study (GWAS) of a European cohort including 2,019 surgically confirmed endometriosis cases and 14,471 controls. Three of the SNPs we identify associated at $P<5\times10^{-8}$ in our combined analysis belong to two loci: LINC00339-WNT4 on 1p36.12 (rs2235529; $P=8.65\times10^{-9}$, OR = 1.29, CI = 1.18–1.40) and RND3-RBM43 on 2q23.3 (rs1519761; $P=4.70\times10^{-8}$, OR = 1.20, CI = 1.13–1.29, and rs6757804; $P=4.05\times10^{-8}$, OR = 1.20, CI = 1.13–1.29). Using an adjusted Bonferoni significance threshold of 4.51×10^{-7} we identify two additional loci in our meta-analysis that associate with endometriosis:, RNF144B-ID4 on 6p22.3 (rs6907340; $P=2.19\times10^{-7}$, OR = 1.20, CI = 1.12–1.28), and HNRNPA3P1-LOC100130539 on 10q11.21 (rs10508881; $P=4.08\times10^{-7}$, OR = 1.19, CI = 1.11–1.27). Consistent with previously suggested associations to WNT4 our study implicate a 150 kb region around WNT4 that also include LINC00339 and CDC42. A univariate analysis of documented infertility, age at menarche, and family history did not show allelic association with these SNP markers. Clinical data from patients in our study reveal an average delay in diagnosis of 8.4 years and confirm a strong correlation between endometriosis severity and infertility (n = 1182, $P<0.001$, OR = 2.18). This GWAS of endometriosis was conducted with high diagnostic certainty in cases, and with stringent handling of population substructure. Our findings broaden the understanding of the genetic factors that play a role in endometriosis.

Citation: Albertsen HM, Chettier R, Farrington P, Ward K (2013) Genome-Wide Association Study Link Novel Loci to Endometriosis. PLoS ONE 8(3): e58257. doi:10.1371/journal.pone.0058257

Editor: Li-Min Huang, National Taiwan University Hospital, Taiwan

Received October 7, 2012; **Accepted** February 1, 2013; **Published** March 5, 2013

Copyright: © 2013 Albertsen et al. This is an open-access article distributed under the terms of the Creative Commons Attribution License, which permits unrestricted use, distribution, and reproduction in any medium, provided the original author and source are credited.

Funding: No current external funding sources for this study.

Competing Interests: The authors have the following interests. Hans M. Albertsen, Rakesh Chettier, Pamela Farrington and Kenneth Ward are employed by Juneau Biosciences LLC, the funder of this study. All authors have direct financial interest in Juneau Biosciences. A US provisional patent application has been filed by Juneau Biosciences that include the results and inventions reported in the manuscript. Title: Genetic Markers Associated with Endometriosis and Use Thereof Serial No.: 61/707,730 Filing date: September 28, 2012. There are no further patents, products in development or marketed products to declare. This does not alter the authors' adherence to all the PLOS ONE policies on sharing data and materials, as detailed online in the guide for authors.

* E-mail: kenw@juneaubiosciences.com

Introduction

Endometriosis affects 5–10% of women in their reproductive years with symptoms including pelvic pain, dyspareunia, dysmenorrhea and infertility [1]. Although ectopic endometrium has been observed in female fetuses [2], symptoms of endometriosis usually don't manifest until adolescence, and some patients with severe endometriosis remain asymptomatic. Definitive diagnosis is often delayed 7–10 years after the onset of symptoms severely impacting quality of life [3–5]. Family history of endometriosis has been reported in multiple studies to increased relative risk about a 5-fold [6,7]. A large twin-study based on the Australian Twin Registry has shown that the ratio of mono-zygotic to fraternal twin pair correlations was in excess of 2 fold, suggesting that 51% of the variance of the liability to endometriosis may be attributable to additive genetic influences with minimal influence from environmental factors [8], and two smaller twin-studies report the concordance rate of endometriosis between monozygotic twins to range between 75% and 87% [9,10]. A large number of candidate genes have been investigated for their role in endometriosis as summarized by Montgomery et al. [11] and Rahmioglu et al. [12], but the first strong evidence to date for genetic association are reported in two large Genome-Wide Association Studies (GWAS). In the first study Uno et al. [13] identified rs10965235 located in an intron of CDKN2BAS on chromosome 9p21 to be associated in a Japanese cohort, and in the second study Painter et al. [14] identified the intergenic SNP rs12700667 on chromosome 7p15.2 to be associated in a European cohort. A meta-analysis of the two studies extend this evidence and identify a total of seven loci associated with endometriosis [15]. To replicate and extend our understanding of the genetic factors that contribute to endometriosis we have undertaken a large two-stage GWAS in a European cohort.

Results and Discussion

GWAS and Replication

We conducted a discovery GWAS on surgically confirmed endometriosis patients and population controls using the Illumina OmniExpress BeadChip. SNPs were limited to the autosomes and

SNPs with an Illumina Gentrain score ≥0.65. We further eliminated SNPs with callrate <0.98, Hardy-Weinberg Equilibrium (hwe) <0.001 and minor allele frequencies (MAF) <0.01. After filtering 580,699 SNPs remained. Next, samples with callrates <0.98 were eliminated. The remaining samples were tested for unknown familial relationships using genome-wide identity-by-state (IBS), and samples closer than 3rd-degree ($\pi > 0.2$) were removed. We used ADMIXTURE (ver. 1.22) [16] to estimate individual ancestry proportions based on a subset of SNPs on the Illumina OmniExpress chip (see *Materials and Methods*) and restricted our analysis to samples with ≥95% European ancestry. The calculated ancestral distribution of samples within Europe is shown in Figure S1. After applying quality, relatedness and ethnicity filters 1,514 case and 12,660 control samples were used for the discovery phase of the association analysis. The genomic inflation factor lambda (λ) was determined to be 1.18, indicating measurable population stratification across the samples. To account for the elevated λ we performed a PCA adjusted association analysis that resulted in a λ-value of 1.05 shown in QQ-plots in Figure S2. We selected the top 100 SNPs with the lowest PCA-adjusted P-values (ranging between 8.20×10^{-5} and 1.36×10^{-7}) for further association analysis in the replication stage (Table S1).

The replication samples included 505 cases and 1811 controls selected for the same criteria as the discovery set. The λ-value for the replication cohort was determined to be 1.01 suggesting no measurable population stratification. After applying the same SNP filters as above we analyzed the top 100 SNPs from the discovery GWAS in the replication set. A significance threshold for the study, allowing for multiple correction, was chosen at 4.51×10^{-7} (0.05/108,699; 108,699 being the number of independent SNPs in the panel of 580,699 filtered SNPs with $r^2<0.20$). A meta-analysis of the discovery and replication results was performed using Cochran-Mantel-Hanzel test and revealed 8 SNPs from 4 genomic regions that passed our genome-wide significance threshold including: LINC00339-WNT4 on 1p36.12 (rs2235529; $P_{meta} = 3.05\times10^{-9}$, OR = 1.30); RND3-RBM43 on 2q23.3 (rs6757804; $P_{meta} = 6.45\times10^{-8}$, OR = 1.20), RNF144B-ID4 on 6p22.3 (rs6907340; $P_{meta} = 2.19\times10^{-7}$, OR = 1.20); and HNRNPA3P1-LOC100130539 on 10q11.21 (rs10508881; $P_{meta} = 4.08\times10^{-7}$, OR = 1.19) and shown in detail in Table 1. Table 1 also show that three SNPs (rs2235529, rs1519761 and rs6757804) pass a conventional genome wide significance threshold of $P<5\times10^{-8}$ in the combined analysis. There was no evidence of heterogeneity between the discovery and replication datasets as judged by the Breslow Day test and shown in Table 1. A second group of 15 SNPs from nine genomic regions that show suggestive replication provide additional candidate loci for endometriosis that merit further investigation. The most significant of these regions encompass IL33 on 9p24.1 (rs10975519; $P_{meta} = 9.26\times10^{-7}$, OR = 1.19). IL33 is a chemokine that has been linked to deep infiltrating endometriosis [17]. A summary of the discovery and replication GWAS, together with the meta and combined analysis for all 100 SNPs is presented in Table S1.

To further characterize the signals from the four most strongly associated regions and the IL33 region, we performed imputation using 1000-Genome and dataset utilizing IMPUTE2 (ver. 2.2.2) [18]. The results from the imputed dataset for the WNT4 region is shown in Table S2a. Figure 1 show a regional association plot around WNT4 and reveal that the associated region extends across 150 kb and include two new genes, HSPC157 (gene symbol: LINC00339) and CDC42, in addition to WNT4. The imputation results identify 25 additional SNPs that are strongly associated to endometriosis and reveal that the imputed SNP, rs10917151, is the most strongly associated SNP in the region ($P_{imputed} = 5.63\times10^{-10}$, OR = 1.3). WNT4 is important for steroidogenesis, ovarian follicle development and the development of the female reproductive tract and a very plausible candidate for endometriosis based on its biological functions [19]. Cell division cycle 42, CDC42, is a small GTPase of the Rho-subfamily, which regulates signaling pathways that control diverse cellular functions including cell morphology, migration, endocytosis and cell cycle progression. CDC42 is in part regulated by estrogen, expressed in endometrium, and has been shown to be differentially expressed in endometriosis [20]. HSPC157 is an alias for the Long Intergenic Non-protein Coding RNA 339 (gene symbol: LINC00339). HSPC157 has been found to be differentially expressed in endometriosis versus autologous uterine endometrium [21]. Based on this biological evidence both CDC42 and LINC00339 must also be considered candidates for endometriosis.

WNT4 has previously been associated with endometriosis, first by Uno et al. (2010) who noted that rs16826658, approximately 16 kb upstream of WNT4, showed a possible association to endometriosis ($P = 1.66\times10^{-6}$, OR = 1.20) in a Japanese population, and again by Painter et al. (2011) who reported that rs7210902, located approximately 22 kb upstream of WNT4, also showed evidence for association in a European cohort ($P = 9.0\times10^{-5}$, OR = 1.16). Our imputation analysis replicate the association of rs7210902 with endometriosis ($P = 6.4\times10^{-5}$,OR = 1.17) and confirm the involvement of the WNT4-region in the pathogenesis of endometriosis. We only found weak evidence of association with rs16826658 (P = 0.05, OR = 1.07), because the minor allele is very common and because of the different ethnic backgrounds between the studies. To further evaluate the signals from the WNT4 region, we performed a haplotype analysis of three key SNPs from our study (rs10917151, rs4654783 and rs2235529) together with rs16826658, and rs7210902 using the imputed data from our population. The haplotype-results are summarized in Table S3 and show that the risk for endometriosis is confined to a single haplotype anchored in rs10917151, rs4654783 and rs2235529 ($P_{HAP-1} = 7.26E-09$, $OR_{HAP-1} = 1.28$), and that this haplotype starts to deteriorate with the addition of rs16826658 and rs7210902 ($P_{HAP-1a} = 8.33E-07$, $OR_{HAP-1a} = 1.25$). This analysis suggests that the risk allele observed in the present study and the two previously published reports is located on the same ancestral haplotype. Imputation was also performed on the three other significant regions on chromosome 2, 6, and 10, and on the region surrounding IL33 on chromosome 9 (Table S2a–e, Figure S3).

Overlap with Other Reported Loci

Uno et al. [13] reported association between endometriosis and rs10965235, located in intron 19 of CDKN2BAS, in a Japanese population. The protective minor allele A, that has a minor allele frequency of 0.20 in the Japanese population, is not observed in the European population preventing a direct comparison between the two ethnic groups. In lieu of a direct comparison between the two ethnic groups we scanned 66 SNPs from a region of 200 kb surrounding rs10965235 in our European population. After correcting for multiple-testing (P-value ≤0.05/66 = 0.00076) we didn't find any evidence that CDKN2BAS is associated with endometriosis in the European population (Table S4a). In contrast, a second SNP (rs13271465) located on 8p22 between MTMR7 and SLC7A2, that Uno et al. identified as being associated with endometriosis ($P_{Combined} = 9.84\times10^{-6}$, OR = 1.18), is present in both studies, show weak association (P = 0.0057, OR = 1.14) in our study, while none of the other 88 SNPs from the 200 kb region surrounding rs13271465 showed

Table 1. Summary of GWAS and replication results.

SNP	gene	Chr	Pos	allele	stage	Case MAF	Control MAF	P[a]	OR[b]	95%CI	P_{het}[d]
rs4654783	WNT4	1	22,439,520	a/g	Discovery	0.34	0.295	2.43E−07	1.23	1.14–1.34	
					Replication	0.323	0.298	1.31E−01	1.13	0.97–1.32	
					Meta[c]			1.40E−07	1.21	1.13–1.30	0.332
					Combined Trend[e]	0.336	0.295	1.17E−07	1.21	1.13–1.29	
rs2235529	WNT4	1	22,450,487	a/g	Discovery	0.188	0.153	1.36E−07	1.28	1.16–1.41	
					Replication	0.182	0.142	1.38E−03	1.36	1.13–1.64	
					Meta[c]			3.05E−09	1.3	1.19–1.41	0.583
					Combined Trend[e]	0.186	0.151	8.65E−09	1.29	1.18–1.40	
rs1519754	RND3 | RBM43	2	151,619,693	c/a	Discovery	0.446	0.403	5.67E−05	1.19	1.11–1.30	
					Replication	0.45	0.405	9.63E−03	1.2	1.04–1.38	
					Meta[c]			1.75E−07	1.2	1.12–1.28	0.964
					Combined Trend[e]	0.447	0.403	1.15E−07	1.2	1.12–1.28	
rs6734792	RND3 | RBM43	2	151,624,882	g/a	Discovery	0.448	0.404	3.52E−05	1.2	1.11–1.29	
					Replication	0.453	0.406	7.48E−03	1.21	1.05–1.39	
					Meta[c]			8.18E−08	1.2	1.12–1.28	0.945
					Combined Trend[e]	0.449	0.404	5.19E−08	1.2	1.12–1.28	
rs1519761	RND3 | RBM43	2	151,633,204	g/a	Discovery	0.445	0.401	3.54E−05	1.2	1.11–1.29	
					Replication	0.452	0.403	5.85E−03	1.21	1.05–1.40	
					Meta[c]			7.30E−08	1.2	1.12–1.29	0.886
					Combined Trend[e]	0.447	0.401	4.70E−08	1.2	1.13–1.29	
rs6757804	RND3 | RBM43	2	151,635,832	g/a	Discovery	0.445	0.401	3.43E−05	1.2	1.11–1.29	
					Replication	0.452	0.403	5.44E−03	1.21	1.06–1.40	
					Meta[c]			6.45E−08	1.2	1.13–1.29	0.876
					Combined Trend[e]	0.446	0.4011	4.05E−08	1.2	1.13–1.29	
rs6907340	RNF144B | ID4	6	19,803,768	a/g	Discovery	0.417	0.371	5.49E−06	1.21	1.12–1.31	
					Replication	0.412	0.378	4.54E−02	1.15	1.00–1.33	
					Meta[c]			2.19E−07	1.2	1.12–1.28	0.579
					Combined Trend[e]	0.415	0.372	1.25E−07	1.2	1.12–1.28	
rs10508881	HNRNPA3P1 | LOC100130539	10	44,541,565	a/g	Discovery	0.45	0.405	3.18E−05	1.2	1.11–1.30	
					Replication	0.42	0.387	6.06E−02	1.15	1.00–1.32	
					Meta[c]			4.08E−07	1.19	1.11–1.27	0.589
					Combined Trend[e]	0.442	0.403	1.57E−06	1.18	1.10–1.26	

The discovery stage included 1,514 endometriosis cases and 12,660 population controls, and the replication stage included 505 cases and 1,811 controls.

[a] The P-values were determined using the Cochrane-Armitage trend test. P-values for the Discovery set reflect PCA adjusted P trend values.

[b] Odds-ratios (OR) and confidence intervals (CI) are calculated using the non-risk allele as the reference.

[c] The Meta analysis was performed using Cochran-Mantel-Haenzel statistics.

[d] P values of heterogeneties (P_{het}) across discovery and replication stages calculated using Breslow-Day Test.

[e] Cochrane-Armitage trend test P-values based on the combined genotypes from the Discovery and Replication data.

Significance threshold is 4.59×10^{-7}, and is determined by 0.05/108,699 where 108,699 is the number of independent SNPs in the panel with r^2 less than 0.20.

doi:10.1371/journal.pone.0058257.t001

any evidence for association with endometriosis (Table S4b). Uno et al. provided a supplementary list of 100 additional candidate SNPs from their study of which 60 are present in our analysis. Among the 60 SNPs only rs2473277 has a P-value <0.001 in our study ($P = 5.97\times10^{-6}$, OR = 1.17). SNP rs2473277 is located between LINC00339 and CDC42 at the left-most boundary of the WNT4 LD-block discussed above (Figure 1), and the risk allele of rs2473277 tag perfectly with the risk haplotype HAP-1 shown in Table S3 (data not shown).

Painter et al. [14] reported significant association of moderate and severe endometriosis with rs12700667 on 7p15.2 ($P_{all} = 2.6\times10^{-7}$, OR = 1.22), with flanking support from

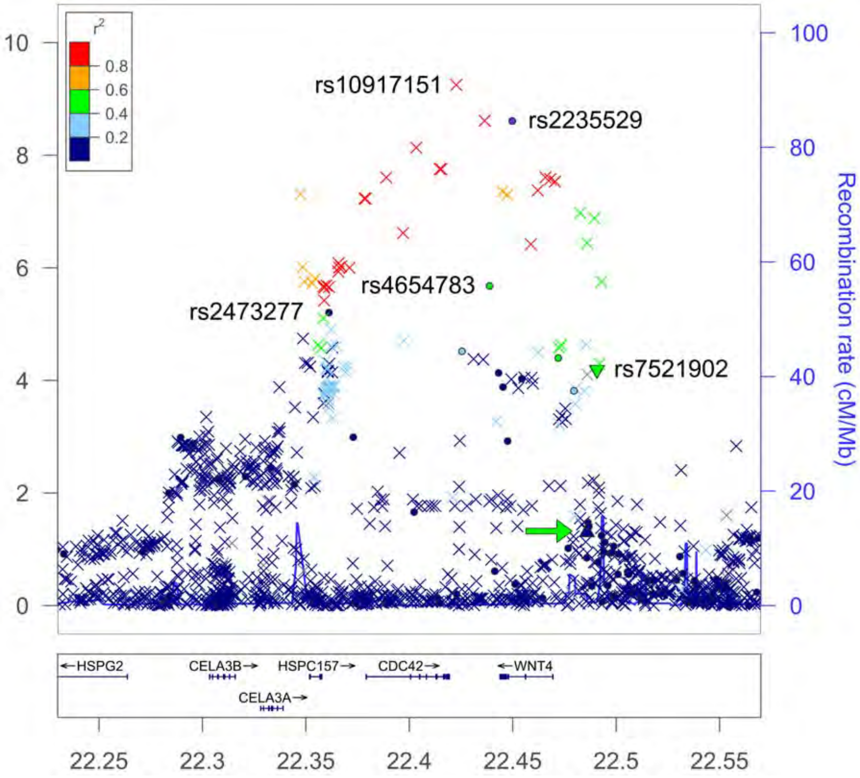

Figure 1. Regional association plot at the WNT4 region on chromosome 1. P-values of genotyped SNPs(●) and imputed SNPs (×) are plotted against their physical position on chromosome 1 as -$\log_{10}$(P-value) on the left (hg19/GRCh37). The plot identify a 150 kb LD-block (22.35 Mb-22.50 Mb) that show association with endometriosis and include WNT4, CDC42 and HSPC157 (gene symbol: LINC00339). Key SNPs are indicated in the Figure with their rsID. Two SNPs, rs16826658 (green arrow) and rs7521902 (green triangle), previously suggested to be associated with endometriosis (Uno et al. 2010; Painter et al. 2011), are located at the right-most boundary of the associated region. A third SNP, rs2473277, located at the left-most boundary of the LD-region was also tentatively associated by Uno et al. (2010). The genetic recombination rates estimated from 1000 Genome samples (EUR) are shown with a blue line according to the scale indicated to the right. The chromosomal position is indicated in Mb at the bottom of the figure.
doi:10.1371/journal.pone.0058257.g001

rs7798431 located 41 kb away. The two SNPs were reported to be in strong linkage disequilibrium (LD), but unfortunately neither SNP is included in our study. A review of the Hapmap3 data from the region show that three SNPs in our study (rs12535837, rs10282436, rs10232819) are in moderate to strong LD with rs12700667 and rs7798431, but we find no evidence for association between endometriosis and any of these markers in our analyses of all endometriosis cases together nor do we find any evidence for association to the moderate and severe subset (Table S4c). A broader scan of the 200 kb region surrounding rs12700667, suggests weak association with rs4722551 ($P = 0.000867$) about 90 kb downstream of rs12700667 (Table S4c). Painter et al. provided a supplementary list of 73 candidate SNPs, but none of the thirty-nine SNPs present in our study reach a P-value threshold <0.001.

A recent meta-analysis published by Nyholt et al. [15] extend the findings by Uno et al. and Painter et al. and report a total of seven SNPs that pass a genome-wide significance ($P<5\times10^{-8}$). A comparison of our results to each of the seven loci show evidence for association to endometriosis for three of the seven loci as detailed in Table S7.

A recent candidate gene study investigating the *LCF6* variant (rs61764370) in the 3′-UTR of *KRAS* showed very strong association with endometriosis among 132 women ($MAF_{case} = 0.311$, $MAF_{control} = 0.076$) [22], and proposed that *let*-7 microRNA play a functional role in the development of endometriosis. We investigated this association by Taqman assay in a set of 1123 cases and 832 controls from our European population and found the allele frequencies to be identical in the two populations ($MAF_{case} = 0.095$, $MAF_{control} = 0.093$). Our result show that the *LCS6* variant of *KRAS* does not provide any value as an indicator for endometriosis risk in a European population in agreement with results reported by Luong et al. [23].

ENDO1 is a susceptibility locus on chromosome 10q26 (OMIM phenotype number 131200) identified by linkage analysis [24], but we find no evidence for SNP association (P-value <0.0001) in this 16 Mb region (data not shown).

Clinical Stratification and Diagnostic Delay

Clinical features commonly used to characterize and stratify endometriosis include infertility, pelvic pain, severity, age-at-menarche and familiality. To determine the diagnostic delay in our patient-population we identified a group of women ($n = 874$) that reported both age at onset-of-symptoms (mean-age-onset = 19.04 years) and age at diagnosis (mean-age-diagnosis = 27.49), and observed an average diagnostic delay of 8.44 years, similar to previous studies. We then went on to examine if our samples showed any clinical correlations using logistic regression. The analysis revealed strong correlations between severity and infertility ($P<0.001$, $OR = 2.19$), and between severity and diagnostic delay ($P<0.001$, $OR = 1.04$) as shown in Table 2. To identify loci associated with the progression of endometriosis, we compared patients with mild endometriosis to patients with moderate or severe endometriosis in a two-stage GWAS. Stage one included 657 patients with mild endometriosis vs. 525 patients with moderate-or-severe endometriosis and a stage two replication set of 318 mild vs. 519 moderate-or-severe patients. A meta-analysis using the CMH test in this limited sample set, found no loci that pass the genome-wide significant threshold which suggest the SNPs identified in the primary study contribute to the general endometriosis risk rather than endometriosis progression. A separate analysis of the top five SNPs using logistic regression also showed no correlation with severity as shown in Table S5a, and Table S5b shows no noticeable increase in effect size when comparing moderate and severe disease against all controls.

Risk Analysis of Endometriosis

After removing markers with $r^2>0.8$ among the top 5 associated regions (incl. the IL33 locus), we conducted multivariate logistic regression using the combined set of 2,019 cases and 14,471 controls. All of the 5 SNPs rs101917151, rs6757804, rs6907340, rs10975519 and rs10508881 analyzed remained significant with OR of 1.3, 1.2, 1.18, 1.17 and 1.17. Each marker appear to be an independent risk factors for endometriosis. Comparison of the OR between the discovery and replication datasets, shown in Table 1, does not suggest any significant inflation of effect size in the discovery dataset (winner's curse), but this conclusion remain tentative due to the difference in size between the two datasets.

Conclusion

A two-stage GWAS and a replication study involving 2,019 cases and 14,471 controls was performed which identified four novel loci strongly associated with endometriosis and confirmed the involvement of a region around WNT4 which previously have been suggested as being associated to endometriosis. Nine other regions identified in the study also hold promise as candidate loci for endometriosis. Utmost care was taken in the clinical classification of patients and only surgically-confirmed cases with >95% European ancestry were considered in this large GWAS of endometriosis. The study is well powered (>90%) to identify a marker at or above 10% minor allele frequency (MAF) with odds-ratio (OR) >1.20, but we estimate the top 5 loci only explain about 1.5% of the phenotypic variance of endometriosis. Since the few risk loci we detected all have odds ratios <1.30 it must be assumed that any new endometriosis loci that contribute to the "missing heritability" must be rare, recent, or show minimal effect. GWAS, by design, detects only very old founder effects. When a phenotype includes infertility, like endometriosis, a high mutation rate would be required to replenish the disease-causing alleles lost from the gene-pool due to infertility. One suitable avenue to investigate under that scenario is to use whole genome sequencing of high-risk families rather than SNP-based GWAS. Little is presently known about the pathophysiology of endometriosis, but we hope that a more detailed investigation of the loci presented in this paper will help elucidate the pathogenesis of endometriosis and clarify its genetic underpinnings.

Materials and Methods

Ethics Statement

All subjects and controls provided written informed consent in accordance with study protocols approved by Quorum Review IRB (Seattle, WA 98101).

Participant Recruitment

Patients included in the present study were invited to participate via an outreach program at www.endtoendo.com, where our research initiative is described in more detail. Briefly, the "End to Endo" website provides general information regarding endometriosis and our research project, and invites women diagnosed with endometriosis to participate in our study.

Medical Review

The inclusion criteria in the endometriosis case population in the present study is surgically confirmed diagnosis of endometriosis with laparoscopy being the preferred method. Trained OB/GYN clinicians performed the medical record review and clinical assessment of each individual patient. Patients were considered to be affected if they had biopsy-proven lesions or if operative reports revealed unambiguous gross lesions. Patients were further categorized by severity, clinical history of pelvic pain, infertility, dyspareunia or dysmenorrhea and family history. Patients were grouped into one of three classes of severity: mild, moderate or severe, following the general guidelines set forth by ASRM [25]. *Exclusion* of endometriosis also requires surgical intervention and we made no attempt to exclude endometriosis in the population controls. Thus, in this analysis we are comparing cases with 100% prevalence of endometriosis to controls with the population prevalence of endometriosis (5–10%), which leads to a systematical underestimation of the true odds ratios and a decrease in statistical power to detect associations.

DNA Extraction

Saliva samples were collected using the Oragene 300 saliva collection kit (DNA Genotek; Ottawa, Ontario, Canada) and

Table 2. Endometriosis severity correlate with infertility and diagnostic delay.

Clinical Feature	Moderate or Severe endometriosis (n = 842)	Mild endometriosis (n = 1177)	Category	OR	Beta	SE	P
Infertility (1182)	525	657	Yes or No	2.19	0.78	0.12	8.52E-11
Family History (1881)	790	1091	Yes or No	0.89	-0.11	0.09	0.23
Age at Menarche (921)	405	516	< = 12 or >12 yrs	1.20	0.18	0.13	0.18
Diagnostic Delay (874)	383	491	0 to 35	1.04	0.04	0.01	2.18E-05

Clinical features were correlated to severity. Only patients that could be unambiguously categorized were included in the analysis with total counts provided in parenthesis next to the clinical feature. P-values (P) are calculated using Wald test. Beta is the regression coefficients and SE the standard error from logistic regression.
doi:10.1371/journal.pone.0058257.t002

DNA was extracted using an automated extraction instrument, AutoPure LS (Qiagen; Valencia, CA), and manufacturer's reagents and protocols. DNA quality was evaluated by calculation absorbance ratio OD_{260}/OD_{280}, and DNA quantification was measured using PicoGreen® (Life Technologies; Grand Island, NY).

Microarray Genotyping

The discovery set of 1514 cases and 12660 controls and replication set of 505 cases and 1811 controls were genotyped using the Illumina Human OmniExpress Chip (Illumina; San Diego, CA) according to protocols provided by the manufacture. Figure S4 show the genotype clusters for the top eight SNPs in our study. All SNPs reported in the present study passed visual inspection for cluster quality. It is our experience that technical replication does not affect genotype calls of SNPs with high quality clusters and due to cost we could not justify independent technical replication.

Taqman Genotyping

A Taqman® 7900 instrument (Life Technologies; Grand Island, NY) and manufacturer's protocols were used to genotype rs61764370. Genotypes were determined using Taqman genotyping software SDS (v2.3) and the genotype cluster was visually inspected. Genotyping QC for rs61764370 passed standard criteria of call rate >95% and no deviation from HWE ($p<0.001$) was observed.

Sample Quality Control

Samples were excluded from the analysis if they missed any of the following quality thresholds:

a) Evidence of familial relationship closer that 3rd-degree ($\pi>0.2$) using genome-wide Identity-By-State (IBS) estimation implemented in PLINK
b) Samples with missing genotypes >0.02
c) Samples with non-European admixture >0.05 as determined by ADMIXTURE

SNP Quality Control

SNPS were excluded from the analysis if they missed any of the following quality thresholds:

a) SNPs with Illumina GenTrain Score <0.65
b) SNPs from copy number variant regions or regions with adjacent SNPs
c) SNPs failing Hardy-Weinberg Equilibrium (HWE) $P\leq10^{-3}$
d) SNPs with minor allele frequency (MAF) ≤0.01 in the control population
e) SNP call rate ≤98%

Admixture

ADMIXTURE (ver. 1.22) was used to estimate the individual ancestry proportion [16]. The software estimates the relative admixture proportions of a given number of a priori defined ancestral groups contributing to the genome of each individual. We used the POPRES dataset [26] as a reference group to create a supervised set of 9 ancestral clusters. Seven of them belong to the European subgroups along with African and Asian groups. Since POPRES dataset utilized Affymetrix 5.0 chip, we used 105,079 autosomal SNPs that overlapped with the Illumina OmniExpress dataset. Among the 105,079 SNPs we selected a subset of 33,067 SNPs that showed greater genetic variation (absolute difference in frequency) among the 9 reference groups. The pair-wise autosomal genetic distance determined by Fixation Index (F_{ST}) using 33,067 SNPs was calculated for the 9 reference groups and show in Table S6 [27]. Subsequently, a conditional test was used to estimate the admixture proportions in the unknown samples as described by Alexander et al. (2009).

Principal Component Analysis (PCA)

PCA was applied to account for population stratification among the European subgroups. We selected the previously identified 33,067 SNPs to infer the axes of variation using EIGENSTRAT [28]. Only the top 10 eigenvectors were analyzed. Most of the variance among the European populations was observed in the first and second eigenvector. The first eigenvector accounts for the east-west European geographical variation while the second accounts for the north-south component. Only the top 10 eigenvectors showed population differences using Anova statistics ($p<0.01$). We then calculated the PCA adjusted Armitrage trend P-values using the top 10 eigenvectors as covariates.

Power Analysis

Power calculations was performed using QUANTO (ver. 1.2), using a log-additive model. The analysis included 2019 cases and 14471 controls with the following assumptions: Type I error = 0.05, a minor allele frequency ≥0.10 and the odds-ratio ≥1.2.

Association Analysis

After the quality of all data was confirmed for accuracy, genetic association was determined using the whole-genome association analysis toolset, PLINK (ver. 1.07) [29].

Differences in allele frequencies between endometriosis patients and population controls were tested for each SNP by a 1-degree-of-freedom Cochran-Armitrage Trend test.

The allelic odds ratios were calculated with a confidence interval of 95%. SNPs that passed the quality control parameters were used to calculate the genomic inflation factor (λ) as well as to generate Quantile-Quantile (QQ) plots (Figure S2), which were generated by ranking a set of $-\log_{10}$ P-values and plotting them against their expected values. PCA adjusted Cochran-Armitrage trend test P-values were also determined. The combined/meta-analysis of discovery and replication dataset was performed using Cochran-Mantel-Hanszel method. Breslow Day test was used to determine between-cluster heterogeneity in the odds ratio for the disease/SNP association. Multivariate Logistic regression was used to test for independence of SNP effects. Univariate Logistic regression was used to test for correlation of clinical factors to the severity of the disease.

Control samples include both male and female samples in approximately equal proportions. The allele frequencies for the 8 strongly associated SNPs and the 15 SNPs with suggested associations did not show any significant gender bias.

Haplotype-based association tests were calculated by 1-degree of freedom χ^2-test, along with their respective odds ratios using PLINK.

The variance explained by logistic regression model is calculated using the Cox Snell and Nagelkerke pseudo R^2 method which is similar to the R^2 concept of linear regression [30].

Imputation Analysis

IMPUTE2 (ver. 2.2.2) was used for imputing SNPs against the 1000-Genome (version 3 of the Phase 1 integrated data). Samples were pre-phased with IMPUTE2 using actual genotypes and then imputed for SNPs included in the 1000-Genome reference panel to form imputed haplotypes. Imputation was carried out within +/ −250 kb of the main marker of interest. Only SNPs that pass the confidence score of > = 0.9 from imputation, call rate of 0.95 and with MAF>0.01 are reported. The imputation was performed on the total dataset of 2,019 cases and 14,471 control subjects.

Software Used

PLINK (version 1.07; http://pngu.mgh.harvard.edu/˜purcell/plink/index.shtml).

QUANTO (version 1.2; http://hydra.usc.edu/gxe).

R (version 2.15.0; http://www.r-project.org/).

Impute2 (version 2.2.2; http://mathgen.stats.ox.ac.uk/impute/impute_v2.html) and haplotype analysis was performed using PLINK (ver. 1.07).

LocusZoom (version 1.1; http://csg.sph.umich.edu/locuszoom/) was used for regional association plots.

EIGENSTRAT (version 3.0; http://genepath.med.harvard.edu/˜reich/Software.htm).

Supporting Information

Figure S1 PCA classification of Case and Control samples. A reference set of samples previously identified as European are shown in Panel A (reference). Samples selected for being 95% European are projected onto the European map and shown in Panel B. The Figure show that our Case and Control populations are geographically identical. A preponderance of the participants have ancestral roots in the north-western part of Europe with a Southern trend towards Italy.
(PDF)

Figure S2 Quantile-quantile plots for the Discovery set of 1,514 endometriosis cases and 12,660 population controls before and after PCA-based adjustment. The unadjusted QQ plot in Panel A is showing a $\lambda = 1.18$. The adjusted QQ plot in Panel B show $\lambda = 1.05$. The association analysis include 580,699 SNPs and included only samples that passed our Ethnicity, SNP and Sample quality filters.
(PDF)

Figure S3 Regional association plots for the five top regions (Panel A–E).
(PDF)

Figure S4 Genotype clusters for the 8 most strongly associated SNPs.
(PDF)

Table S1 Top 100 SNPs from Discovery and Replication GWAS.
(PDF)

Table S2 a Genotyped and Imputed P-values for the LINC00339-WNT4 region on 1p36.12. b Genotyped and Imputed P-values for the RND3-RBM43 region on 2q23.3. c Genotyped and Imputed P-values for the RNF144B-ID4 region on 6p22.3. d Genotyped and Imputed P-values for the IL33-TPD52L3 region on 9p24.1. d Genotyped and Imputed P-values for the HNRNPA3P1-LOC100130539 region on 10q11.21.
(PDF)

Table S3 Haplotype analysis for the WNT4-region.
(PDF)

Table S4 a No association with CDKN2BAS on 9p21 in Europeans. b Tentative replication of rs13271465 located on 8p22 between MTMR7 and SLC7A2. c SNP rs12700667 fails replication.
(PDF)

Table S5 a Severity of endometriosis is independent of the five top loci by logistic regression analysis. b Severity of endometriosis is independent of the top five loci by association analysis.
(PDF)

Table S6 Pair-wise autosomal genetic distance among ethnic groups as measured by the Fixation Index (F_{ST}).
(PDF)

Table S7 Support for endometriosis association in a Caucasian cohort found at 3 of 7 loci reported by Nyholt et al.
(PDF)

Acknowledgments

We would like to extend our sincere gratitude to all our study participants. It is because of them that this study has been possible. We also extend our thanks to our colleagues in Juneau's Family Studies Group and our Laboratory for their untiring efforts on this endometriosis project.

Author Contributions

Conceived and designed the experiments: HA RC KW. Performed the experiments: HA RC. Analyzed the data: HA RC PF KW. Contributed reagents/materials/analysis tools: KW. Wrote the paper: HA RC KW.

References

1. Giudice LC, Kao LC (2004) Endometriosis. Lancet 364: 1789–1799.
2. Signorile PG, Baldi F, Bussani R, D'Armiento M, De Falco M, et al. (2009) Ectopic endometrium in human foetuses is a common event and sustains the theory of mullerianosis in the pathogenesis of endometriosis, a disease that predisposes to cancer. J Exp Clin Cancer Res 28: 49.
3. Husby GK, Haugen RS, Moen MH (2003) Diagnostic delay in women with pain and endometriosis. Acta Obstet Gynecol Scand 82: 649–653.
4. Ballard K, Lowton K, Wright J (2006) What's the delay? A qualitative study of women's experiences of reaching a diagnosis of endometriosis. Fertil Steril 86: 1296–1301.
5. Arruda MS, Petta CA, Abrao MS, Benetti-Pinto CL (2003) Time elapsed from onset of symptoms to diagnosis of endometriosis in a cohort study of Brazilian women. Hum Reprod 18: 756–759.
6. Hansen KA, Eyster KM (2010) Genetics and genomics of endometriosis. Clin Obstet Gynecol 53: 403–412.
7. Stefansson H, Geirsson RT, Steinthorsdottir V, Jonsson H, Manolescu A, et al. (2002) Genetic factors contribute to the risk of developing endometriosis. Hum Reprod 17: 555–559.
8. Treloar SA, O'Connor DT, O'Connor VM, Martin NG (1999) Genetic influences on endometriosis in an Australian twin sample. Fertil Steril 71: 701–710.
9. Hadfield RM, Mardon HJ, Barlow DH, Kennedy SH (1997) Endometriosis in monozygotic twins. Fertil Steril 68: 941–942.
10. Moen MH (1994) Endometriosis in monozygotic twins. Acta Obstet Gynecol Scand 73: 59–62.
11. Montgomery GW, Nyholt DR, Zhao ZZ, Treloar SA, Painter JN, et al. (2008) The search for genes contributing to endometriosis risk. Hum Reprod Update 14: 447–457.
12. Rahmioglu N, Missmer SA, Montgomery GW, Zondervan KT (2012) Insights into Assessing the Genetics of Endometriosis. Curr Obstet Gynecol Rep 1: 124–137.
13. Uno S, Zembutsu H, Hirasawa A, Takahashi A, Kubo M, et al. (2010) A genome-wide association study identifies genetic variants in the CDKN2BAS locus associated with endometriosis in Japanese. Nat Genet 42: 707–710.
14. Painter JN, Anderson CA, Nyholt DR, Macgregor S, Lin J, et al. (2011) Genome-wide association study identifies a locus at 7p15.2 associated with endometriosis. Nat Genet 43: 51–54.

15. Nyholt DR, Low SK, Anderson CA, Painter JN, Uno S, et al. (2012) Genome-wide association meta-analysis identifies new endometriosis risk loci. Nat Genet.
16. Alexander DH, Novembre J, Lange K (2009) Fast model-based estimation of ancestry in unrelated individuals. Genome Res 19: 1655–1664.
17. Santulli P, Borghese B, Chouzenoux S, Vaiman D, Borderie D, et al. (2012) Serum and peritoneal interleukin-33 levels are elevated in deeply infiltrating endometriosis. Hum Reprod 27: 2001–2009.
18. Howie BN, Donnelly P, Marchini J (2009) A flexible and accurate genotype imputation method for the next generation of genome-wide association studies. PLoS Genet 5: e1000529.
19. Franco HL, Dai D, Lee KY, Rubel CA, Roop D, et al. (2011) WNT4 is a key regulator of normal postnatal uterine development and progesterone signaling during embryo implantation and decidualization in the mouse. FASEB J 25: 1176–1187.
20. Goteri G, Ciavattini A, Lucarini G, Montik N, Filosa A, et al. (2006) Expression of motility-related molecule Cdc42 in endometrial tissue in women with adenomyosis and ovarian endometriomata. Fertil Steril 86: 559–565.
21. Hu WP, Tay SK, Zhao Y (2006) Endometriosis-specific genes identified by real-time reverse transcription-polymerase chain reaction expression profiling of endometriosis versus autologous uterine endometrium. J Clin Endocrinol Metab 91: 228–238.
22. Grechukhina O, Petracco R, Popkhadze S, Massasa E, Paranjape T, et al. (2012) A polymorphism in a let-7 microRNA binding site of KRAS in women with endometriosis. EMBO Mol Med.
23. Luong HT, Nyholt DR, Painter JN, Chapman B, Kennedy S, et al. (2012) No evidence for genetic association with the let-7 microRNA-binding site or other common KRAS variants in risk of endometriosis. Hum Reprod.
24. Treloar SA, Wicks J, Nyholt DR, Montgomery GW, Bahlo M, et al. (2005) Genomewide linkage study in 1,176 affected sister pair families identifies a significant susceptibility locus for endometriosis on chromosome 10q26. Am J Hum Genet 77: 365–376.
25. American Society for Reproductive Medicine (1997) Revised American Society for Reproductive Medicine classification of endometriosis: 1996. Fertil Steril 67: 817–821.
26. Nelson MR, Bryc K, King KS, Indap A, Boyko AR, et al. (2008) The Population Reference Sample, POPRES: a resource for population, disease, and pharmacological genetics research. Am J Hum Genet 83: 347–358.
27. Holsinger KE, Weir BS (2009) Genetics in geographically structured populations: defining, estimating and interpreting F(ST). Nat Rev Genet 10: 639–650.
28. Price AL, Patterson NJ, Plenge RM, Weinblatt ME, Shadick NA, et al. (2006) Principal components analysis corrects for stratification in genome-wide association studies. Nature Genetics 38: 904–909.
29. Purcell S, Neale B, Todd-Brown K, Thomas L, Ferreira MA, et al. (2007) PLINK: a tool set for whole-genome association and population-based linkage analyses. Am J Hum Genet 81: 559–575.
30. Nagelkerke NJD (1991) A note on a general definition of the coefficient of determination. Biometrika 78: 691–692.